6-24-2015

Molecular Dynamics Simulations of A Suspended Particle In A Fluid Near A Wall

Jianwei Ju

Jianwei Ju

Candidate

Mechanical Engineering

Department

This dissertation is approved, and it is acceptable in quality and form for publication:

Approved by the Dissertation Committee:

Professor Peter Vorobieff , Chairperson

Professor Juan C. Heinrich

Professor Svetlana Poroseva

Dr. Edward Kober

Molecular Dynamics Simulations of A Suspended Particle In A Fluid Near A Wall

BY

Jianwei Ju

B.S., Mechanical Engineering, Zhejiang University, China, 2001
M.S., Mechanical Engineering, University of New Mexico, 2004

DISSERTATION

Submitted in Partial Fulfillment of the
Requirements for the Degree of Doctor of Philosophy, Engineering

Doctor of Philosophy

Engineering

The University of New Mexico
Albuquerque, New Mexico

May, 2015

Molecular Dynamics Simulations of A Suspended Particle In A Fluid Near A Wall

by

Jianwei Ju

B.S., Mechanical Engineering, Zhejiang University, China, 2001

M.S., Mechanical Engineering, University of New Mexico, 2004

PhD, Engineering, University of New Mexico, 2015

Abstract

The behavior of the suspended particles in a fluid is an important subject in fluid flow studies. Earlier research works mostly were performed using a continuum treatment on a macro scale level. Recent developments in the field of micro- and nanofluids have led to a renewed interest in molecular hydrodynamics phenomena. The micro hydrodynamic interactions between particles and solid surfaces have been shown to play important roles in the ordering of particles in vibrated fluids, self-organization of biological cells, and collective dynamics of swimming particles[Voth2002, Riedel2005, Hernandez2005], micro-electronic fluid behaviors and also have great prospects in industry applications.

Though a lot of researches have been done in this area, some problems are still unclear. For example, the boundary conditions of the interaction surfaces. For hundreds of years it has relied on the no-slip boundary condition at the solid-liquid interface in the continuum theory, and it was also applied to model many macroscopic experiments[Batchelor00]. However, the no-slip boundary started to break down in molecular level, for certain scenarios such as in the near field between a colloidal particle and a solid surface, what kind of boundary condition may be applied to the interface are still not clear. Another problem is the microscopic particle size. There is no clear theory for the effective particle size. As a result, lot of studies all assumed an ad hoc position for the wall that is not been defined in terms of the actual interactions with the fluid. This introduced some ambiguity

in the determination of the correct comparison to the continuum theory as well as to the general force versus distance results. Further more, in a number of more recent studies, researchers applied either the repulsive Weeks-Chandler-Andersen (WCA) potentials, or some cut off and shifted Lennard-Jones (LJ) potentials. The WCA potential is a pure repulsive potential, though the regular LJ potential with a finite cutoff distance, has both repulsive and attractive parts, LJ potential usually has a discontinuity where it is cut-off, this non-smoothness may affect the results. A new potential model is needed to conserve the simulation system energy better.

In this research we focused on the hydrodynamic interactions experienced by colloidal particles in the vicinity of a solid surface. We developed a new potential model, which was smoothly cut at the finite cutoff distance with both the repulsive and attractive parts. Using this new potential model, we investigated the wall-particle interaction and the solvation forces for a single suspended particle in a LJ fluid. We also focused especially on the phenomena when the suspended sphere is positioned quite close to the wall. Additionally, we explored how moving a non-interacting sphere through the particle wall, can be used to determine the effective radius of the suspended particle. Next, we analized the dynamic drag force of spherical particles of different radii with various velocities to assess the validity of Brenner's expression as the suspended particle approaches the wall. The study finally determined the slip or no-slip boundary conditions in the microscale hydrodynamics.

TABLE OF CONTENTS

Chapter 1

INTRODUCTION

The behavior of the suspended particles in a fluid is an important subject in fluid flow studies. Earlier research works mostly were performed using a continuum treatment on a macro scale level. Recent developments in the field of micro- and nanofluids have led to a renewed interest in molecular hydrodynamics phenomena. The micro hydrodynamic interactions between particles and solid surfaces have been shown to play important roles in the ordering of particles in vibrated fluids, self-organization of biological cells, and collective dynamics of swimming particles[Voth2002, Riedel2005, Hernandez2005], micro-electronic fluid behaviors and also have great prospects in industry applications.

Though a lot of researches have been done in this area, some problems are still unclear. For example, the boundary conditions of the interaction surfaces. For hundreds of years it has relied on the no-slip boundary condition at the solid-liquid interface in the continuum theory, and it was also applied to model many macroscopic experiments[Batchelor00]. However, the no-slip boundary started to break down in molecular level, for certain scenarios such as in the near field between a colloidal particle and a solid surface, what kind of boundary condition may be applied to the interface are still not clear. Another problem is the microscopic particle size. There is no clear theory for the effective particle size. As a result, lot of studies all assumed an ad hoc position for the wall that is not been defined in terms of the actual interactions with the fluid. This introduced some ambiguity

in the determination of the correct comparison to the continuum theory as well as to the general force versus distance results. Further more, in a number of more recent studies, researchers applied either the repulsive Weeks-Chandler-Andersen (WCA) potentials, or some cut off and shifted Lennard-Jones (LJ) potentials. The WCA potential is a pure repulsive potential, though the regular LJ potential with a finite cutoff distance, has both repulsive and attractive parts, LJ potential usually has a discontinuity where it is cut-off, this non-smoothness may affect the results. A new potential model is needed to conserve the simulation system energy better.

In this research we focused on the hydrodynamic interactions experienced by colloidal particles in the vicinity of a solid surface. We developed a new potential model, which was smoothly cut at the finite cutoff distance with both the repulsive and attractive parts. Using this new potential model, we investigated the wall-particle interaction and the solvation forces for a single suspended particle in a LJ fluid. We also focused especially on the phenomena when the suspended sphere is positioned quite close to the wall. Additionally, we explored how moving a non-interacting sphere through the particle wall, can be used to determine the effective radius of the suspended particle. Next, we analized the dynamic drag force of spherical particles of different radii with various velocities to assess the validity of Brenner's expression as the suspended particle approaches the wall. The study finally determined the slip or no-slip boundary conditions in the microscale hydrodynamics.

1.1 Previous Research

The problem of a sphere slowly moving with a constant velocity in a viscous fluid (Re << 1, where Re=rU/ν, r is the radius of the sphere, U is the constant velocity and ν is the dynamic viscosity) is one of the basic problems in hydrodynamics. Stokes' Law defines the drag force as proportional to the particle's radius, velocity and the fluid viscosity.

$$F = 6\pi\mu r U \tag{1.1}$$

Brenner[Brenner61] obtained exact solutions of the Stokes equations in a viscous fluid of a spherical particle moving steadily toward and away from a planar surface of infinite extent. For the case of a solid surface with no-slip boundary condition, incompressible follow, and Low Reynolds number, Brenner found that the drag force, F, on the particle is given by

$$F = 6\pi\mu r U\lambda, \tag{1.2}$$

where μ is the viscosity, *r* the radius of the sphere, *U* its velocity, 6 for no-slip conditions, and λ is a correction factor given by

$$\lambda = \frac{4}{3}\sinh\alpha\sum_{n=1}^{\infty}\frac{n(n+1)}{(2n-1)(2n+3)}\left[\frac{2\sinh(2n+1)\alpha+(2n+1)\sinh 2\alpha}{4\sinh^2(n+1/2)\alpha-(2n+1)^2\sinh^2\alpha}-1\right], \tag{1.3}$$

with

$$\alpha = \cosh^{-1}\left(\frac{h}{b}+1\right), \tag{1.4}$$

where h is the distance from the center of the sphere to the plane. At a large distance from the surface, $h \to \infty$, λ tends to one, so that Eq. (2) would simplify to Stokes' law.

At short separation distances from the plane surface (compared to the radius of the sphere), this continuum force (Eq.(2)) should diverge as b/h. At short distances compared to molecular dimensions, the continuum assumption must break down because of the molecular nature of the fluid, and one expects that the drag force remains finite. The assumptions required for Brenner's solution are no-slip boundary conditions, a constant fluid density and infinitely smooth solid and colloid surfaces. In real atomistic systems, these assumptions are not completely valid at sufficiently small length scales, so discrepancies should arise.

As the no-slip boundary conditions break, Luo and Pozrikidis[Luo2008] improved Eq.(1) as:

$$F = c\pi\mu r U = 6\frac{\beta+2}{\beta+3}\pi\mu r U \tag{1.5}$$

where β is the Basset parameter. As $\beta \to 0$, the Stokes' law coefficient of 6 tends 4, indicating a substantial reduction in the drag force.

In addition, a number of researchers have suggested the no-slip boundary conditions were no longer supported in the micro-scale fluid behaviors. There have been a couple of previous studies on the validity of Stokes' law for the case of a spherical particle moving toward a wall by employing molecular dynamics. Vergeles *et al.* [Vergeles96, Vergeles97] studied the translational and rotational motion of a colloid particle in a viscous Lennard-Jones fluid both near and away from a flat surface. Their study, which included both spherical and atomistically structured colloids showed that the drag and torque on the sphere in an essentially unbounded fluid agree with the continuum hydrodynamics results captured by Stokes' law. Similar studies were also performed by Heyes *et al* [Heyes96, Nuevo97]. As the solute approaches the wall, Vergeles et al concluded that the Brenner model was supported by their data, although some variations were observed at separation distances comparable to the solvent radius. These authors also concluded that the no-slip condition breaks down near the wall.

In a more recent molecular dynamics study that apployed repulsive Weeks-Chandler-Andersen (WCA) potentials, Challa and van Swol revisited parts of the Vergeles study [Challa06]. In their analysis, they found that as a sphere approaches a flat surface the drag force on the sphere can be represented by a superposition of two contributions: a static solvation force and the hydrodynamic force. They inferred that the solvation force contributes most prominently at small distances between the sphere and the planar surface and at small velocities. For a smooth wall, they found that the static force can lead to a total force that oscillates between positive and negative values (depending on the discrete size of the solvent molecules), an effect that is not included in the continuum

hydrodynamic result [Batchelor00]. After compensating for this, however, they found that they did not observe a divergence in the hydrodynamic force as strong as that predicted by Brenner.

Kohale and Khare [Kohale2008] provided simulations of a colloid sphere moving inside fluid between two confined surfaces. They measured the friction forces between the colloid sphere and the fluid and found the values of the friction forces follow the same qualitative trend as the continuum results but are consistently lower than the continuum values. The continuum results were obtained for the case of no-slip boundary condition on the sphere surface; they claim this no-slip boundary condition is clearly not supported in their simulations. In their research, in addition to a pure repulsive potential, Kohale and Khare also tried a regular LJ potential with a finite cutoff distance, so the interaction forces could have both repulsive and attractive parts. Because their LJ potential has a discontinuity where it is cut-off, this non-smoothness may affect their results.

Several researchers followed up to justify the no-slip boundary condition on the microscopic level. Horn *et al* [Vinogradova2000] presented data describing the squeeze-film drainage of an " ideal elastic" or "Boger fluid"(an elastic liquid with a constant viscosity) in submicron films between curved solid surfaces. The thin film does not follow the predictions based on the bulk rheological properties of Boger fluid. The film is thinning more rapidly than prediction of Newtonian theory with no-slip conditions. To

explain this, they invoked slippage at the fluid-solid interface and interpreted the results with a simple slip length model.

Zhu et al [Zhu2006] developed a stable spread-sheet algorithm for the calculation of the hydrodynamic forces measured by colloid probe atomic force microscopy to be used in investigations of interfacial slip. They claimed their model is accurate enough in the large separation limit (large with respect to the radius of the microsphere), and can be used to predict the hydrodynamic drainage force instead of Brenner equation. But they also admitted that their results for a relatively soft cantilever significantly overestimated.

With increasing interest in micro- and nanofluidics, many researchers have focused on the modeling of the motion of liquids over surfaces, and led to the concept of the effective tensorial slip. Vinogradova and Belyaev[Vinogradova2010] discussed the issue of boundary conditions at smooth hydrophobic and rough hydrophilic surfaces, and then given the especial emphasis to the derivation of effective boundary conditions for a flow past hydrophobic solid surfaces with special textures that can exhibit greatly enhanced properties, compared to analogous flat or slightly disordered surfaces. They derived accurate formulas describing effective boundary conditions for pressure-driven flow past super-hydrophobic textures. They analyzed both thin and thick channel situations, and in some special cases, obtained exact solutions valid for an arbitrary thickness of the channel. They also gave the exact solutions for optimization of the transverse flow and analytical results for the hydrodynamic resistance to the approach of two surfaces. Furthermore, they discussed the electrokinetic pumping in microfluidic devices. In 2011

Asmolov, Belyaev, and Vinogradova[Vinogradova2011] analyzed theoretically a high-speed drainage of liquid films squeezed between a hydrophilic sphere and a textured superhydrophobic plane that contains trapped gas bubbles. They showed that at a thinner gap the force reduction becomes more pronounced, and that it depends strongly on the faction of the gas area and local slip lengths. For small separations they derived an exact equation, which introducess a correction for effective slip to texture parameters.

Bocquet and Barrat [Bocquet2007] have recently reviewed slippage at atomistic scales and shown the connection with slip length models. They suggested the friction coefficient κ and hence the slip length b ($b=\mu/\kappa$), depend strongly on the strength of the solid-liquid interactions. They found that slip length achieved for modified Lennard-Jones (LJ) models may vary between a few molecular diameters for a traditional (LJ) potential and 50 to 60 molecular diameters for reduced interactions; the slip length is highly dependent on the value of the interaction parameter that defines the solid-liquid attraction.

In order to make comparisons to the continuum models, these studies all assumed the sizes of the fluid and suspended particles (as well as the particles that form the wall if a non-smooth wall is employed) to be fixed at some nominal value determined by the parameters of the applied potentials. For example, if the range of the Lennard-Jones interaction is σ, the radius of the particle is often taken to be $\sigma/2$. In the analyses of these studies, the position of the wall was assumed to be at either the origin of the potential, where the potential becomes zero (for WCA type models), or at a distance $\sigma/2$ from the atomic centers for LJ-type models. However, due to the softness of the interactions, it is

reasonable to expect that the effective sizes, particularly near the flat surface, to be determined by the competing interactions of the fluid molecules located between the spherical particle and the wall. This also means that the effective particle sizes can become subtle functions of the conditions of the simulations (eg. temperature and pressure). As a result, the studies cited above all assume some ad hoc position for the wall that has not been defined in terms of the actual interactions with the fluid. This introduces ambiguity in the determination of the correct comparison to Brenner's expression (2) as well as to general force versus distance results. The fundamental issue of defining the size of the solute or the position of the wall impacts a large number of similar studies comparing fluid-flow analyzed by molecular dynamics simulations [for example, [Kohale10], [Koplik89]], especially where it is of interest to obtain a quantitative comparison with the continuum theories and to assess slip/no-slip interactions. As it is now possible to perform measures on the colloid and surface interactions at molecular level resolution it is important to clarify how such results can be interpreted.

1.2 Narrative Summary

In our investigation our interest is investigating the wall-particle interactions, including solvation forces for a single suspended spherical particle in a viscous fluid, the friction coefficient, and the boundary conditions. In the first part of the research, we focus both on the effective size of colloid particles suspended in a fluid in the vicinity of a rigid wall and on the effective position of the wall. We calculate the solvent forces on spherical

particles of different radii as a function of varying positions near and overlapping the wall and compare them to continuum models. Based on those data, the effective sizes of the particles and the position of the wall are investigated using several different metrics.

In addition, the study determined the slip or no-slip boundary conditions in the microscale hydrodynamics. We calculated the friction coefficient of spherical particles with different masses and radii that moves freely inside a viscos fluid with an initial velocity. The friction coefficient can be determined by measuring the velocities and mean square displacements of the sphere. Slip or no-slip boundary conditions can be analyzed by investigating those results.

Next, we analysis the dynamic drag force of a spherical particle of different radii with various velocities and to assess the validity of Brenner's expression as the suspended particle approaches the wall. The simulations focused on the analysis of equilibrium simulations with a colloid particle moving with a constant velocity approaching and leaving both the smooth wall and an atomic wall, and apply continuum analogies to the behavior of those resulting forces with respect to radius and separation distances.

Chapter 2

THE EFFECTIVE PARTICLE SIZE

In this charpter, we investigate the effective particle size of the colloidal particle suspended in a fluid in the vicinity of a rigid wall. In order to determine the effective size of the particles, we calculate the solvent forces on spherical particles of different radii as a function of different positions near and overlapping the wall and compare them to continuum models. In addition, this procedure also determines the effective position of the wall. All simulations reported here are performed with the LAMMPS package [LAMMPS] for molecular dynamics.

2.1 Simulation Approach

2.1.1 Interaction Potentials

The fluid particles have a mass *m*, and interact via a pairwise potential. For the fluid-fluid interaction potentials, we used two different variations of the Lennard-Jones (LJ) potential. For the first set of simulations, we used the well-known repulsive WCA potential [Challa06] that was used in many previous studies:

$$\phi(r) = \begin{cases} \phi_{12-6}(r) - \phi_{12-6}(r_c), & r < r_c \\ 0, & r > r_c \end{cases} \tag{2.1}$$

with

$$\phi_{12-6}(r) = 4\varepsilon\left[\left(\frac{\sigma}{r}\right)^{12} - \left(\frac{\sigma}{r}\right)^{6}\right], \tag{2.2}$$

the cutoff radius is chosen at the minimum of the LJ potential, $r_c/\sigma = 2^{1/6} \approx 1.12$ and r is the distance between the center of the two fluid particles. The parameter ε is the depth of the LJ potential, and represents our fundamental energy unit, and similarly σ is the fundamental length unit. The potential between the fluid particles and the suspended sphere is described using a shifted WCA potential, as was used in previous studies.

$$\phi(r) = \begin{cases} \infty, & 0 < r < b_0 \\ \phi_{12-6}(r - b_0) - \phi_{12-6}(r_c), & b_0 < r < r_c + b_0 \\ 0, & r > r_c + b_0 \end{cases} \tag{2.3}$$

Here b_0 is the radius of the hard-core region of the sphere (which allows its effective size to be arbitrarily adjusted) and r is the distance between the center of the sphere and the center of a fluid particle. These potentials are continuous and smooth to arbitrary order (except at the inner cut-off b_0 which shouldn't be accessible), and short-ranged. Consequently, there are no complicating factors in their numerical evaluation and for the standard time step of $\Delta t = 0.005\sigma\sqrt{m/\epsilon}$, there is a very high degree of energy conservation.

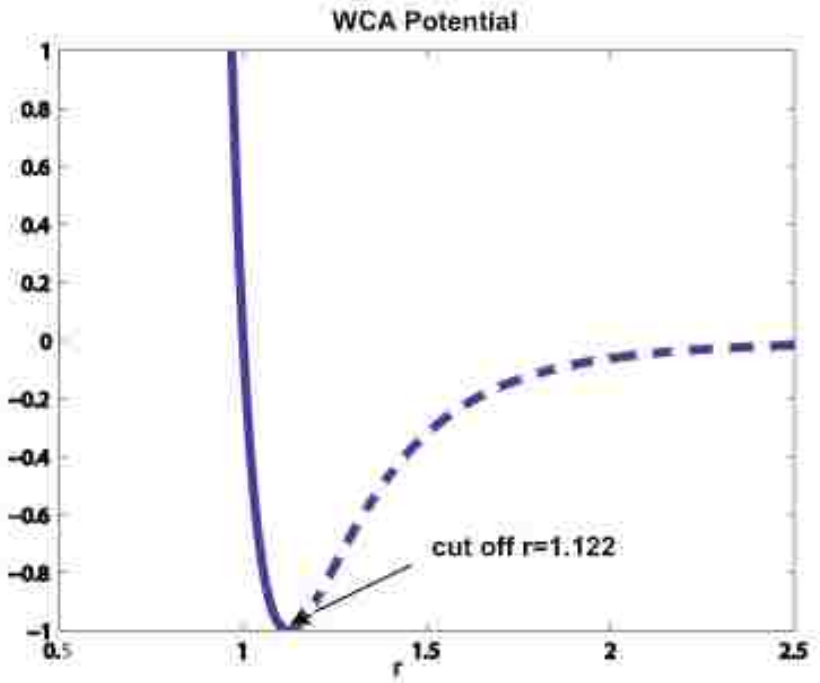

Fig. 2.1. WCA potential and cut off at r=1.122.

In order to explore the effect of attractive forces under similar simulation conditions, we then use a quadratic LJ-spline pair potential to do the similar simulation to add the attractive part to the force. Because of the moderately long range of the LJ potential, many previous studies either cut-off the interaction at an arbitrary distance (resulting in an interaction that is neither continuous nor smooth at the cut-off), or employed a cut-and-shifted potential form that is continuous at the cut-off, but not smooth. Consequently, the simulations do not conserve energy during the dynamics runs, and the method of simulation and/or the analyses require corrections for this defect. Other resolutions of this problem are either to include a very large range of pairwise interactions (which is very computationally intensive) or to more smoothly truncate the tail of the LJ potential [Holian]. Here, we define a modified LJ form that smoothly (to second order) approaches

zero at a distance r_{max}. This potential consists of the standard LJ potential up to its inflection point at $r_{spl} = (26/7)^{1/6}\ \sigma \approx 1.24\ \sigma$, as proposed earlier [Holian]. There (and distinct from [Holian]), it switches to a quartic polynomial spline that is smoothly (to second order) matched at this point and goes smoothly to zero at a non-arbitrary value r_{max}.

The LJ-spl potential is built by using the usual LJ 12-6 potential for separations $r < r_{spl} = (26/7)^{1/6}\ \sigma \approx 1.24\ \sigma$[1],

$$\phi_{12-6}(r) = 4\varepsilon\left[\left(\frac{\sigma}{r}\right)^{12} - \left(\frac{\sigma}{r}\right)^{6}\right] \qquad (2.4)$$

Where r_{spl}, is the distance of maximum attractive force, i.e., $\phi''_{spl} = 0$.

Between r_{spl} and $r_{\max} = \frac{55}{36}\left(\frac{26}{7}\right)^{1/6}\sigma = \frac{55}{36}r_{spl}\sigma \approx 1.90\sigma$, ϕ is a 4th order spline:

$$\phi_{spl}(r) = A(r - r_{\max})^4 + B(r - r_{\max})^3 \qquad (1.5)$$

with A and B chosen such that at $r = r_{spl}$:

$$\begin{cases} \phi = \phi_{spl} \\ \phi' = \phi'_{spl} \\ \phi'' = \phi''_{spl} = 0 \end{cases} \qquad (2.6)$$

When $r > r_{\max}$:

$$\phi = \phi' = 0. \qquad (2.7)$$

From (2.5), (2.6) and (2.7), our results of A and B are: $A = \frac{5184}{133}\left(\frac{936}{133}\right)^2\left(\frac{7}{26}\right)^{14/3}\frac{\varepsilon}{\sigma^4} \approx 4.23\frac{\varepsilon}{\sigma^4}$, and $B = 2\frac{5184}{133}\left(\frac{936}{133}\right)\left(\frac{7}{26}\right)^{7/2}\frac{\varepsilon}{\sigma^{3.}} \approx 5.56\frac{\varepsilon}{\sigma^3}$.

Fig. 2.2 shows the LJ-spline potential. Fig. 2.3 shows the forces derived from the 4th order spline. Both the potential and the force go smoothly to zero at $r_{\max}$.

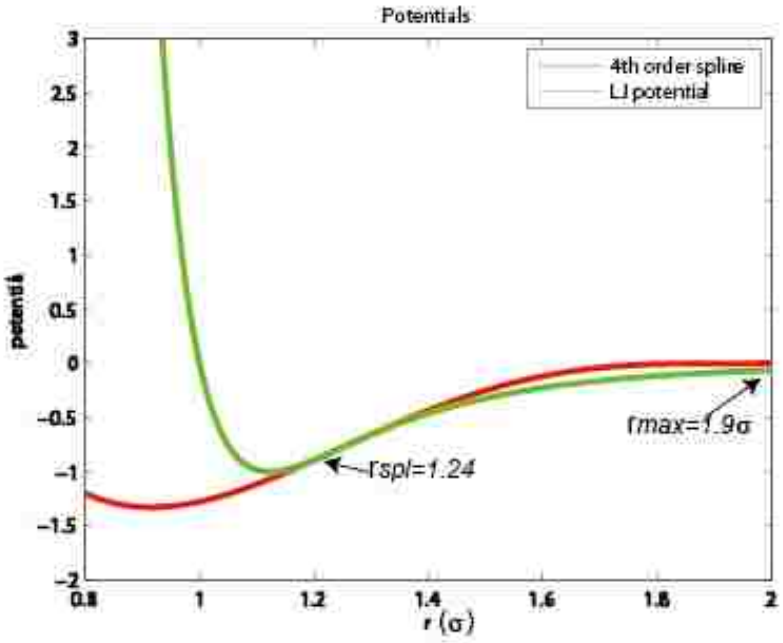

Fig. 2.2. LJ-spline pair potential. The dotted line is the 4th order spline; the solid line is the LJ 12-6 potential. The new potential contains two parts, the 1st part is the LJ 12-6 potential when $r < r_{spl}$, the 2nd part is the 4th order spline, when $r_{spl} < r < r_{\max}$.

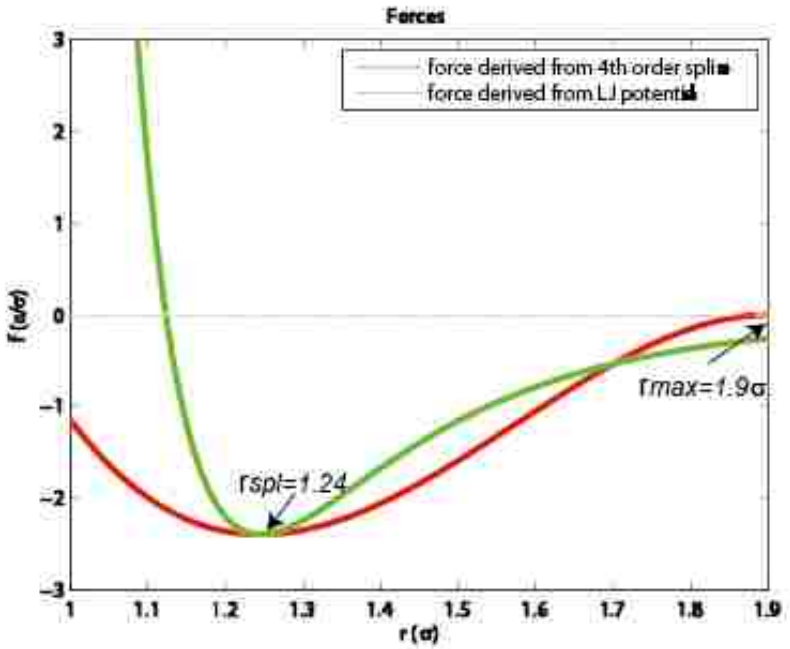

Fig. 1.3. Forces vs. separation. The dotted line is the 4th order spline force; the solid line is the LJ 12-6 force. The minimum occurs at $r = 2^{1/6}\sigma$.

We use this LJ-spline potential as the interactive potential between fluid-fluid particles, and wall particles. The shifted LJ-spline potential is the interactive potential between fluid particles and the sphere. Since both the potential and the force go smoothly to zero at $r_{\max}$. Consequently, the simulations conserve energy during the dynamics runs.

Fig. 2.4 shows the energy and temperature in a test simulation. We use the same system try an NVE simulation, with our newly designed 4th order spline potential. The figure shows a good energy conservation. We set the initial temperature at $kT/\varepsilon=3$, then let the system reach the thermo-equilibrium (at step 60000), after that let the simulation start and note down the temperature, pressure and energy of the system.

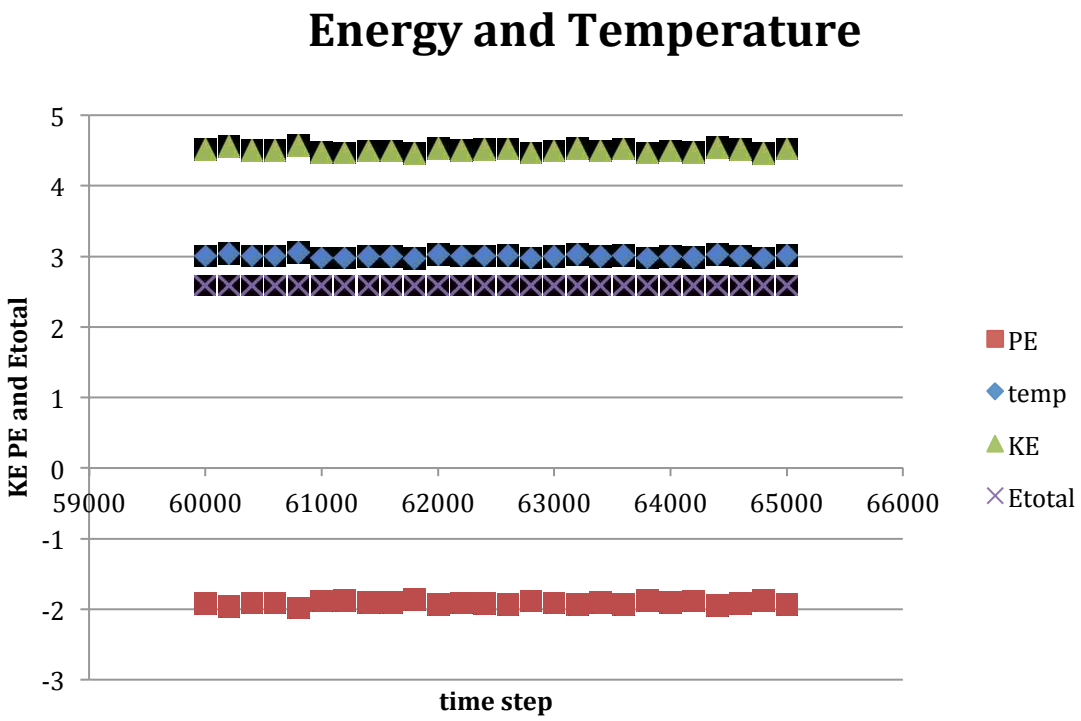

Fig. 2.4. Energy and temperature in the NVE simulation. The energy conserved well in the system.

2.1.2 Simulation Procedure

The simulations were performed in a box of dimensions $L_x/\sigma \times L_y/\sigma \times L_z/\sigma = 13.68 \times 13.68 \times 32.20$ with periodic boundary conditions applied to the x and y directions, while a pair of parallel walls was placed normal to the z direction near the two ends of the box. The atomistic wall that was used to explore the behavior of the suspended spherical particle consisted of two layers each of 200 atoms. These were placed in a face centered cubic (fcc) arrangement with a lattice spacing of 1.094σ to form a wall that would be impervious to the solvent atoms. The inner most layer of wall atoms was positioned

with their atomic centers at z=0. These wall atoms interacted with the solvent atoms with the same potential as a solvent-solvent interaction, but they were not allowed to move during the simulations. The wall at the far end of the simulation box (z = 32.20) was a simple smooth wall that interacted with the solvent atoms by a planar 9-3 potential as used in earlier work [Vergeles96,97]. The potential energy between the suspended sphere and the wall particles was set to zero so that the wall exerted no direct force on the sphere. In all simulations described here, the position of the colloid with respect to the wall was fixed during the data acquisition periods, so the magnitude of this interaction has no significance on the simulation.

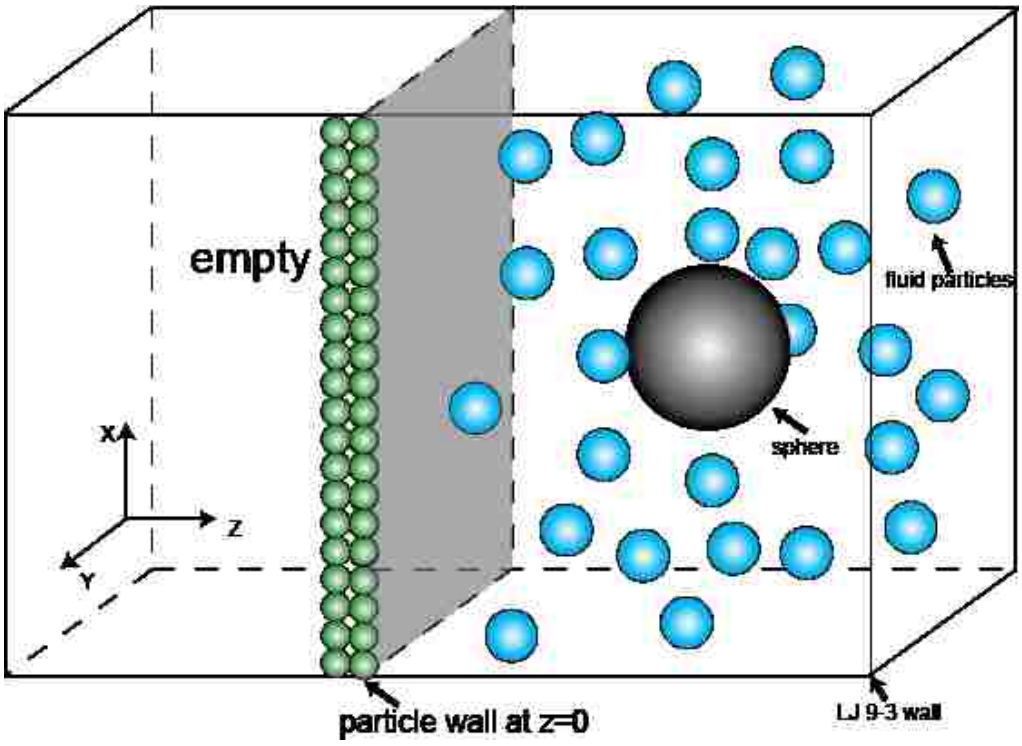

Fig. 2.5. Simulation box and the initialization of the system.

The simulations were initialized by filling up the region to the right of the wall with fluid particles (see Fig. 2.5). The fluid particles were initiated in an fcc crystal structure with a

lattice constant 1.094σ giving an initial solvent density of $\rho\sigma^3$=0.8. The first layer of solvent was placed at z = 1.094 σ. Then, a colloid sphere with a core radius of b_0 and mass M was placed at an arbitrarily selected initial point. Any solvent particle whose center was within $b_0 + x\sigma$ of the colloid center was then removed. In order to get a relatively consistent pressure values, the x values were carefully chosen. For the WCA cases, x was around 0.7; for the LJ-spline cases, x was around 0.9. This method generated fairly consistent solvent densities regardless of the size and initial position of the colloid. The system was then randomized for 40000 time steps using a Nose-Hoover thermostat and setting the temperature to a high value of $kT/\varepsilon = 3$ to liquify the solvent. The temperature was then lowered to a value of either $kT/\varepsilon = 1.2$ or $kT/\varepsilon = 1.6$, again using a Nose-Hoover thermostat, and the system was allowed to equilibrate for 20000 time steps. After this, the simulation was continued in an NVE ensemble, and the z-component of net solvent force on the sphere was evaluated 1000 times, collecting a static snapshot every 200 time steps.

This procedure was performed for 100 different static positions of the suspended sphere for each selected core radius, potential set and temperature. The range of initial positions was incremented from starting at a location where the center of the sphere was well separated from the wall, and was repeated until the sphere had moved completely through the wall and there was no longer any perturbation to the solvent. Effectively, this tracks the equilibrium forces resulting from moving the colloid from the bulk fluid and through the wall. By reinitializing the simulations for each new initial colloid position, a fairly constant solvent density and thermodynamic state was maintained.

The pressure of the simulation system was calculated by averaging the total interaction force on the smooth wall at the far end of the simulation box. We set up a region close to the smooth wall ($27.93<z<32.30$), during the simulation, if the fluid particles fell into that region, the interaction forces between the fluid particles and the wall would be noted down and accumulated, eventually, this total interaction force value was be averaged by the area of the smooth wall. We use this value as the system pressure for the simulation (See figures in the Appendix for the pressure values).

2.2 Solvation Force

Figure 2.6 shows a schematic of the geometry as the sphere approaches the wall. Because the fluid particles interact with the wall, there is a region of thickness Δ_1 between the center of the first layer of wall atoms and the center of the closest layer of fluid molecules where the density of the fluid vanishes. Similarly, the radius of the suspended particle, as defined in the potential energy of Eq. (2.3), is b_0 and we assume that there is a region of thickness Δ_2 that defines its effective size. We intend to calculate these parameters in a non-ambiguous manner by determining the net solvation force on the spherical particle obtained from the simulations and equating it to the force one would calculate assuming that this solvation force arises from a continuous fluid exerting a hydrostatic pressure. Also note that because we do not have an interaction between the suspended sphere and the wall, the parameters Δ_1 and Δ_2 originate purely from the interactions between the fluid and the wall and the fluid and the suspended particle.

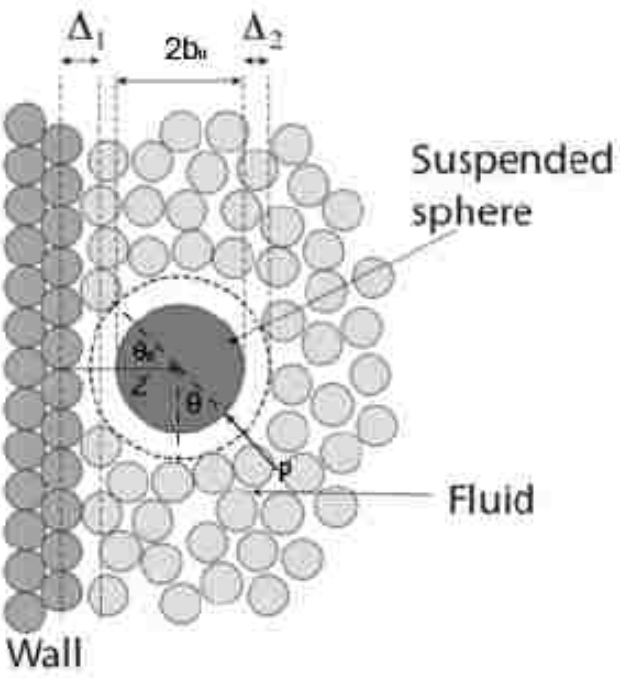

Fig. 2.6. Schematic of the geometry as the sphere approaches the wall.

In the continuum limit, the solvent force on the colloid comes from the hydrostatic pressure, p, that is exerted by the fluid normal to the surface of the suspended particle. In this coordinate system, the net force in the z direction is given by the difference of the force on the right hemisphere minus the force on the left hemisphere. The net forces in the perpendicular directions (x,y) will be zero because of the cylindrical symmetry of the system. As the sphere starts penetrating the wall (Fig. 2.6), the intersection plane can be defined by the angle θ_a with respect to the equatorial plane of the sphere. Our convention is to define θ as positive for the left half of the sphere, and it will be negative if the intersection is on the right half of the sphere.

We assume that the hydrostatic pressure, p, is exerted by the fluid on the suspended particle, the net force is given by the difference of the force on the right hemisphere minus the force exerted by the fluid particles located between the suspended particle and the wall. The area in this case is not necessarily that of the entire left hemisphere because of the region of thickness Δ_1 that is devoid of fluid molecules.

The net force along the *z* direction on the hemisphere on the right side can be calculated by integrating the *z* component of the force exerted by the fluid on the right hemisphere, $-p \sin\theta$, over a circular element of area, $2\pi (d + \Delta_2)^2 \cos\theta\, d\theta$, that is

$$F_{right} = -2\pi p \int_0^{\pi/2} d\theta \left(b_0 + \Delta_2\right)^2 \cos\theta \sin\theta = -\pi p \left(b_0 + \Delta_2\right)^2 \tag{2.8}$$

The corresponding force on the left side of the sphere is

$$F_{left} = 2\pi p \int_{\theta_0}^{\pi/2} d\theta \left(b_0 + \Delta_2\right)^2 \cos\theta \sin\theta = \pi p \left(b_0 + \Delta_2\right)^2 \cos^2\theta_0 = \pi p \left(z - \Delta_1\right)^2, \tag{2.9}$$

where $\cos\theta_0 = (z - \Delta_1)/(d + \Delta_2)$; θ_0 being half the angle subtended at the center of the sphere by the spherical cap defined by the plane at Δ_1. The net force is then

$$F = F_{right} + F_{left} = -p\pi\left[\left(b_0 + \Delta_2\right)^2 - \left(z - \Delta_1\right)^2\right] = p\pi\left[z^2 - 2\Delta_1 z + \Delta_1^2 - \left(b_0 + \Delta_2\right)^2\right]. \tag{2.10}$$

This is a parabolic equation giving the force as a function of the distance between the suspended particle and the wall. As we will see below, the force versus distance curves we obtain from the simulations are approximately parabolic.

2.3 Results and Discussion

Simulations where run for five different sphere sizes with radii b_0/σ = 0, 1, 2, 3, and 4. The case where b_0/σ = 0 corresponds to the "suspended" particle being exactly equivalent to a fluid particle. The remaining cases correspond to an increasingly larger sphere, though the range and energetics of the interactions between the sphere and solvent was maintained fixed. Since the simulation box size is fixed, the number of fluid particles in the box decreases as the sphere size is increases by the algorithm we employed in the set-up. Similarly, as the sphere passes into the wall, the number of fluid particles increases to compensate for the sphere's incomplete presence. Overall, the set-up algorithm we employed kept the solvent pressure (and presumably its density as well) maintained at a fixed value +- 4% (See the Appendix for figures of pressures).

Repulsive Weeks-Chandler-Andersen potential: The first set of simulations we carried out using the repulsive WCA potential of Eqs. (2.1) and (2.3). The z component of the solvation force for d/σ = 0, 1 , 2, 3 , and 4 at temperatures kT/ε = 1.2 and kT/ε = 1.6 are shown in Fig. 2.7. The pressures for these two sets of runs are around σ^3/ε=6.5 and σ^3/ε=8.2. (See the Appendix figures). This figure reports the solvation force ($F\sigma/\varepsilon$) as the sphere is moved toward and through the wall. For the sphere approaching the wall, the force oscillates between positive (repulsive) and negative (attractive) values with a period that is associated with the size of the fluid particles. This phenomena has been noted previously and is associated with discrete layering of the solvent between the colloid and the surface. As the sphere moves through the wall the force becomes

increasingly attractive as predicted by Eq. (2.10). The magnitude of the force is maximally attractive exactly at the point where only the right hemisphere of the suspended sphere is exposed to the fluid. From this point on as the sphere continues to move through the wall the force decreases in magnitude until it is zero at the point where the sphere is no longer exposed to the fluid.

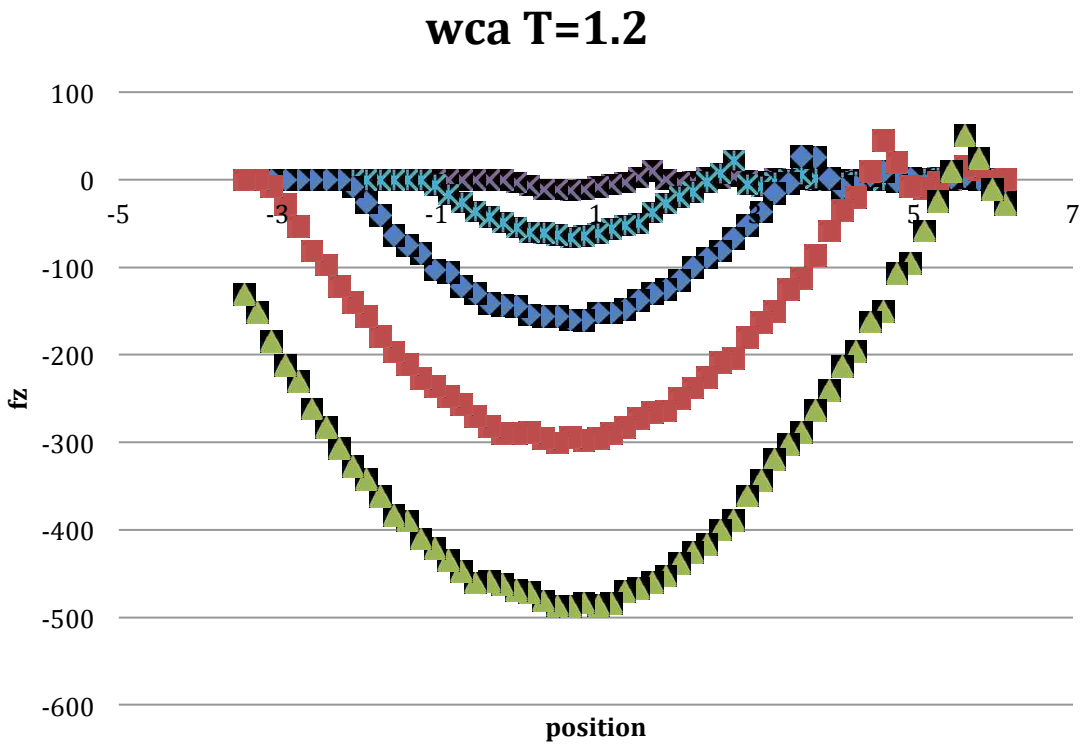

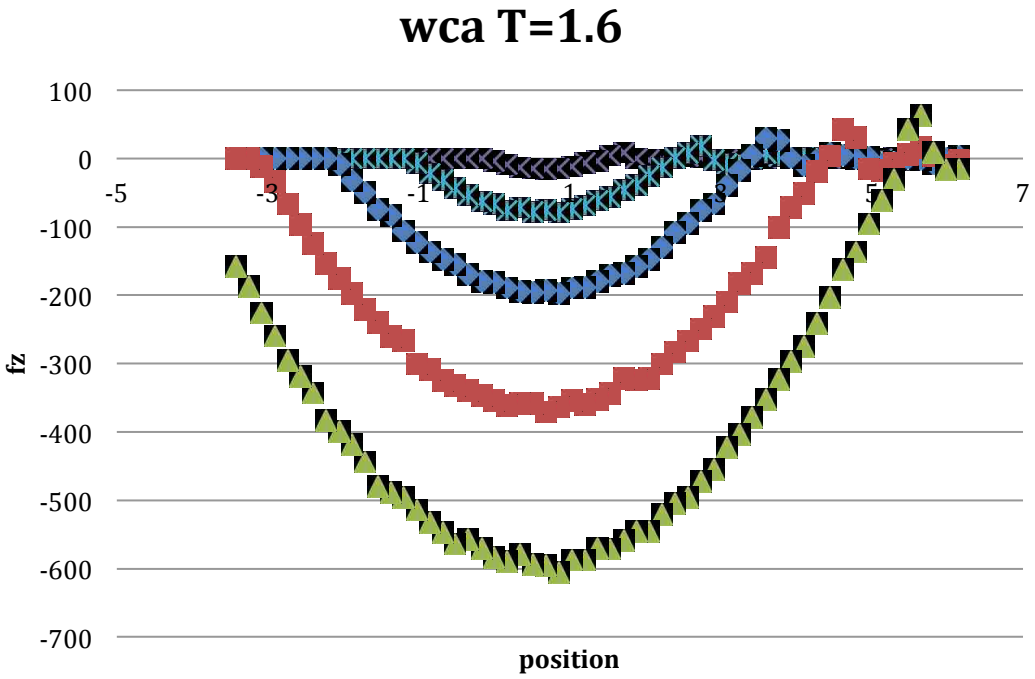

Fig. 2.7. The *z* component of the solvation force. The cross symbols are the force values of colloid $b_0 = 0$, star symbols are the force values of colloid $b_0 = 1$, diamond symbols are the force values of colloid $b_0 = 2$, square symbols are the force values of colloid $b_0 = 3$, triangle symbols are the force values of colloid $b_0 = 4$.

LJ-spline potential: We use the same simulation approach as for the WCA potential to run simulations. The values of the sphere radius are again $b_0 = 0$, 1, 2, 3, and 4 and the temperatures are $kT/\varepsilon = 1.2$ and $kT/\varepsilon = 1.6$. The pressures for these two sets of runs are around $\sigma^3/\varepsilon = 3.2$ and $\sigma^3/\varepsilon = 4.8$. (See the Appendix). Note that P(LJ $kT/\varepsilon = 1.6$) = P(WCA $kT/\varepsilon = 1.2$) which was purposefully done. The results are plotted in Fig. 2.8 and it is seen that they are qualitatively similar to what was we found for the WCA fluid. The most striking difference is that the attractive force is significantly larger in the case

of the WCA potential. This is a result of the pressure in the system being larger in this case. Note differences between this and WCA.

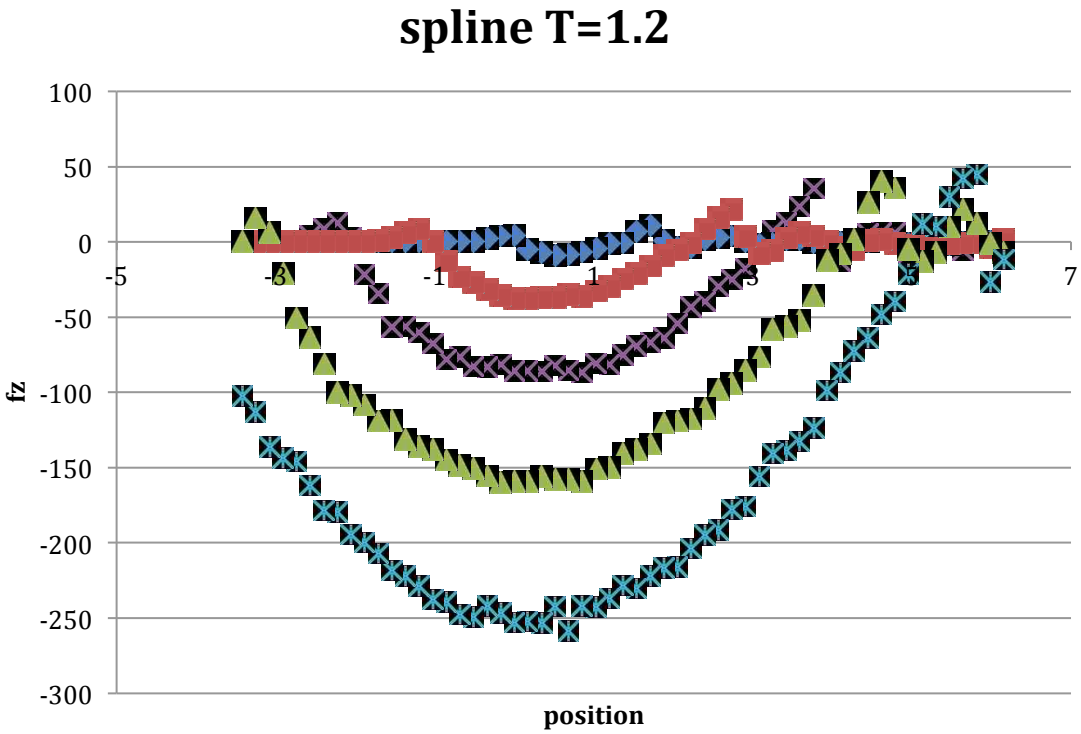

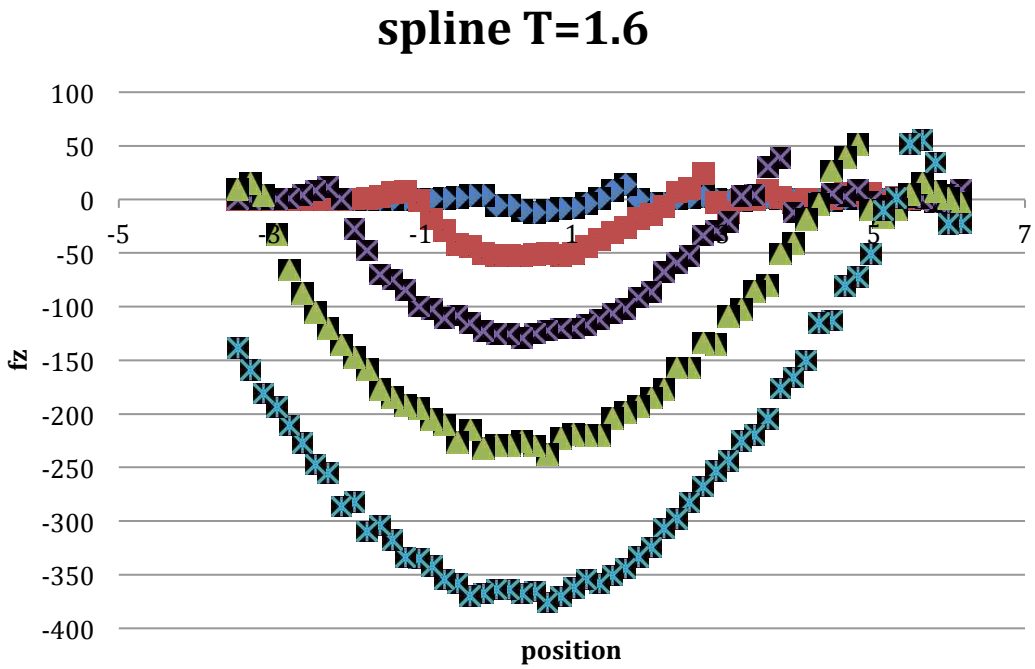

Fig. 2.8. The z component of the solvation force. The diamond symbols are the force values of colloid $b_0 = 0$, square symbols are the force values of colloid $b_0 = 1$, cross symbols are the force values of colloid $b_0 = 2$, triangle symbols are the force values of colloid $b_0 = 3$, star symbols are the force values of colloid $b_0 = 4$.

From Eq.(2.10) we know it is a parabolic equation giving the force as a function of the distance between the suspended particle and the wall. We performed a parabolic fitting to the solvation data we got from the simulations, and extract the Δ1, Δ2 values (See the Appendix for the fittings).

The position parameters Δ_1 and Δ_2 defined in Fig.2.6 can now be obtained by fitting Eq. (2.10) to the part of the data shown in Fig. 2.7 that represents the direct contact between the sphere and the wall. It is clear from Eq. (2.10) that these parameters can be obtained

without explicit knowledge of the pressure p. The parameters obtained for different radii are reported in Tables 2.1 Table 2.2, and plotted in Fig. 2.9.

Table 2.1. Fitted values of Δ_1 and Δ_2 as a function of the hard-core radius b_0 at two different temperatures kT/ε =1.2 and kT/ε =1.6 for a WCA fluid.

WCA	Δ_1	Δ_1	Δ_2	Δ_2
b_0	kT/ε = 1.2	kT/ε = 1.6	kT/ε = 1.2	kT/ε = 1.6
0	0.66	0.66	0.80	0.79
1	0.64	0.62	0.75	0.76
2	0.64	0.63	0.77	0.76
3	0.63	0.63	0.72	0.76
4	0.64	0.63	0.74	0.73

It is noteworthy than in this case the size parameters a roughly independent of the temperature and only decrease slightly as the sphere is increased. Also, it is seen that Δ_2 which is related to the size of the sphere is slightly larger that Δ_1, which is related to the position of the wall. From the definition of these parameters (Fig.2.6) it appears that they are probing similar physics so it is reasonable to assume that the slight difference in their values is related to the curvature of the surface they are associated with.

Table 2.2. Fitted values of Δ_1 and Δ_2 as a function of the hard-core radius b_0 at two different temperatures kT/ε =1.2 and kT/ε =1.6 for a LJ-spline fluid.

LJ-spline	Δ_1	Δ_1	Δ_2	Δ_2
b_0	kT/ε = 1.2	kT/ε = 1.6	kT/ε = 1.2	kT/ε = 1.6
0	0.58	0.61	0.65	0.72
1	0.48	0.56	0.67	0.77
2	0.40	0.48	0.72	0.76
3	0.40	0.47	0.72	0.74
4	0.24	0.37	0.85	0.84

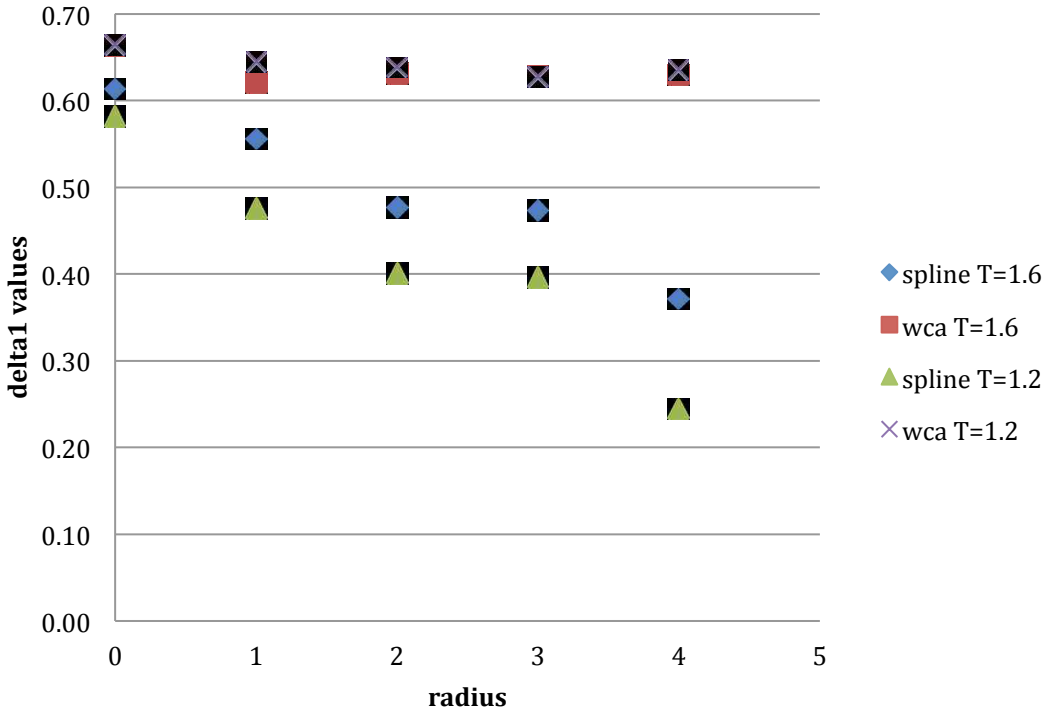

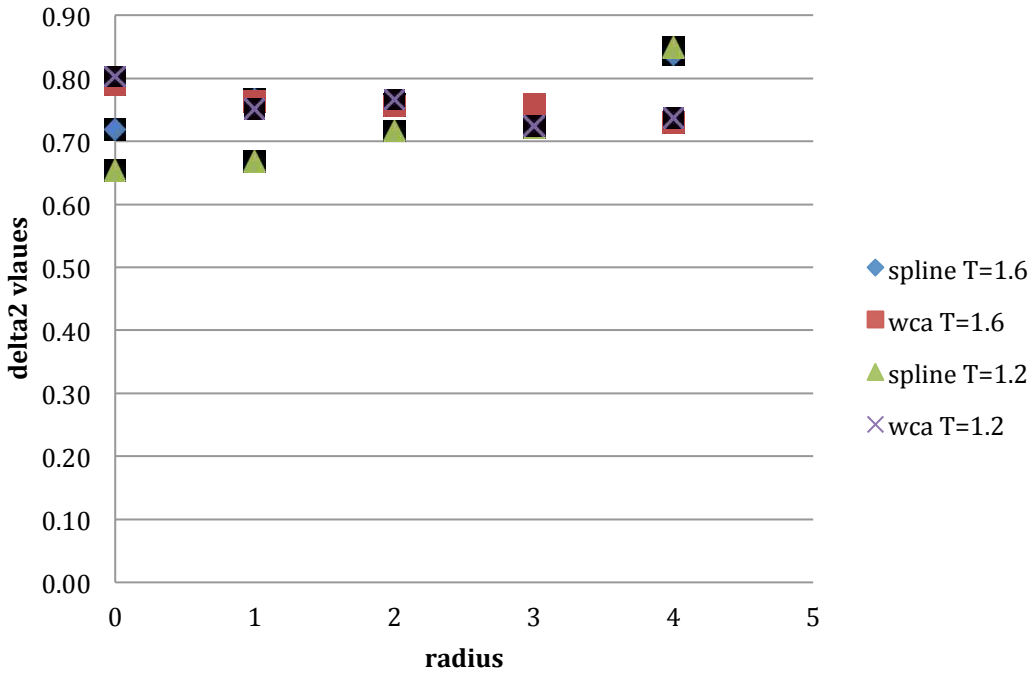

Figure 2.9. Values of Δ_1 and Δ_2 as a function of the hard-core radius b_0 at two different temperatures kT/ε =1.2 and kT/ε =1.6 for both WCA and LJ-spline fluid.

From Table 2.2 we see that Δ_2 is roughly independent of temperature and of the size of the sphere. Furthermore, its values are essentially as for the WCA case. In contrast Δ_1 depends on temperature as well as on the size of the sphere.

The reported values of Δ_1 and Δ_2 where as mentioned obtained from Eq. (2.10) without explicit use of values for the pressure. However, as a consistence check we can also make use of the pressure to estimate Δ_2 by noticing that the maximum attractive force on the sphere is given by

$$F = -p\pi(\Delta_2 + b_0)^2 \,, \tag{2.11}$$

where we have used the notation Δ_2 to distinguish this quantity from Δ_2. Since the minimum force can be obtained from Figs. 2.7 and 2.8 and since the pressure is known we can use Eq. (2.11) to obtained a value for Δ_2. The results are given in Table 2.3 and plotted in Fig. 2.10.

Table 2.3. Δ_2 values obtained using Eq. (11).

b_0	WCA, kT/ε = 1.2	WCA, kT/ε = 1.6	LJ-spline, kT/ε = 1.2	LJ-spline, kT/ε = 1.6
0	0.73	0.76	0.91	0.85
1	0.74	0.72	0.91	0.84
2	0.72	0.73	0.91	0.84
3	0.73	0.71	0.91	0.82
4	0.72	0.73	0.87	0.80

Figure 2.10 shows that Δ_2 is very similar to Δ_2 for both the WCA potential and for the LJ-spline potential.

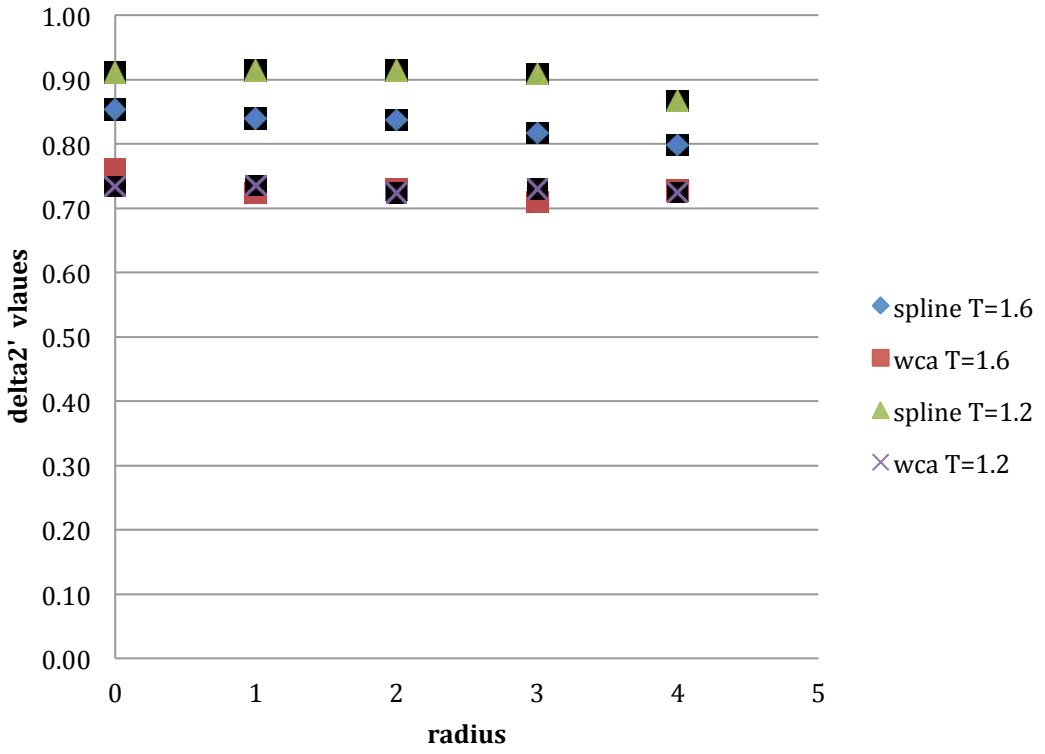

Fig.2.10. Values of Δ_2 as a function of the hard-core radius b_0 at two different temperatures kT/ε =1.2 and kT/ε =1.6 for both WCA and LJ-spline fluid.

In our simulations we noticed that before the sphere pushed out of the fluid, there was a small region the interaction forces became positive (forces pushing to the colloid away from particle walls). These values were smaller than the solvent diameter (1.0σ). Table 2.4 and figure 2.11 show these values.

Table 2.4. Values of distance as a function of the hard-core radius b_0 at two different temperatures kT/ε =1.2 and kT/ε =1.6 for both WCA and LJ-spline fluids.

b_0	WCA, kT/ε = 1.2	WCA, kT/ε = 1.6	LJ-spline, kT/ε = 1.2	LJ-spline, kT/ε = 1.6
0	0.68	0.77	0.51	0.51
1	0.51	0.68	0.77	0.60
2	0.51	0.85	0.77	0.51
3	0.77	0.51	1.03	0.68
4	0.51	0.51	0.68	0.60

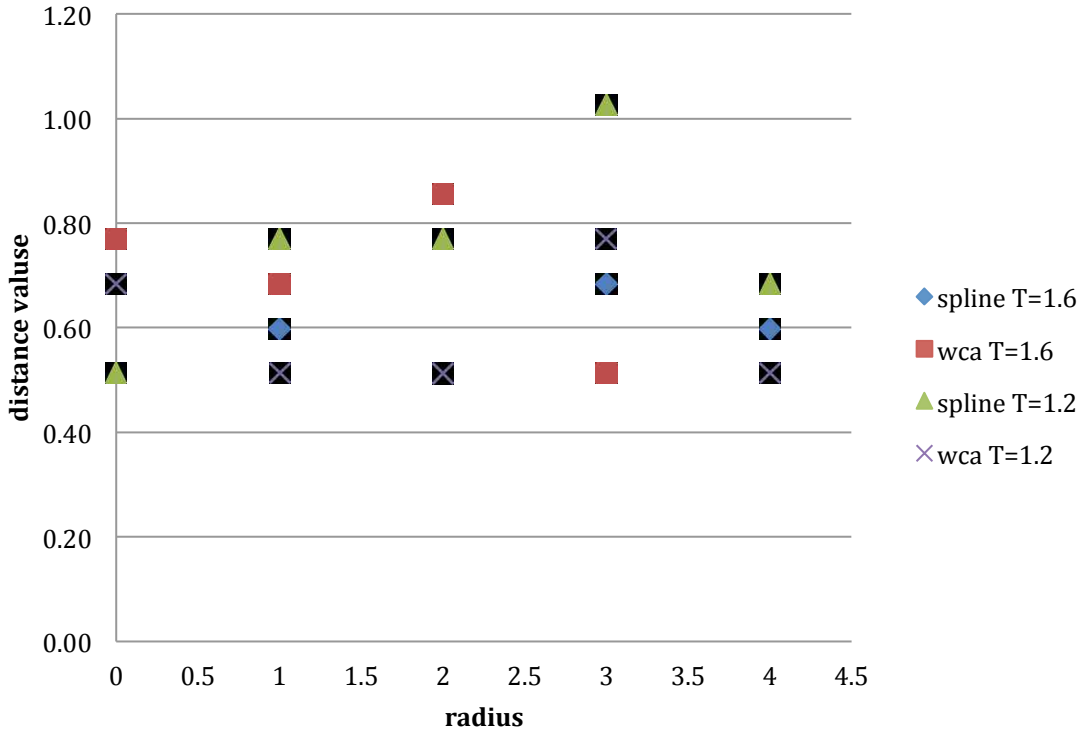

Fig. 2.11. Values of distance as a function of the hard-core radius b_0 at two different temperatures kT/ε =1.2 and kT/ε =1.6 for both WCA and LJ-spline fluids.

2.4 Conclusions

We have used molecular dynamics simulations to investigate the hydrodynamics forces on a sphere embedded in a viscous fluid closed to a solid wall. We have applied two different LJ-type potentials to model the fluid-fluid, fluid-wall, and fluid-sphere interactions. In addition to the purely repulsive WCA potential we have used a LJ-spline potential with a finite-range minimum to model these interactions. We have shown that the obtained force versus distance curves can be captured in a continuum framework that require a reinterpretation of the wall position as well as the sphere size. The effective position of the wall as given by the quantity Δ_1 was shown to depend on the applied potential (WCA or LJ-spline) as well as on, temperature and sphere size. The temperature and size dependence was most pronounced for the softer LJ-spline potential. In contrast we found the effective radius of the sphere, $r=r_0+\Delta_2$, to be remarkably independent of the interaction potential and temperature. We believe that our finds will prove to be useful when making connections between atomic scale simulations and continuum theories should as Brenners' results Eq. (1.2).

In earlier researches, the effective radius of the sphere was usually considered as half the distance where the minimum potential occurs. For LJ type potentials including WCA potential, the minimum occurs at $2^{1/6}\sigma \approx 1.12\sigma$, so the sphere radius was often considered about 0.56σ. While the results in our simulations showed the effective radii were larger then that value. Figure 2.12 shows the schematic of the interaction force and particle positions as the sphere approaches the wall.

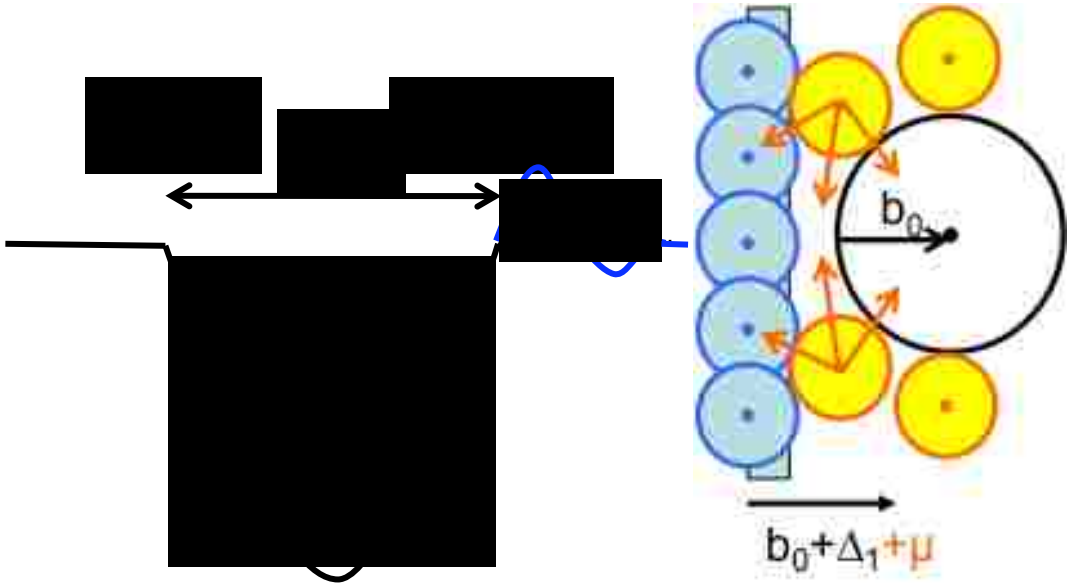

Fig. 2.12. Schematic of the interaction force and geometries of particle positions as the sphere approaches the wall.

The zero net solvent force on colloid requires a balancing force pushing colloid away from wall. From figure 2.11 and table 2.4, it was a small gap (less than solvent diameter) gets this extra tangential force from solvent force to fill the gap. This builds to a positive force (away from wall) when gap is close to solvent diameter and pressure fills the gap. This makes the effective sphere radius larger than the earlier assumed value 0.56σ.

Chapter 3

FRICTION COEFFICIENT AND DIFFUSION COEFFICIENT

In this Chapter, we investigate the friction and diffusion coefficients associated a large smooth sphere moving inside of a viscous fluid. This is a problem with a large history, whose mathematical analysis goes back to Stokes in the middle of the 19th century [Batchelor, p. 229]. For this analysis, one needs to know the sphere radius, the effective solvent viscosity, and the slip / no-slip boundary conditions appropriate for this situation. Previous analyses have assumed values for the radius and taken the effective solvent viscosity to be the same as the equilibrium bulk value [literature refs]. Here, we will use the radius values that have been derived in the previous chapter. As shown there, they include the effects of the discreteness of the fluid molecules and thus, they are different from what has been used in the previous analyses. This will affect our interpretation of the viscosity and boundary conditions, as we will see below.

For this analysis, we construct an atomistic simulation with a large smooth sphere located in the central region of a large box of a viscous Lennard-Jones fluid with periodic boundary conditions. Initially, the sphere will be constrained to move with an initial velocity with respect to the solvent box to establish a quasi-equilibrated flow situation, and then it will be allowed to freely move in that box such that the relative velocities of the particle and the solvent equilibrate. We will use Stokes' Law and the Stokes-Einstein model to analyze the results and calculate the friction coefficient and diffusion coefficient from these trajectories. All simulations reported here are performed with the LAMMPS

package [LAMMPS] for molecular dynamics, and the simulation conditions will be similar to the ones used in the previous chapter.

3.1 Drag and Boundary Conditions

The problem of a sphere slowly moving with a constant velocity in a viscous fluid (Re<<1) is one of the basic problems in hydrodynamics. The primary quantity of our interest is the friction force experienced by the spherical particle that is moving though the fluid with a fixed velocity. According to the Stokes' Law, the slip or no-slip boundary conditions for this flow behavior can be determined by the relation between the friction forces the sphere experiences and the velocity with which the sphere moves.

Stokes' law gives the force acting on a sphere of a radius b_0 moving with a velocity U in a fluid with viscosity μ: (Kohale & Khare)

$$F = -c\pi\mu bU = -\xi U . \qquad (3.1)$$

The coefficient *c* assumes the values of 4 and 6 for slip and no-slip (stick) boundary conditions, respectively. These are the Maxwell and Stokes limits, respectively, that are commonly cited in the literature. The drag coefficient is defined as $\xi = c\pi\mu b$; it depends on both the particle radius and the local viscosity. This quantity is then situation dependent and has units of mass/time. The value of the coefficient *c* in expression (3.1) can be evaluated in several ways. First, it can be evaluated from the friction coefficient, which is obtained by measuring the velocity and mean square displacement of a large (with

respect to the size of the fluid molecules) sphere moving inside a viscous fluid. Secondly, it can be determined by focusing on the behavior of the fluid, specifically, the velocities of each fluid particle.

3.2 Diffusion and Friction Coefficients

From the discussion in 3.1, one of the methods to evaluate the constant c is investigating the Friction Coefficient of the large colloidal sphere, that is, by studying the diffusion of the particle in the fluid.

The simplest model describing the diffusion of a spherical particle in a viscous fluid is the Stokes-Einstein model [REFERENCE], which gives the following mean square displacement of the diffusing particle at large time: (A. Einstein, "Investigations on the Theory of the Brownian Motion" (Dover, New York, 1956) OR R, M, Mazo, "Brownian Motion, Fluctuations, Dynamics and Applications" (Oxford University Press, Oxford, 2002))

$$\left\langle r^2 \right\rangle = 6Dt \tag{3.2}$$

where

$$D = kT/\xi = kT/(c\pi\mu b) \tag{3.3}$$

is the diffusion coefficient (which has the units of mass^2/time).

Because of the hydrodynamic and inter-particle forces, the colloid experiences Brownian motion. We use the averaged velocity square and mean square displacement to describe this phenomenon.

Consider the velocity of the Brownian particle it obeys the Langevin equation: [stochastic processes in physics and chemistry]

$$m\dot{V} = -\xi V + L(t) = -m\gamma V + L(t) \tag{3.4}$$

The last term on the right hand side is the random force exerted by the molecules of the surrounding fluid. Here, γ (the friction coefficient) is defined as ksi/m and has units of 1/time. This is the friction coefficient and is seen to play the role of fundamental time decay constant for the system. $L(t)$ acts as an random fluctuation force, which is caused by the collisions of the individual molecules of the surrounding fluid and varies rapidly and randomly as a function of time This is expressed by the postulate for its autocorrelation function $\langle L(t)L(t')\rangle = \Gamma\delta(t-t')$, where Γ is a constant. Its average vanishes, $\langle L(t)\rangle = 0$. If the initial velocity is $V(0) = V_0$, then equations (3.4) can be solved explicitly:

$$V(t) = V_0 e^{-\gamma t} + \frac{e^{-\gamma t}}{m}\int_0^t e^{\gamma t'} L(t')dt. \tag{3.5}$$

We average (?) this equation over a sub ensemble of Brownian particles all having the same initial V_0. Since $\langle L(t)\rangle = 0$, and $L(t')$ for $t' > t$ is independent of V_0, we have

$$\langle V(t)\rangle_{V_0} = V_0 e^{-\gamma t}. \tag{3.6}$$

After squaring we abtain:

$$\left\langle \left\{V(t)\right\}^2 \right\rangle_{V_0} = V_0^2 e^{-2\gamma t} + \frac{\Gamma}{2\gamma m^2}\left(1 - e^{-2\gamma t}\right). \tag{3.7}$$

The constant Γ can be identified by invoking the fact that for $t \to \infty$ the mean square velocity must have the known thermal value namely

$$\left\langle \left\{V(\infty)\right\}^2 \right\rangle = \frac{\Gamma}{2\gamma m^2} = \frac{3kT}{m}. \tag{3.8}$$

Thus, we can get the expression for the averaged squared velocity:

$$\left\langle V^2 \right\rangle = \left(V_0^2 - \frac{3kT}{m} \right) e^{-2\gamma t} + \frac{3kT}{m}. \tag{3.9}$$

Using a similar argument we can get the mean square displacement

$$\begin{aligned} \left\langle \left[r(t) - r(0)\right]^2 \right\rangle &= \left[V_0^2 - \frac{3KT}{m} \right] \left[\frac{1 - \mathrm{e}^{(-\gamma t)}}{\gamma} \right]^2 + \frac{6KT}{m\gamma} \left[t - \frac{1 - \mathrm{e}^{(-\gamma t)}}{\gamma} \right] \\ &= \left[V_0^2 - \frac{3KT}{m} \right] \frac{1}{\gamma^2} \left[1 - 2\,\mathrm{e}^{(-\gamma t)} + \mathrm{e}^{(-\gamma t)} \right] + \frac{6KT}{m} \frac{1}{\gamma^2} \left[\gamma t - 1 + \mathrm{e}^{(-\gamma t)} \right] \end{aligned} \tag{3.10}$$

For $\gamma t \geq 1$, the exponential is negligibly small (for $\gamma t \geq 5$ which means exp ($-\gamma t$) ≤ 0.01), yielding:

$$\left\langle \left[r(t) - r(0)\right]^2 \right\rangle \approx \left[V_0^2 - \frac{3kT}{m} \right] \frac{1}{\gamma^2} + \frac{6kT}{m} \frac{1}{\gamma^2} \left[\gamma t - 1 \right], \tag{3.11}$$

$$\left\langle \left[r(t) - r(0)\right]^2 \right\rangle \approx \left[V_0^2 - \frac{9kT}{m} \right] \frac{1}{\gamma^2} + \frac{6kT}{m\gamma} t. \tag{3.12}$$

Hence, at longer times one should observe linear behavior with a slope of $6kT / m\gamma = 6D$, and an intercept given by the first term.

In each simulation, we note down the velocity and displacement of the colloid particle, and calculate the squared velocity and mean square displacement. After that, use equation (3.9) and (3.10) to do a nonlinear least squares fit to get the value of the friction coefficient γ. This method works better for the large time intervals (100<t/ $\sigma\sqrt{m/\epsilon}$<300).

A second way to calculate the friction coefficient is to focus on the fluid particle behavior. Since the colloid is moving inside the fluid, Newton's Second Law gives

$$m_f \frac{dv_f}{dt} = \xi(v_c - v_f) \tag{3.13}$$

where ξ is the drag constant. From the discussion above, we can conclude that $\gamma = \xi / m$, so equation (3.13) can be written as

$$\frac{dv_f}{(v_c - v_f)} = \frac{\xi}{m_f} dt, \tag{3.14}$$

where m_f is the mass of the fluid particles. Let $\alpha = \xi / m_f = \gamma m / m_f$, equation (3.14) can be solved and we get

$v_c - v_f = v_{c(0)} e^{(-\alpha t)}$.

In the simulations reported here, before t = 100, the colloid moves at a constant velocity, so that,

$$v_f = v_{c(0)}[1 - e^{(-\alpha t)}], \tag{3.15}$$

From the same simulations, we note down the velocities of each fluid particle, using the data from the beginning short time period (0<t/ $\sigma\sqrt{m/\epsilon}$<100) and equation (3.15), we get another way to calculate the friction coefficient γ.

3.3 Simulation Method

All simulations reported here were performed with the LAMMPS package for molecular dynamics.

For the fluid-fluid interaction potentials, we used two different variations of the Lennard-Jones (LJ) potentials. In order to study the effect of attractive forces we use a modified version of the Lennard-Jones potential. It is the same LJ-Spline potential we discussed in Chapter 2.1. Then we used the well-known repulsive WCA potential to redo the same simulations and compare the results.

The simulation box size is L/σ=27.3596 in all 3 directions, with periodic boundary conditions. The mass of the colloid particle is 200, the core radius changes from b_0/σ=0 (a marked fluid particle) to b_0/σ=3. The mass of fluid particle is set to be 1. The fluid particles were initiated in a FCC crystal structure with a lattice constant 1.094σ corresponding to a typical liquid argon volume density of $\rho\sigma^3$=0.8. The initial temperature of the system is set at $kT/\varepsilon = 3$ and the system is left to thermalize. After the system is thermalized, the colloid particle starts to move at $v = 1.4\,\tau/\sigma$ without any force exerted on it, during the time interval $t = 0\ \sigma\sqrt{m/\epsilon}$ and $t = 100\ \sigma\sqrt{m/\epsilon}$. After $t = 100\ \sigma\sqrt{m/\epsilon}$, the colloid particle starts to experience the hydrodynamic and inter-particle forces. For each simulation case (the colloid has a different radius), the simulation was repeated for 30 time with different initial random thermal velocities, to get the averaged value of the mean square displacement and averaged velocity square. The value of

friction coefficient was then valued from the fitting of the averaged velocity square and mean square displacement of the colloid.

3.4 Data Analysis

In Section 3.2, we discussed the analytical solution of the mean square displacement and the velocity squares. In our systems, once the large colloid starts to move at a fixed velocity with respect to the fixed box frame, the fluid also begins to pick up a velocity by the drag interaction. Thus, the center of mass of the system also acquires a net velocity. In order to use the equations in Section 3.2, after each simulation, we let LAMMP dumps the positions and velocities of all the fluid particles at every time step, thus, the velocity and displacement of the mass center can be calculated. Then, the relative velocity of the colloid to the fluid and relative displacement of the colloid to the fluid can be obtained. These relative velocity and relative displacement are the data that can be fit to equation (3.9) and equation (3.12). Examples of data are shown in **Figure 3.1** and **Figure 3.2**. From the figures we can see that in both cases there are oscillations and a lot of noises and in early stage the fit is not very good. In order to have a better way to get more accurate fitting data, we tried different ways fitting methods as talked in the next section.

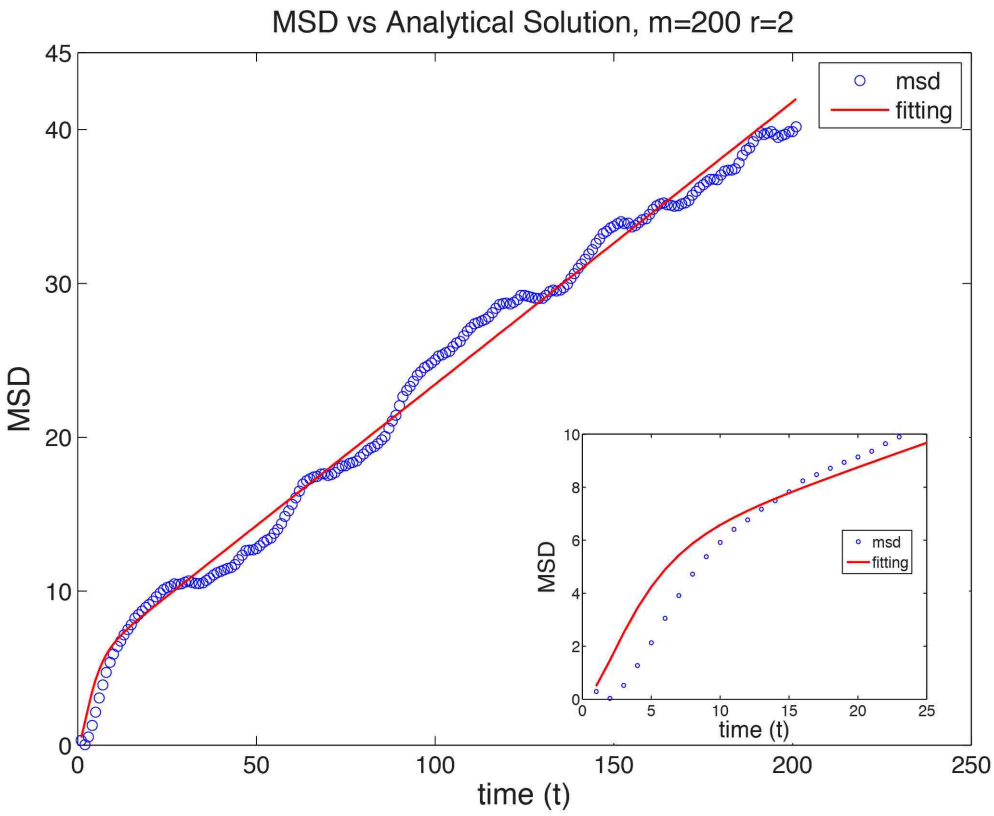

Figure 3.1 Mean Square Displacement and the Analytical Solutions of colloidal sphere with mass=200 and core radius=2. The simulation potential is LJ-Spline potential.

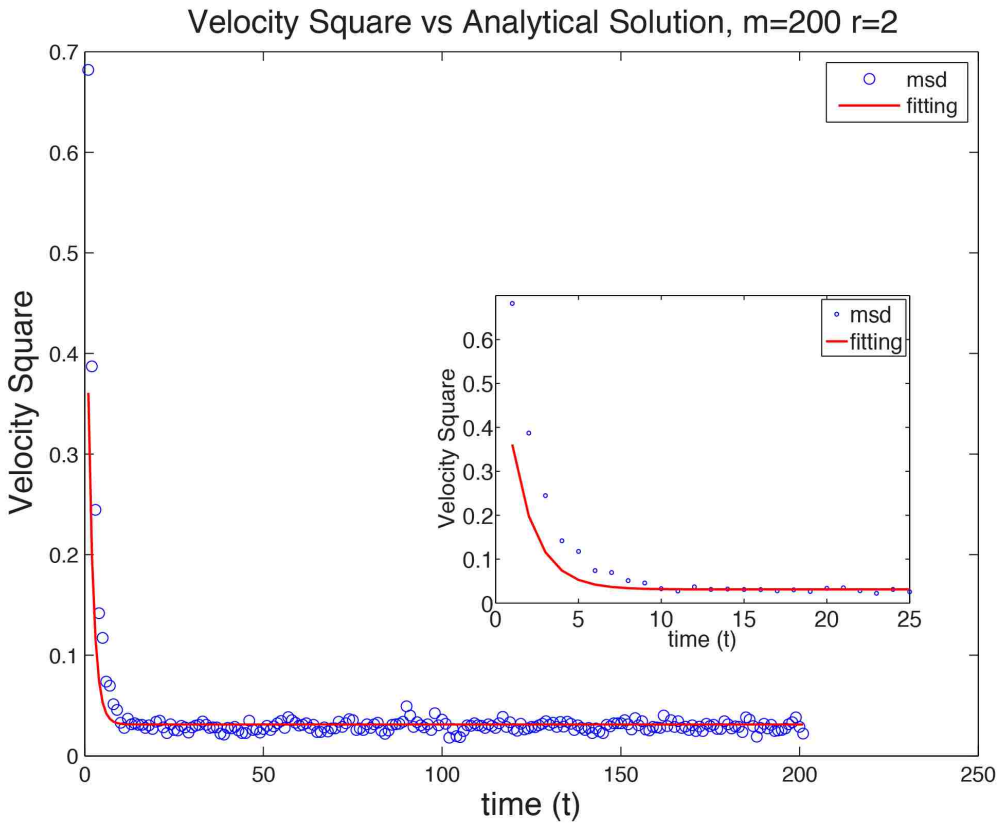

Figure 3.2 Velocity Square and the Analytical Solutions of colloidal sphere with mass=200 and core radius=2. The simulation potential is LJ-Spline potential.

3.5 Fitting Method

3.5.1 Friction Coefficient From Both Velocity and Displacement

First, we fit the velocity data at late times to get an accurate value for T from equation (3.9). Second, fit the diffusion data at late times to get an accurate value for the linear slope. Then turn that into a value for γ using the value of T from step 1 and the slope from equation (3.12). From the sample data **Figure 3.1**, we can tell, just as equation (3.12)

described that in "later times" we observe linear behavior with a slope of $6kT / m\gamma = 6D$. Because "late times" is somewhat subjective, redefine late times rigorously as $\gamma t \geq 5$ using γ from step 2, and redo steps 1 and 2 appropriately so that the analysis is self-consistent.

The following are the results we get from the fittings.

Table 3.1 Fitted values of T and γ as a function of "real" radius $b_0+\Delta_2$ and mass.

WCA

m	$b_0+\Delta_2$	T fit	γ
100	2+0.76	2.27	0.98
200	2+0.76	2.20	0.42
300	2+0.76	2.21	0.20
200	0+0.76	2.04	0.05
200	1+0.76	2.12	0.21
200	2+0.76	2.20	0.42
200	3+0.76	2.32	0.67

Table 3.2 Fitted values of T and γ as a function of the "real" radius $b_0+\Delta_2$ and mass.

LJ-spline

m	$b_0+\Delta_2$	T fit	γ
100	2+0.76	1.97	0.86
200	2+0.76	1.90	0.34
300	2+0.76	1.95	0.22
200	0+0.76	1.87	0.06
200	1+0.76	1.84	0.27
200	2+0.76	1.90	0.34
200	3+0.76	2.05	0.71

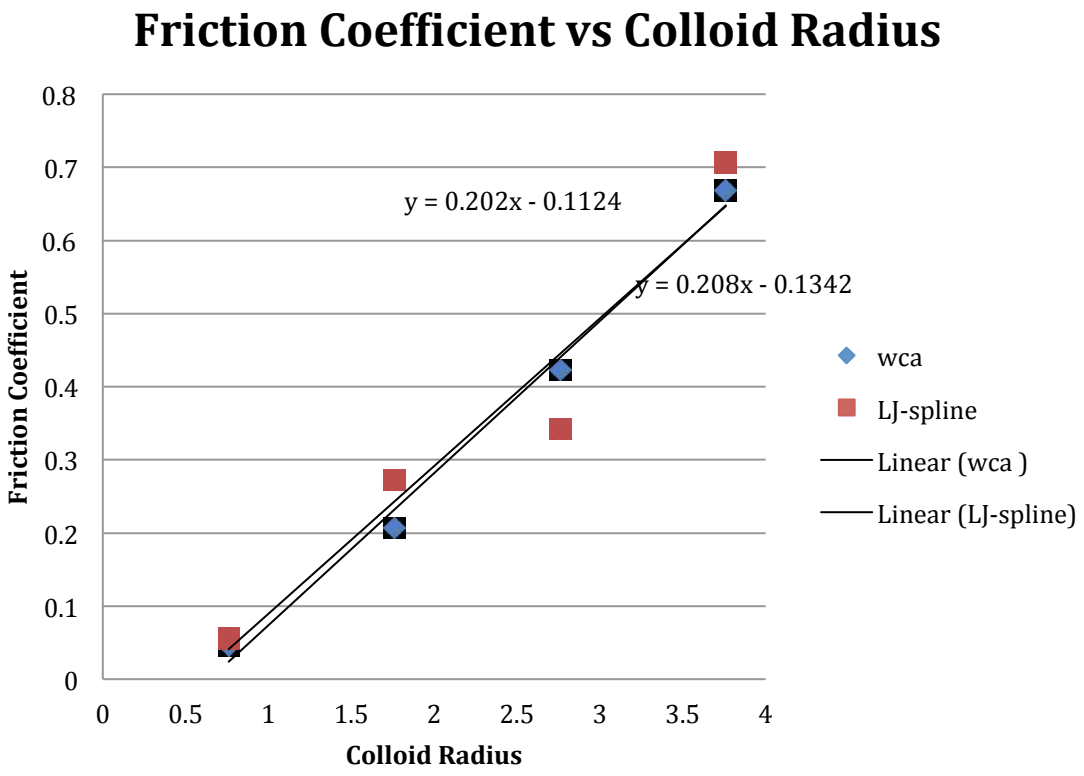

Figure 3.3 Fitted values of γ as a function of hard-core radius for both WCA and LJ-spline fluid. The mass of the colloid is 200. The interception is not zero but near zero. The slope of the line should be cπμ/m.

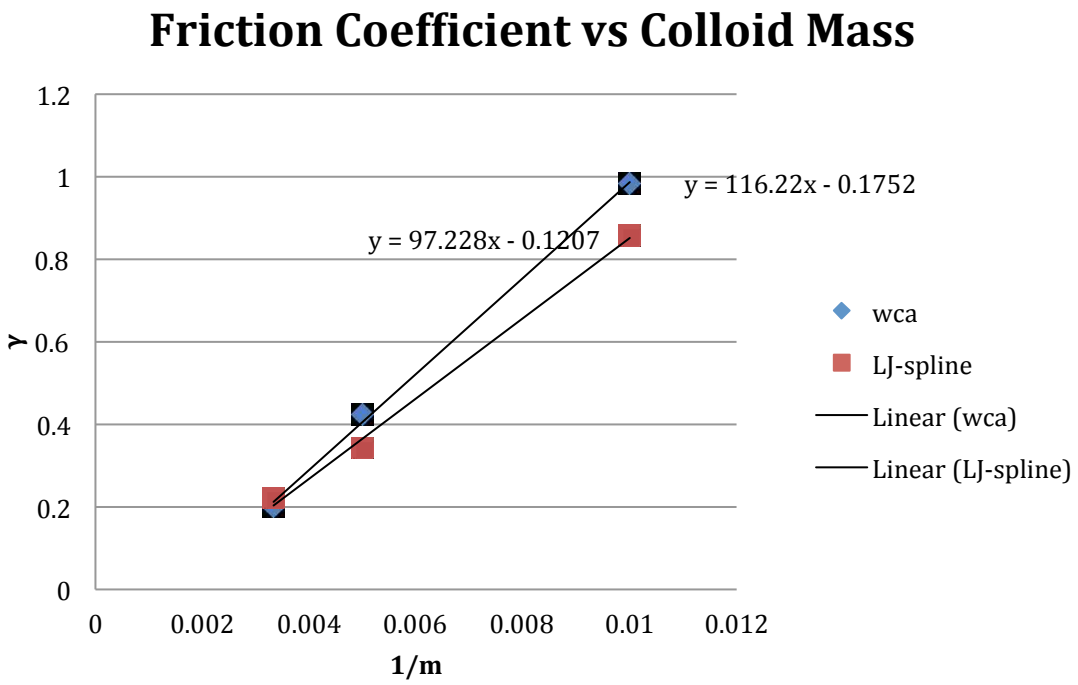

Figure 3.4 Fitted values of γ as a function of 1/ mass for both WCA and LJ-spline fluid. The intercept is very near zero, and the slope should be cπμr based on equation 3.3.

3.5.2 Friction Coefficient From Self-Correlation Function

Equation 3.2 and 3.3 show the relations between mean square displacement and the friction coefficient. We calculated the self-correlation function of the mean square displacement.

$$\left\langle \left[r(t) - r(t+\Delta t) \right]^2 \right\rangle = \int_t^{t+\Delta t} dt' dt'' \left\langle v(t') v(t'') \right\rangle = \frac{1}{N} \sum_{i=1}^{N} r_i r_{i+n} \tag{3.16}$$

According to the equipartition theorem,

$$\frac{1}{2} m \left\langle v(t) v(t) \right\rangle = \frac{3}{2} k_B T ,$$

thus

$$\left\langle v(t)v(t^{'})\right\rangle = \frac{3k_BT}{m}\exp\left(-\frac{\xi}{m}\left|t-t^{'}\right|\right).$$

Then equation 3.16 can be written as:

$$\begin{aligned}\left\langle\left[r(t)-r(t+\Delta t)\right]^2\right\rangle &= \frac{3k_BT}{m}\int_t^{t+\Delta t} dt^{'}\,dt^{''}\exp\left[-\frac{\xi}{m}\left|t^{'}-t^{''}\right|\right] \\ &= 2\cdot\frac{3k_BT}{m}\int_0^{\Delta t}(\Delta t-t^{'''})\exp\left[-\frac{\xi}{m}\left|t^{'''}\right|\right] \\ &= 6D\Delta t-\frac{6Dm}{\xi}\left(1-\exp(-\frac{\xi}{m}\Delta t)\right)\end{aligned} \tag{3.17}$$

with $\tau \equiv m/\xi$ and $\Delta t >> \tau$

$$\left\langle\left[r(t)-r(t+\Delta t)\right]^2\right\rangle \approx 6D\Delta t \tag{3.18}$$

that is the same result as equation 3.2 shows.

Once we get the slope of the fitting, from equation 3.2, the friction coefficient can be calculated from the slop. **Figure 3.5** and **Figure 3.6** show the example data of the simulation where the colloid mass is 200, radius is 2, and the LJ-Spline was used for the simulation. Just as we mentioned in section 3.4, in figure 3.5, the data are noisy to get a clear slope from it. When we tried the self-correlation function of it, we can tell from figure 3.6, the data are much more smoother, and we can calculate the slope from it.

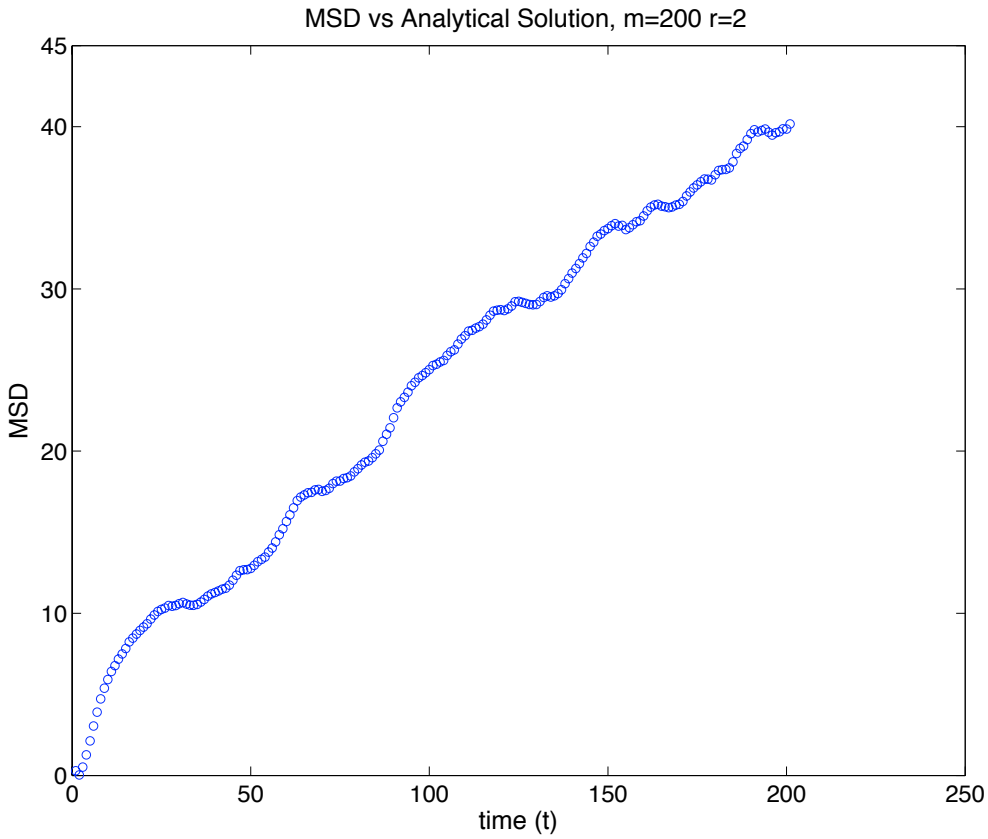

Figure 3.5 Mean Square Displacement data of the colloidal particle with mass=200 and radius=2.

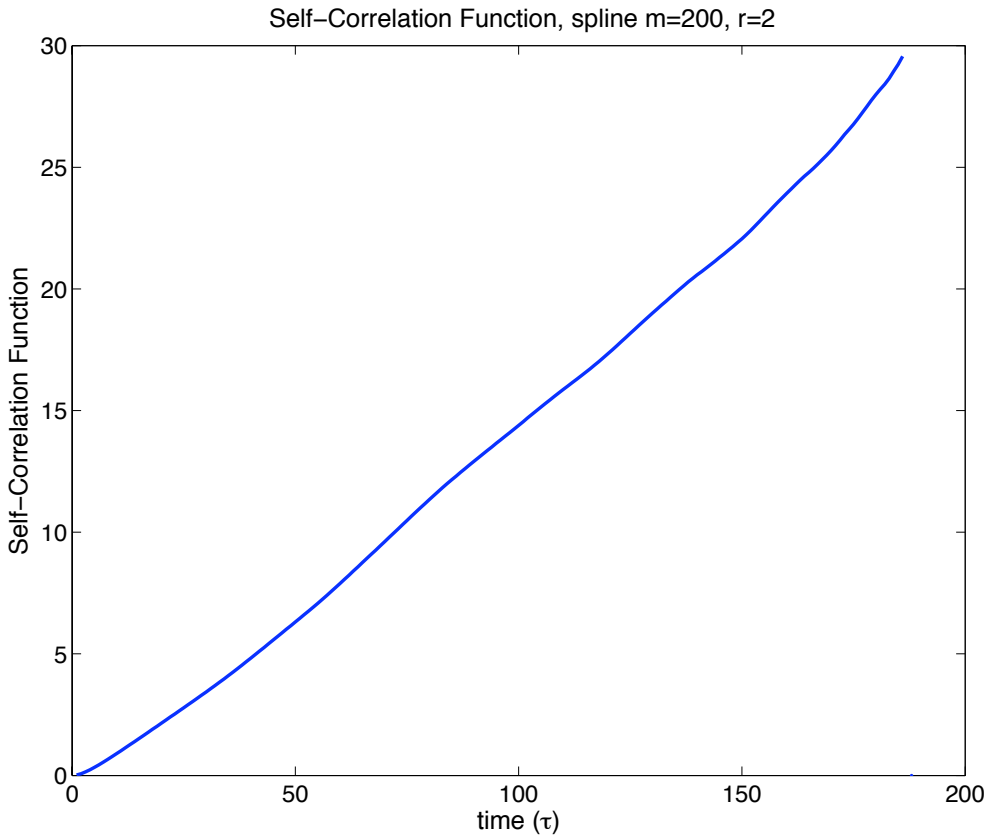

Figure 3.6 Self-Correlation Function of displacement for the same colloidal particle.

The following are the results we get from the fittings.

Table 3.3 Fitted values of T and γ as a function of the "real" radius $b_0+\Delta_2$ and mass.

WCA

m	$b_0+\Delta_2$	slope	γ
100	2+0.76	0.17	0.80
200	2+0.76	0.16	0.43
300	2+0.76	0.17	0.27
200	0+0.76	0.88	0.07
200	1+0.76	0.30	0.22
200	2+0.76	0.16	0.43
200	3+0.76	0.10	0.68

Table 3.4 Fitted values of T and γ as a function of the "real" radius $b_0+\Delta_2$ and mass.

LJ-spline

m	$b_0+\Delta_2$	slope	γ
100	2+0.76	0.14	0.88
200	2+0.76	0.15	0.40
300	2+0.76	0.16	0.25
200	0+0.76	0.73	0.07
200	1+0.76	0.22	0.26
200	2+0.76	0.15	0.40
200	3+0.76	0.08	0.73

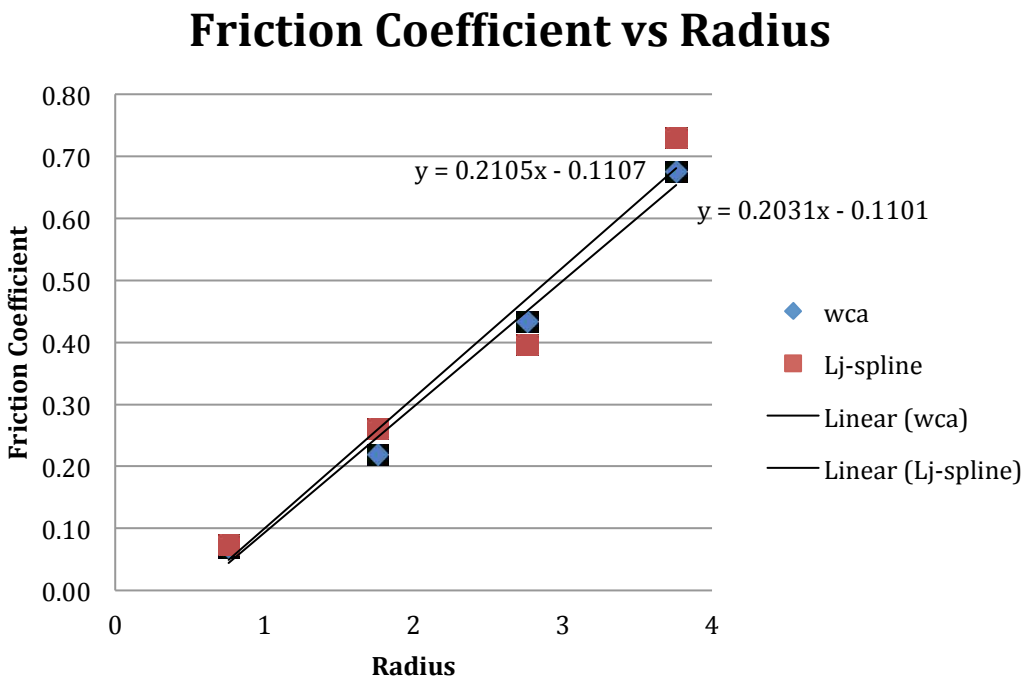

Figure 3.7 Fitted values of γ as a function of colloid radius for both WCA and LJ-spline fluid. The interception is not zero but near zero. The slope of the line should be $c\pi\mu/m$.

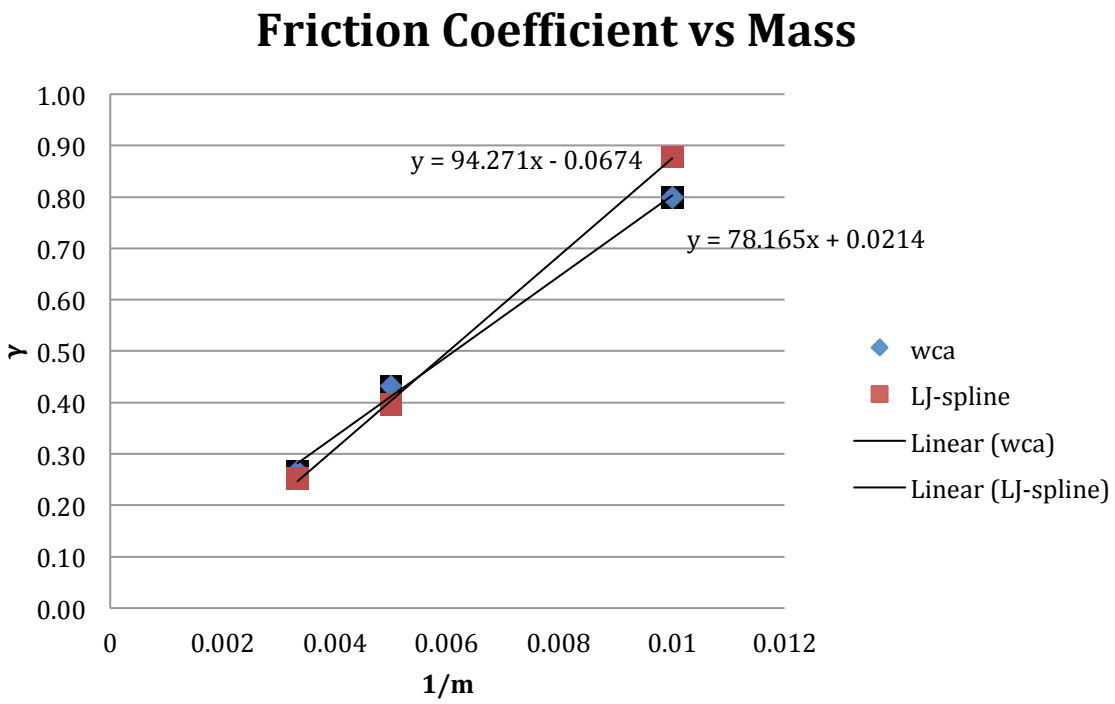

Figure 3.8 Fitted values of γ as a function of 1/ mass for both WCA and LJ-spline fluid. Add linear fit. The intercept is very near zero, and the slope should be cπμr.

3.5.3 Friction Coefficient From The Fluid

In section 3.2, we also missioned, from the same simulations, instead of focusing on the colloidal sphere, we note down the velocities of each fluid particle, using the data from the beginning short time period ($0<t/\sigma\sqrt{m/\epsilon}<100$) and equation (3.15), we get another way to calculate the friction coefficient γ.

The following are the results using this way to simulate the friction coefficients.

Table 3.5 Fitted values of γ as a function of the "real" radius b_0 and fixed mass.

m	$b_0+\Delta_2$	γ (LJ-spline)	γ (WCA)
200	0+0.76	0.07	0.07
200	1+0.76	0.22	0.20
200	2+0.76	0.39	0.36
200	3+0.76	0.59	0.55

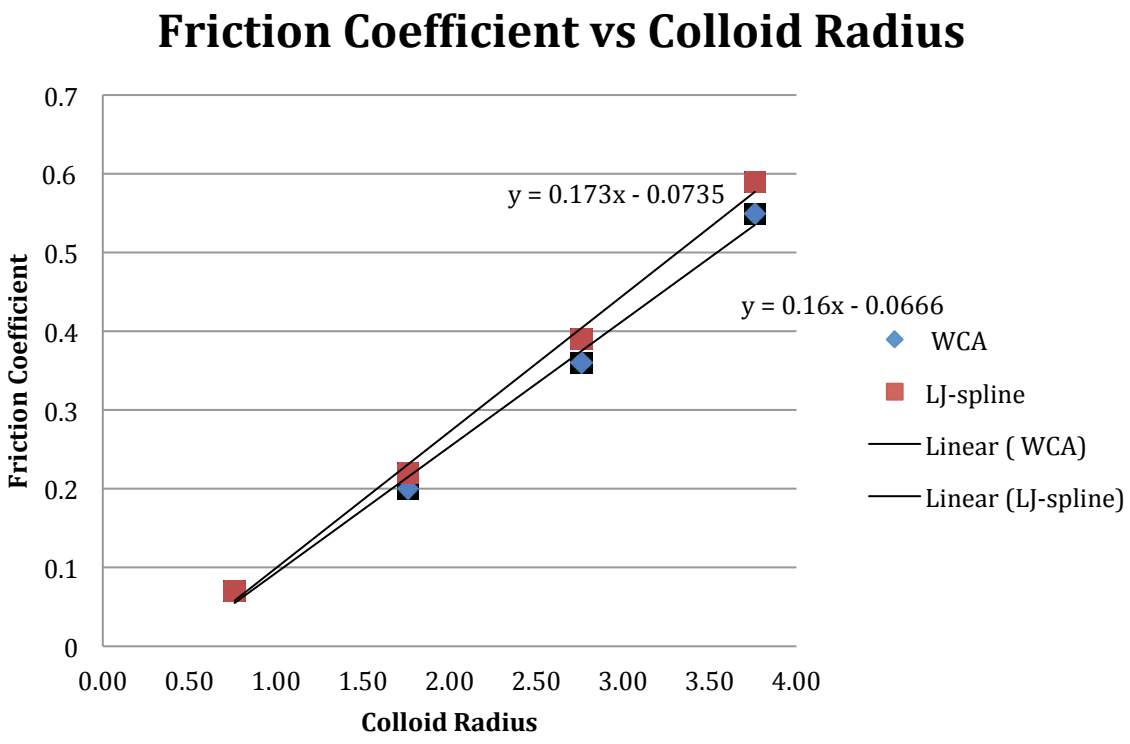

Figure 3.9 Fitted values of γ as a function of colloid radius for both WCA and LJ-spline fluid. The interception is very near zero. The slope of the line should be cπμ/m.

3.6 Viscosity

LAMMPS gives several ways to simulate the viscosity of a fluid, in our work we perform a reverse non-equilibrium MD simulation, which implements the rNEMD algorithm of Muller-Plathe [Muller99]. Momentum in one dimension is swapped between atoms in two different layers of the simulation box in a different dimension. This induces a velocity gradient which can be monitored by LAMMPS, which tallies the cummulative momentum transfer that it performs. Figure 3.6 shows the viscosity model we used in our simulations.

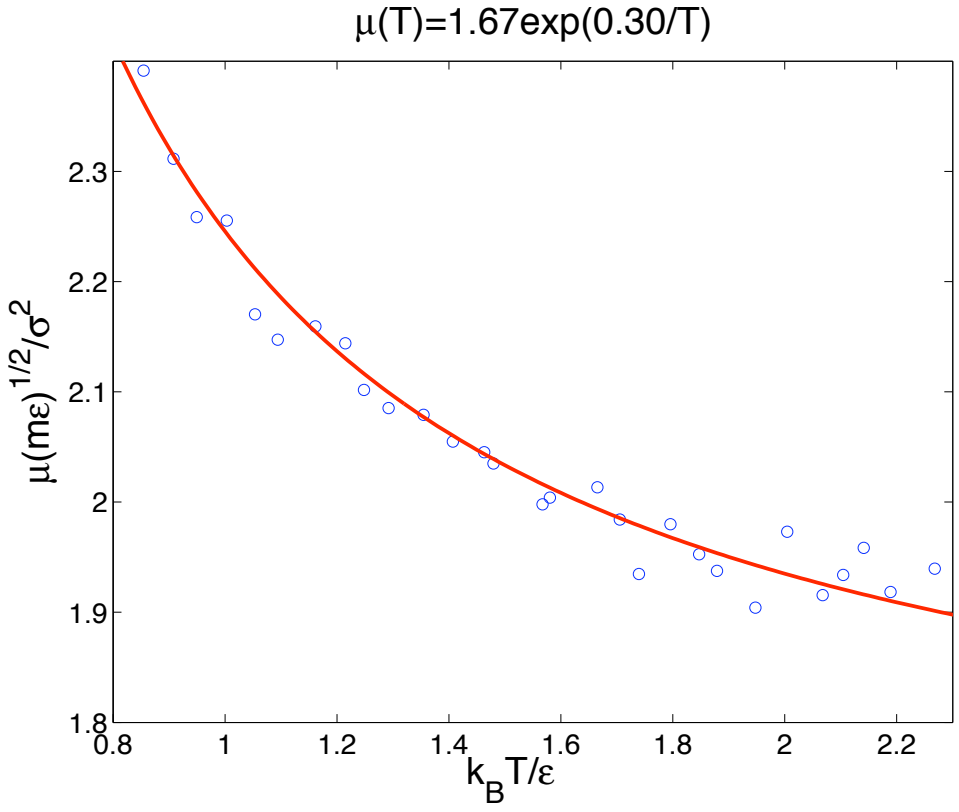

Figure 3.10 Viscosity model using the algorithm of Muller-Plathe.

3.7 Results and Discussion

3.7.1 Results

From these results, we can consider to two major alternative approaches interpret the data. The first approach follows the more conventional method of interpretation which is to assume that the value of the viscosity can be taken as the bulk equilibrium value, and one then derives values for c which would depend upon the value for the radius. We will also examine a second approach where we assume that c must be equal to 4, because the colloid particle is smooth and there is no inherent mechanism to create stick (partial or complete) with respect to the solvent. [Supporting evidence for this model will be presented in the next chapter.] With that assumption, one then derives a value for the viscosity as a function of the radius.

From the first model we can calculate the coefficient c in equation 3.1. Since

$$F = c\pi\mu b \tag{3.19}$$

which means

$$m\gamma = c\pi\mu b \tag{3.20}$$

$$c = \frac{m\gamma}{\pi\mu b} \tag{3.21}$$

The coefficient c assumes the values of 4 and 6 for slip and no-slip (stick) boundary conditions respectively.

The following tables show the c value from our friction coefficient γ. In order to make the radius of the colloidal particle more accurate, we use the value of (b_0+Δ_2) that was determined in Chapter 2 as the core radius of the colloidal particle.

Table 3.6 c values from the velocity and displacement fitting (section 3.5.1).

WCA

m	b_0	γ	Δ2	μ	c
100	2	0.98	0.76	1.91	5.93
200	2	0.42	0.76	1.91	5.08
300	2	0.2	0.76	1.91	3.63
200	0	0.05	0.76	1.93	2.17
200	1	0.21	0.76	1.92	3.96
200	2	0.42	0.76	1.91	5.08
200	3	0.67	0.76	1.90	5.97

LJ-spline

m	b_0	γ	Δ2	μ	c
100	2	0.86	0.76	1.94	5.11
200	2	0.34	0.76	1.94	4.04
300	2	0.22	0.76	1.94	3.92
200	0	0.06	0.76	1.97	2.55
200	1	0.27	0.76	1.96	4.99
200	2	0.34	0.76	1.94	4.04
200	3	0.71	0.76	1.93	6.22

Table 3.7 c value from the fittings of self-correlation function of the MSD (section 3.5.2).

WCA

m	b_0	γ	Δ2	μ	c
100	2	0.8	0.76	1.91	4.84
200	2	0.43	0.76	1.91	5.20
300	2	0.27	0.76	1.91	4.90

200	0	0.07	0.76	1.93	3.03
200	1	0.22	0.76	1.92	4.15
200	2	0.43	0.76	1.91	5.20
200	3	0.68	0.76	1.90	6.06

LJ-spline

m	b_0	γ	Δ2	μ	c
100	2	0.88	0.76	1.94	5.23
200	2	0.4	0.76	1.94	4.75
300	2	0.25	0.76	1.94	4.45
200	0	0.07	0.76	1.97	2.97
200	1	0.26	0.76	1.96	4.81
200	2	0.4	0.76	1.94	4.75
200	3	0.73	0.76	1.93	6.39

Table 3.8 c values from fitting of the fluid particles (section 3.5.3).

fluid

m	b_0	γ (WCA)	Δ_2	μ	c
200	0	0.07	0.76	1.93	3.03
200	1	0.2	0.76	1.92	3.77
200	2	0.36	0.76	1.91	4.35
200	3	0.55	0.76	1.90	4.90

m	b_0	γ (LJ-spline)	Δ_2	μ	c
200	0	0.07	0.76	1.97	2.97
200	1	0.22	0.76	1.96	4.07
200	2	0.39	0.76	1.94	4.63
200	3	0.59	0.76	1.93	5.17

The problem with these results is that the values of c are very scattered and can be outside the accepted bounds. Consequently, we consider an alternative analysis where we assume a fixed value of c = 4 and determine what the value of viscosity would be under that assumption.

The corresponding results are shown in **Table 3.9**, **Table 3.10** and **Table 3.11**.

Table 3.9 Viscosity values from the velocity and displacement fitting with fixed c. (section 3.5.1).

WCA

m	b_0	γ	Δ2	c	μ
100	2	0.98	0.76	4.00	2.83
200	2	0.42	0.76	4.00	2.42
300	2	0.2	0.76	4.00	1.73
200	0	0.05	0.76	4.00	1.05
200	1	0.21	0.76	4.00	1.90
200	2	0.42	0.76	4.00	2.42
200	3	0.67	0.76	4.00	2.84

LJ-spline

m	b_0	γ	Δ2	c	μ
100	2	0.86	0.76	4.00	2.48
200	2	0.34	0.76	4.00	1.96
300	2	0.22	0.76	4.00	1.90
200	0	0.06	0.76	4.00	1.26
200	1	0.27	0.76	4.00	2.44
200	2	0.34	0.76	4.00	1.96
200	3	0.71	0.76	4.00	3.01

Table 3.10 Viscosity values from the fittings of self-correlation function of the MSD with fixed c. (section 3.5.2).

WCA

m	b_0	γ	Δ2	c	μ
100	2	0.8	0.76	4.00	2.31
200	2	0.43	0.76	4.00	2.48
300	2	0.27	0.76	4.00	2.34
200	0	0.07	0.76	4.00	1.47
200	1	0.22	0.76	4.00	1.99
200	2	0.43	0.76	4.00	2.48

200	3	0.68	0.76	4.00	2.88

LJ-spline

m	b_0	γ	Δ2	c	μ
100	2	0.88	0.76	4.00	2.54
200	2	0.4	0.76	4.00	2.31
300	2	0.25	0.76	4.00	2.16
200	0	0.07	0.76	4.00	1.47
200	1	0.26	0.76	4.00	2.35
200	2	0.4	0.76	4.00	2.31
200	3	0.73	0.76	4.00	3.09

Table 3.11 Viscosity values from fitting of the fluid particles with fixed c. (section 3.5.3).

fluid

m	b_0	γ (WCA)	Δ_2	c	μ
200	0	0.07	0.76	4.00	1.47
200	1	0.2	0.76	4.00	1.81
200	2	0.36	0.76	4.00	2.08
200	3	0.55	0.76	4.00	2.33

m	b_0	γ (LJ-spline)	Δ_2	c	μ
200	0	0.07	0.76	4.00	1.47
200	1	0.22	0.76	4.00	1.99
200	2	0.39	0.76	4.00	2.25
200	3	0.59	0.76	4.00	2.50

3.7.2 Discussion

In section 3.7.1, we calculated the c values which indicate the boundary conditions of our simulation. From the results we have, the c values change from less than 3 to more than 6, it seems we can not tell the exact boundary conditions of the simulations. While, in our simulations, the large colloidal particle is smooth and we also use smooth interaction potentials, we believe the boundary conditions should be a smooth one, though from the c values we can not tell the boundary conditions. A recent research by Luo and Pozrikidis [Luo2006] on the motion of a spherical particle in infinite linear flow and near a plane wall, indicates that the slip velocity reduces the drag force, torque, and the effective viscosity of a dilute suspension. They derived a more general form of the drag resistance. That means our viscosity model for the simulation is too simply and cannot reflect the "true" values of the viscosity. According to their research, the force exerted on the sphere is $F = -8\pi\mu ag = -6\pi a \frac{\beta_p + 2}{\beta_p + 3}(V - U)$. As $\beta_p \rightarrow 0$, the Stokes-law coefficient of six tends to four, indicating a substantial reduction in the drag force. That also emphasizes our belief that the c values should be close to 4 and the viscosities may change in the region near the large colloidal particle surface.

We also calculated the drag constant ξ. From equation (3.3) we can tell the drag constant $\xi = m\gamma$. From section 3.5.1 and 3.5.2, in each case, for the same radius $b_0 = 2$, we have 3

different friction coefficient data for different mass. As an example we calculated the drag constant using the data in section 3.5.1.

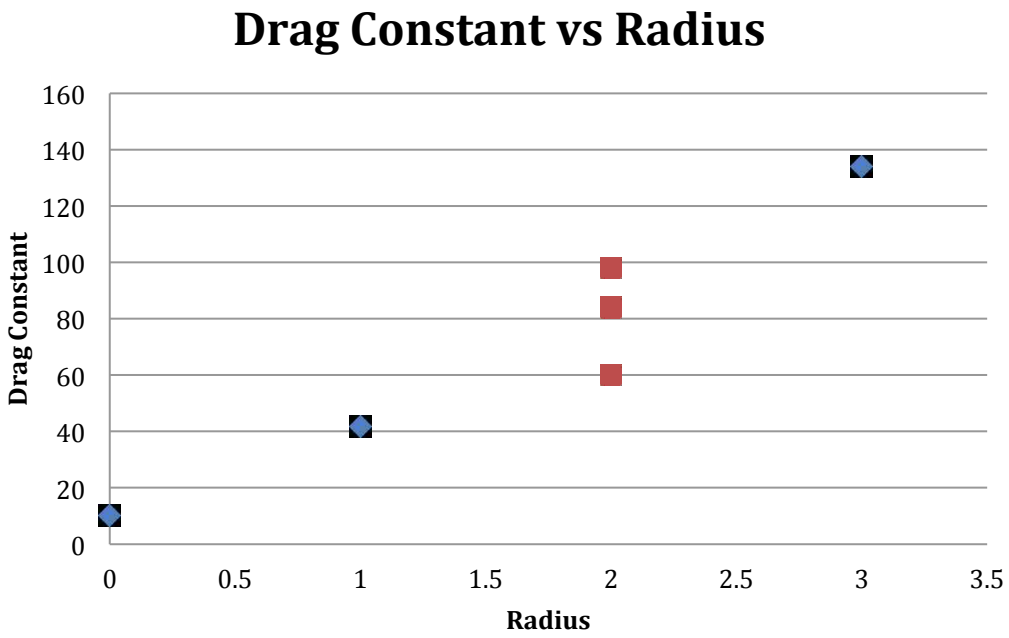

Figure 3.11 Drag Constant as a function of colloid radius for wca fluid. (Data are from section 3.5.1).

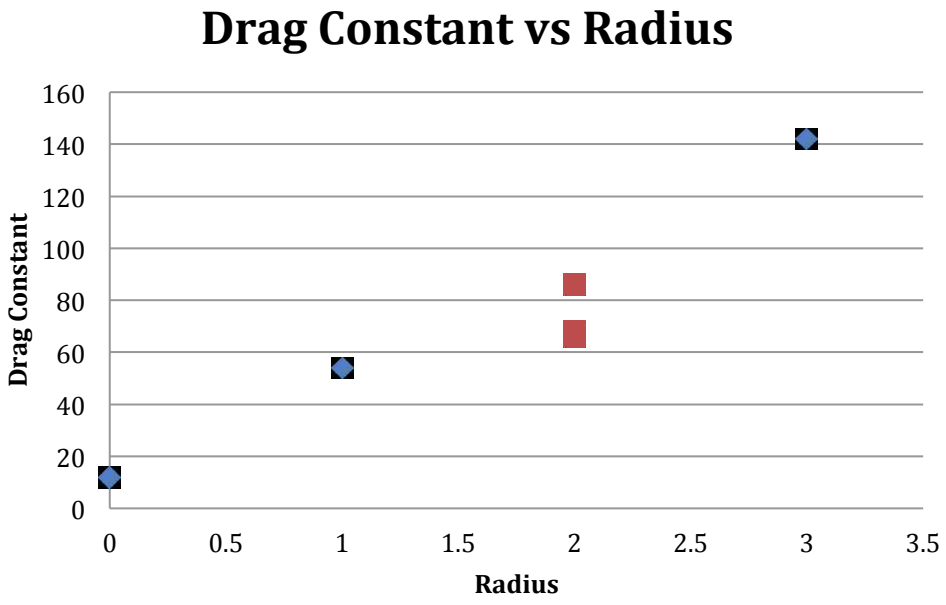

Figure 3.12 Drag Constant as a function of colloid radius for LJ-spline fluid. (Data are from section 3.5.1).

The drag constant should only be a linear function of radius, but our results show that for the same radius ($b_0 = 2$) we are obtaining distinctly different drag constant values. This means that the product of c and μ is not behaving as a constant. Within each set of simulations (WCA and LJ), the interactions between the solvent and sphere are equivalent, and the assumption of c being constant would appear to be appropriate. Also, because the potentials are radially symmetric for the smooth particles, there is no mechanical means by which to exert a transverse force during a sphere-solvent interaction. Consequently, the value of c for these simulations with a smooth sphere should be 4. Other researchers have previously made this argument. In 1986, Gaskell *et al*. [Gaskell86] reported the computer simulation data for the generalized wavevector-dependent shear viscosity in a Lennard-Jones fluid. The results were carefully compared

with simple viscoelectric theory. The latter was found to give a respectable description of the data, and discrepancies were pointed out. A group of Australia researchers Hansen *et al*. [Hasen2007] also reported that the viscosity can change with the radius and mass of the colloid particle. The real space viscosity kernel has a width of 2 to 3 atomic diameters, that means that the generalized hydrodynamic constitutive relation is required if the stain rate varies significantly over this distance. They also pointed out that in general only for fluid flows in which the gradient of the strain rate is constant or zero can the classical Navier-Stokes equation with constant transport coefficients be considered exact [Todd2008]. Again, they emphasized that the strain rate varies appreciably over the width of the kernel in real space. Such conditions are likely to be dominant for nanofluidic flows. Furthermore, they suggested the viscosity must be treated as nonlocal property of the fluid, they showed that a gradient expansion of the nonlocal constitutive equation gives a reasonable approximation to the shear stress in the small wave vector limit [Todd2008].

The resolution of our results would then be that viscosity is not a constant. Assuming c = 4, values for viscosity are shown in Table3.9, 3.10 and 3.11. There does appear to be a trend the viscosity value depends on the radius of the sphere. The Australian group has performed MD simulations showing gradients in velocities can have a significant impact on the effective value of the viscosity. Our systems will have such gradients as the solvent flows past the sphere, and they should increase with the radius of the sphere for a fixed velocity. Our results are consistent with this argument and we believe this is the

preferred way to resolve our results. Studies in the next chapter support our assertion that we should treat c=4 for these smooth sphere simulations.

Chapter 4

MOVING COLLOIDAL PARTICLE

In this chapter, we investigate the static and dynamic components of the drag force as a function of separation for a colloid particle moving toward an atomic wall or a smooth wall. We also compare the results with Brenner's solution, and again try to determine the appropriate boundary condition for the system. All simulations reported here are performed with the LAMMPS package [LAMMPS] for molecular dynamics.

In the earlier work, the solvation force near a wall was determined by observing a large colloid moving in close proximity to the wall. Vergeles et al. performed a study of both transitional and rotational motions of a single sphere in a Lennard-Jones fluid as it approaches a planar wall. Van Swol specifically separated the contributions of the drag force experienced by a smooth sphere as it approaches a smooth planar surface, and static solvation forces (the same that cause the force oscillations discussed in Chap 2/3) by observing the colloid motions when the colloid moves away from a planar wall. An issue that was not specifically addressed by those researches is that when the colloid moves to a position that is very near the wall, some fluid particles may get trapped in the small region between the wall and the colloid surface. The solvent force values may become too large in the small gap between the surface of the colloid and the wall, thus making the results of the drag force is unreliable.

To avoid those situations, in our simulations, we do not stop the colloid when it is close to the wall. Instead, we let the colloid continue to penetrate through the wall, by ignoring the forces between the colloid and the wall. If a solvent atom as becomes trapped between the particle and the wall, the force between the solvent and the particle and the wall will diverge and cause the simulation to terminate. The results from such simulations were discarded. We will vary the wall character, particle size and velocity and compare with previous results and the Brenner solution.

4.1 Simulation Approach

The simulations were performed in a box of dimensions $Lx/\sigma \times Ly/\sigma \times Lz/\sigma = 13.68 \times 13.68 \times 32.20$ with periodic boundary conditions applied to the *x* and *y* directions, while a pair of parallel walls was placed normal to the *z* direction near the two ends of the box. The back wall was smooth and used to evaluate the pressure as in Chap 2/3. The front wall was defined as either rough or smooth to determine how that effects the results.

First we describe the rough wall, which is made of atoms. The atomistic wall that was used to explore the behavior of the suspended spherical particle consisted of two layers each of 200 atoms. These were placed in a face centered cubic (fcc) arrangement with a lattice spacing of 1.094s to form a wall that would be impervious to the solvent atoms. The inner most layer of wall atoms was positioned with their atomic centers at z=0. These wall atoms interacted with the solvent atoms with the same potential as a solvent-

solvent interaction, but they were not allowed to move during the simulations. In our current work, we use the WCA potential as the interaction potential.

$$\phi(r) = \begin{cases} \phi_{12-6}(r) - \phi_{12-6}(r_c), & r < r_c \\ 0, & r > r_c \end{cases} \tag{4.1}$$

with

$$\phi_{12-6}(r) = 4\varepsilon\left[\left(\frac{\sigma}{r}\right)^{12} - \left(\frac{\sigma}{r}\right)^{6}\right] \tag{4.2}$$

The cutoff radius is chosen at the minimum of the LJ potential, $r_c/\sigma = 2^{1/6} \approx 1.12$ and r is the distance between the center of the two fluid particles. The parameter ε is the depth of the LJ potential, and represents our fundamental energy unit, and similarly σ is the fundamental length unit. The potential between the fluid particles and the suspended sphere is described using a shifted WCA potential, as was used in previous studies.

$$\phi(r) = \begin{cases} \infty, & 0 < r < b_0 \\ \phi_{12-6}(r - b_0) - \phi_{12-6}(r_c), & b_0 < r < r_c + b_0 \\ 0, & r > r_c + b_0 \end{cases} \tag{4.3}$$

Here b_0 is the radius of the hard-core region of the sphere (which allows its effective size to be arbitrarily adjusted) and r is the distance between the center of the sphere and the center of a fluid particle. These potentials are continuous and smooth to arbitrary order (except at the inner cut-off b_0 which shouldn't be accessible), and short-ranged. Consequently, there are no complicating factors in their numerical evaluation and for the standard time step of $\Delta t = 0.005\sigma\sqrt{m/\varepsilon}$, there is a very high degree of energy conservation.

The wall at the far end of the simulation box (z = 32.20 s) was a simple smooth wall that interacted with the solvent atoms by a planar 9-3 potential as used in earlier work[van Swol2006].

$$\emptyset(\mathrm{r}) = (\frac{2}{5})^{1/2}\left[\frac{1}{5}\left(\frac{\sigma}{r}\right)^{9} - \frac{3}{2}\left(\frac{\sigma}{r}\right)^{3}\right] \qquad (4.4)$$

The potential energy between the suspended sphere and the wall particles was set to zero so that the wall exerted no direct force on the sphere.

The simulations were initialized by filling up the region to the right of the wall with fluid particles. Those particles were set in an fcc crystal structure with a lattice constant 1.094σ giving an initial solvent density of $\rho\sigma^3=0.8$. A colloid sphere with a core radius of b_0 and mass M was placed at an arbitrarily selected initial point. Any solvent particle whose center was within $b_0 + \sigma$ of the colloid center was then removed in order to establish a fairly consistent solvent density for the systems with different colloid radii. The system was then randomized for 40000 steps in NVE ensemble, to disorder the solvent. To obtain the 300 different starting configurations discussed below, different random number seeds were chosen for the initial velocities of the solvent atoms. The temperature was the rescaled back to $kT/\varepsilon = 1.2$ using a Nose-Hoover thermostat, and the system equilibrated for 20000 steps. After this, the simulation was continued in an NVE ensemble, a constant velocity U was set on the colloid at z direction to keep the colloid moving towards the wall, and the z-component of net solvent force on the sphere was collected every time step and these were averaged over sets of 200 time steps. This

procedure was performed for 300 different configurations of the fluid particles (generated by the different random thermalization procedure described above) for each selected core radius, potential set and temperature. We then averaged the results of these three hundred configurations over the discrete time window of 200 time steps. Because a constant particle velocity is being applied, this also corresponds to a discrete window of the suspended particle position.

As we mentioned in the beginning, we will let the colloid push through the wall. After the colloid has pushed through the wall, we let it stay for 10000 time steps (U=0) to let the temperature and pressure of fluid particles re-equilibrate back to $kT/\varepsilon = 1.2$ Then, the colloid was given the same constant velocity but in the reversed direction -U to have the colloid re-emerge from the wall and move back to its initial position. The z-component of net solvent force on the sphere was collected and averaged the same way as before.

As part of our analysis, we monitor the pressure of the system. It should remain approximately constant until the particle overlaps with the wall, except for minor heating due to the forced particle translation. Since in our simulations, the wall is also made of particles, and those particles constrained not to move in the simulation procedure, the LAMMPS calculated pressure value will be larger than that of the real system pressure. Consequently, we used a separate method to calculate the system pressure. This was determined by summing the forces on the right wall of the simulation box (a smooth planar LJ-9-3 wall), and dividing by its area (defined by the x-y dimensions of the simulation box) to get the actual system pressure.

4.2 Static and Dynamic Components

The molecular-dynamics results for the drag forces are qualitatively different when the colloid moves toward and away from the wall in the near field (i.e., $h/b_0 < 1$). When leaving the wall, the colloid experiences a drag force that is not only the negative of the drag force when moving toward the wall, the magnitude of the force is considerably less negative near the wall than antisymmetry would suggest.

Challa & van Swol pointed out that the antisymmetry to the hydrodynamic theory is not shared by the actual MD simulations, and the drag force can be extracted into a static and a dynamic component:

$$F_{static}(U,h) = \frac{1}{2}[F(U,h) + F(-U,h)] \tag{4.5}$$

$$F_{dynamic}(U,h) = \frac{1}{2}[F(U,h) - F(-U,h)] \tag{4.6}$$

where h is the separation between the surface of the colloid and the wall, U is the colloid velocity. The static force (4.5) vanishes for large h, while the dynamic force (4.6) should approach a non-zero value, namely the Stokes drag. Again, Challa & van Swol's study did not show a clear view of the colloid effective size and the wall position. That may cause ambiguity in the determination of the correct comparison to Brenner's expression. Our study presents a more reliable way in comparison with continuum theory.

As with previous simulations, we observe that when the fluid particles interact with the wall, there was a region of space between the center of the first layer of wall atoms and the center of the closest layer of fluid molecules. If one defines the volume of space associated with either the solvent or the wall by simply the region sampled by the nuclear positions, then this region does not belong to either element. In the earlier work of other researches, this issue has never been thoroughly addressed. In both Vergeles and van Swol's work, none of them investigated what would constitute a better definition of the wall position. Similarly, they lacked a rigorous definition of the particle radius.

In our previous work (the second chapter), we determined a correction term for the wall position Δ_1, and a correction term for the colloid radius Δ_2. Similarly, the radius of the suspended particle, as defined in the potential energy of Eq. (4.3), is b_0 and we assume that there is a region of thickness Δ_2 that defines its effective size. From our early work, we have found out the correction term of this simulation, when r=4, Δ_1= 0.5664, and Δ_2=0.7059. So the separation was calculated as $h= z-\Delta_1-\Delta_2$, where $z=|z_i-z_w|$ means the distance of the colloid particle from the center of the closest layer of the atomic wall. We now use these definitions for our analysis.

4.3 Results

4.3.1 Rough Wall Results

Figure 4.1 shows an example of the colloid with a radius 4 in the near field of the atomic wall. We plot the total force in z-direction on the colloid as a function of the separation. The force oscillates with a period that closely reflects the molecular size of the fluid particles, 1σ, in our simulations. The oscillations increase when the colloid in the near region of the wall. Though the interaction potential is purely repulsive, the solvation force is negative (attractive) almost in all the positions when the colloid moves away from the wall, and positive (repulsive) when approaching the wall. The two curves remain perfectly in phase with each other. **Figure 4.1** also shows the static and dynamic components of the drag force for the colloid of a core radius 4.

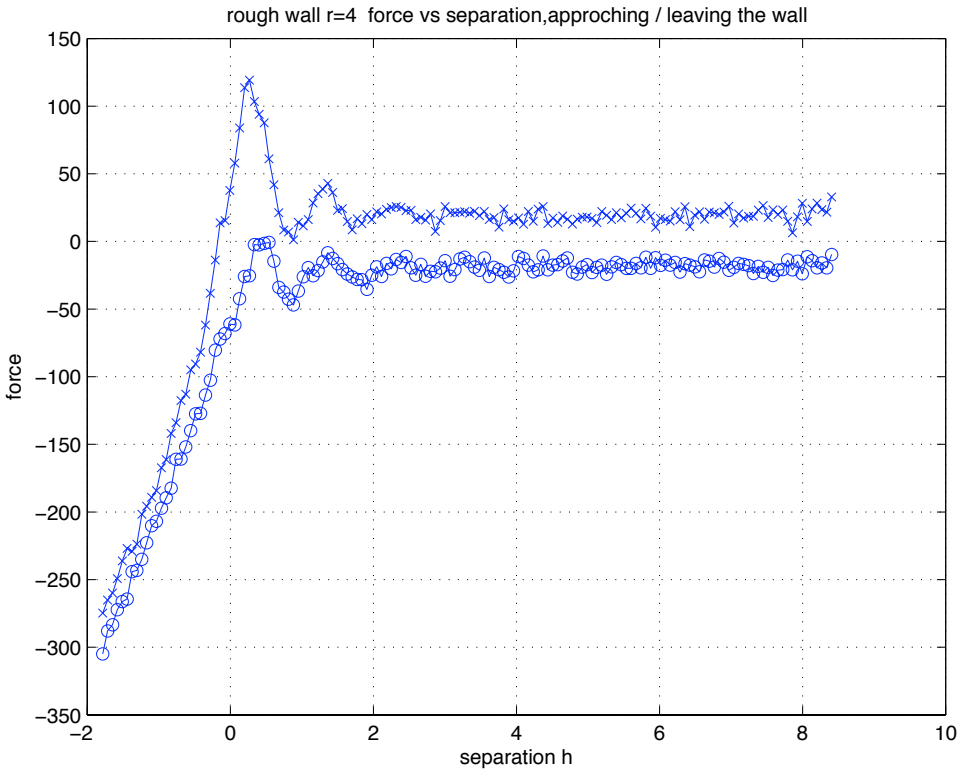

Figure 4.1 The drag force as a function of separation for a colloid of radius 4, moving toward (and away) from the atomic wall at a velocity U=0.068. The solid curve with

crosses denotes the force while the colloid approaching the wall; the curve with circles denotes the force while moving away from the wall.

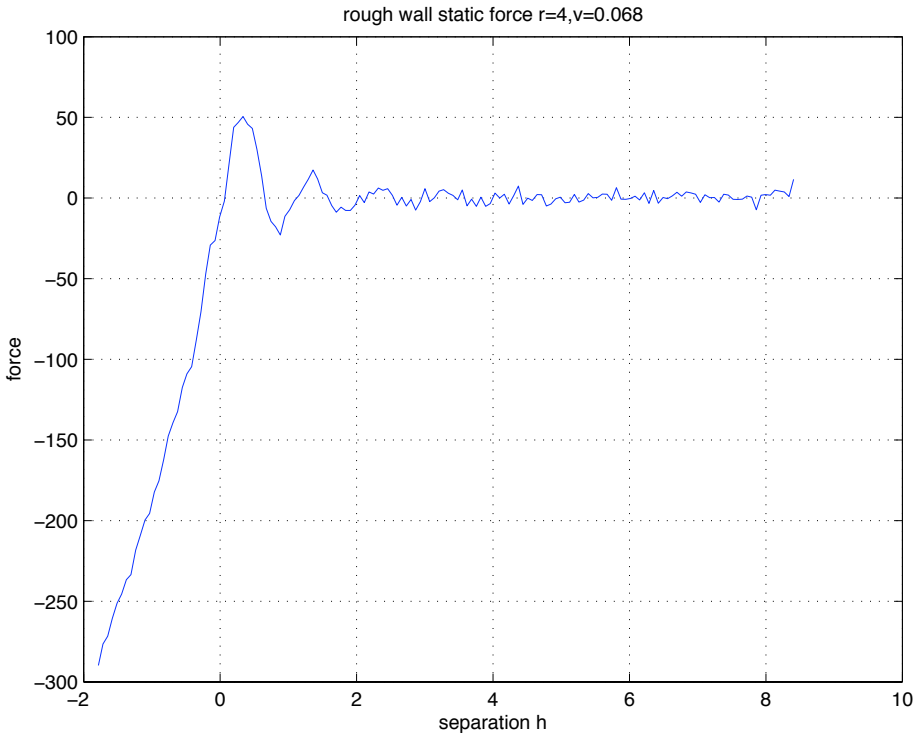

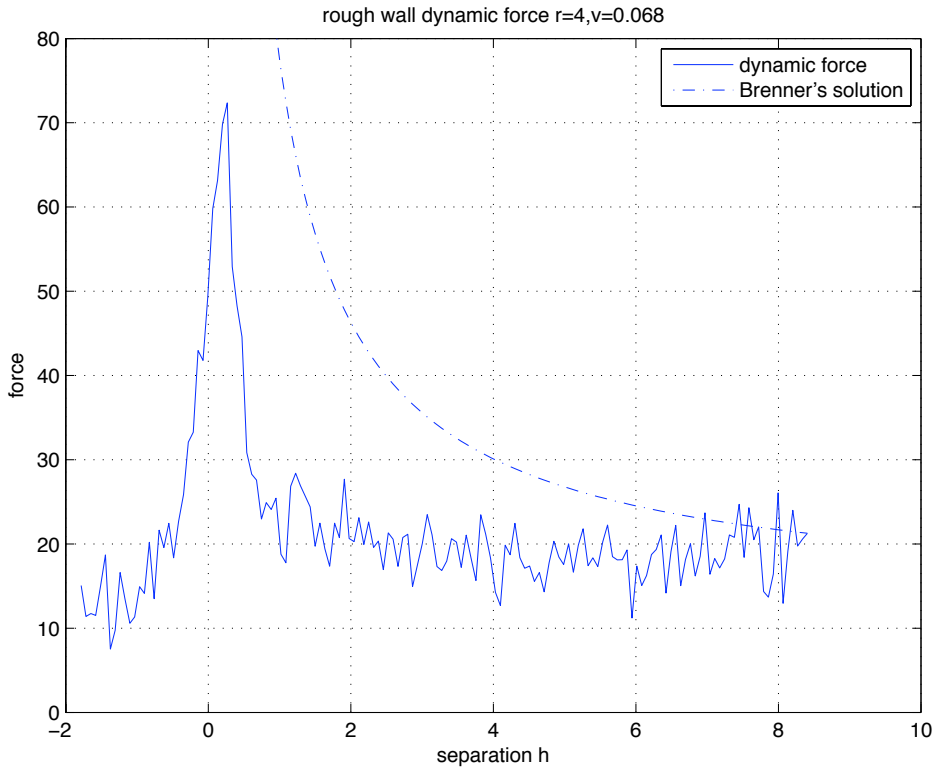

Figure 4.2 The static and dynamic component of the drag force as a function of separation for a colloid particle moving toward an atomic wall with a velocity U=0.068. The broken curve is Brenner's solution.

In **Figure 4.2** (a), the intercept of the curve and z-direction is 0, that is to say, when separation is zero, the static force is zero too. Which indicates both the wall position and colloid size are consistent with each other, and our correction terms Δ_1 and Δ_2 are reasonable. Also from **Figure 4.2** (a), when the separation h is large, the net static force is 0, as predicted. **Figure 4.2** (b) shows the dynamic force and Brenner's solution. The dynamic term of the drag force displays a strong upturn when the colloid is very close to

the wall. The curve shows the same tendency as Brenner's curve, and approaches the non-zero value as Brenner's solution suggested for large h.

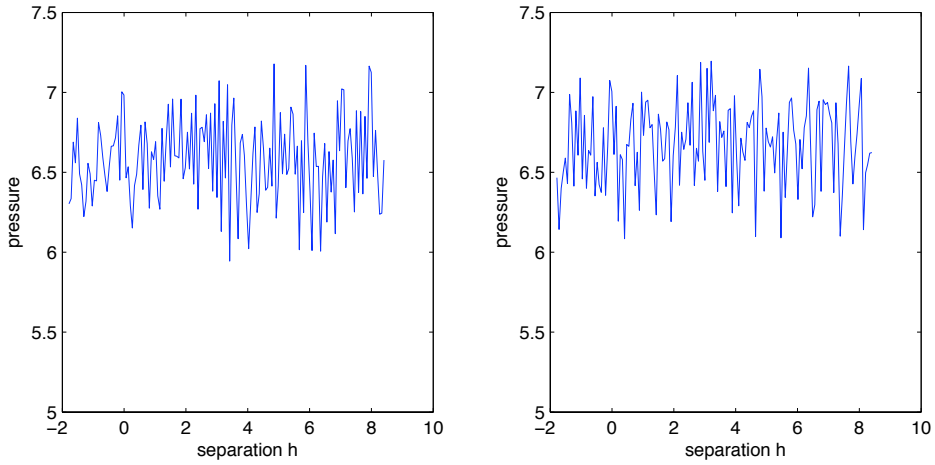

Figure 4.3 The system pressure as a function of separation for a colloid particle moving toward and away from an atomic wall with a velocity U=0.068. (left) colloid particle approached the wall. (right) colloid particle left the wall.

Figure 4.3 shows the system pressure when the colloid moves toward and away from the atomic wall. The system pressure is quite stable, before the colloid penetrates the wall. After the colloid begins to push through the wall, the system pressure starts to drop. When the colloid moves back to the simulation box, the pressure increases back to the stable value.

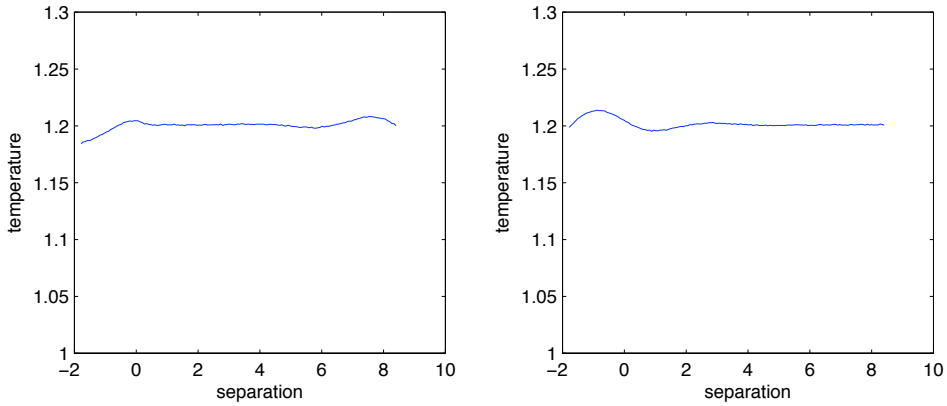

Figure 4.4 The system temperature as a function of separation for a colloid particle moving toward and away from an atomic wall with a velocity U=0.068. (left) colloid particle approached the wall. (right) colloid particle left the wall.

Figure 4.4 shows the system temperature. The system temperature keeps a stable value, despite the considerable noise present.

Similarly **Figure 4.5**, **Figure 4.6** show the static and dynamic components of the drag force for the colloid of a core radius 2 and comparison with Brenner's solution. **Figure 4.7** and **Figure 4.8** show the system pressure and temperature. These results agree with those of the r=4 simulations.

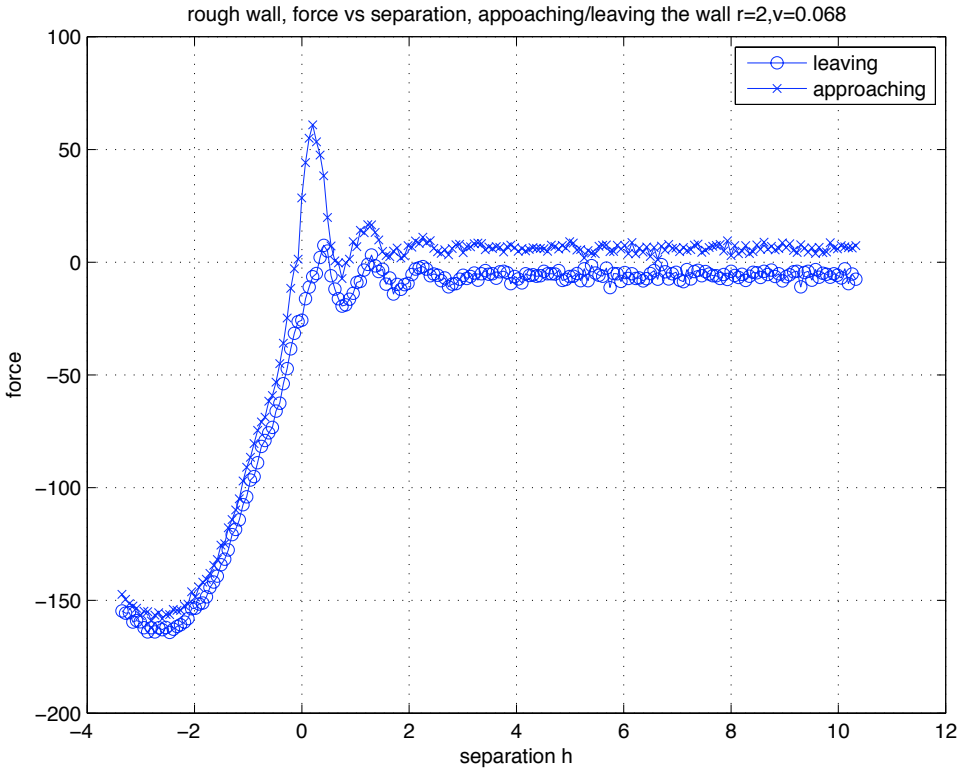

Figure 4.5 The drag force as a function of separation for a colloid of radius 2, moving toward (and away) from the atomic wall at a velocity U=0.068. The solid curve with crosses denotes the force while the colloid approaching the wall; the curve with circles denotes the force while moving away from the wall.

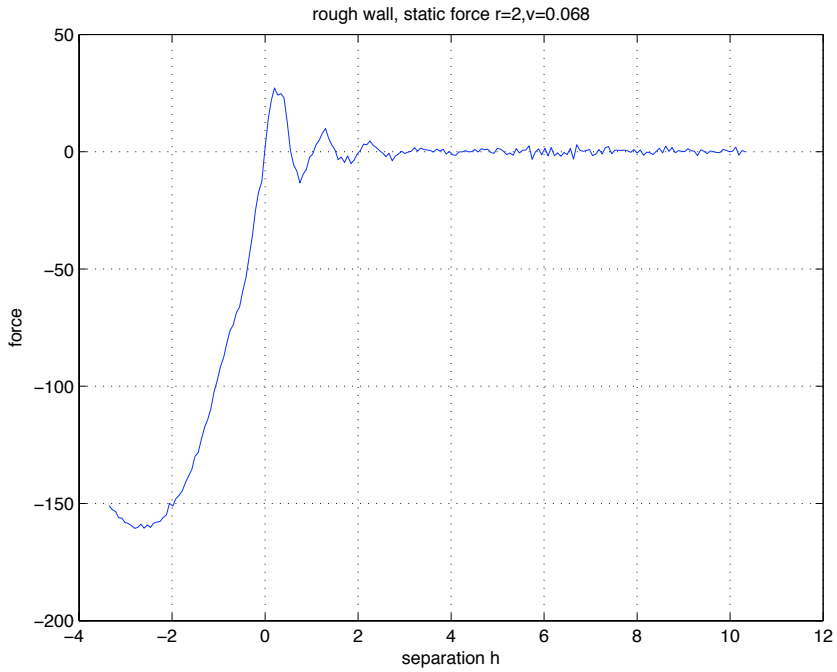

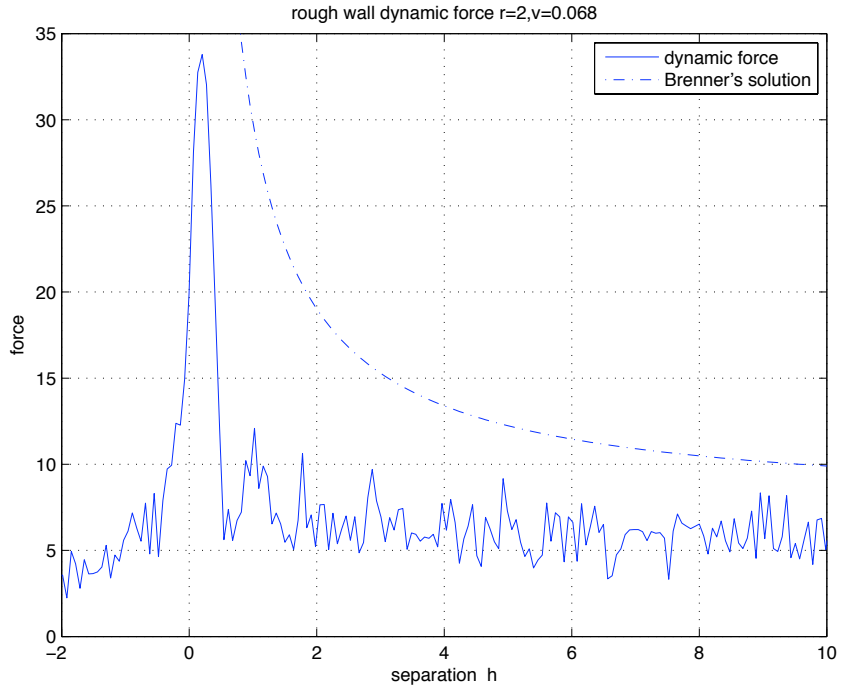

Figure 4.6 The static and dynamic component of the drag force as a function of separation for a colloid particle moving toward an atomic wall with a velocity U=0.068. The broken curve is Brenner's solution.

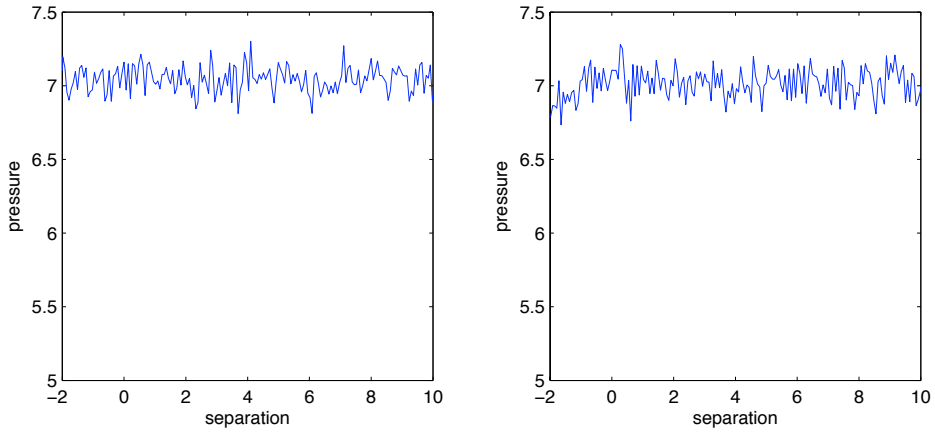

Figure 4.7 The system pressure as a function of separation for a colloid particle moving toward and away from an atomic wall with a velocity U=0.068. (left) colloid particle approached the wall. (right) colloid particle left the wall.

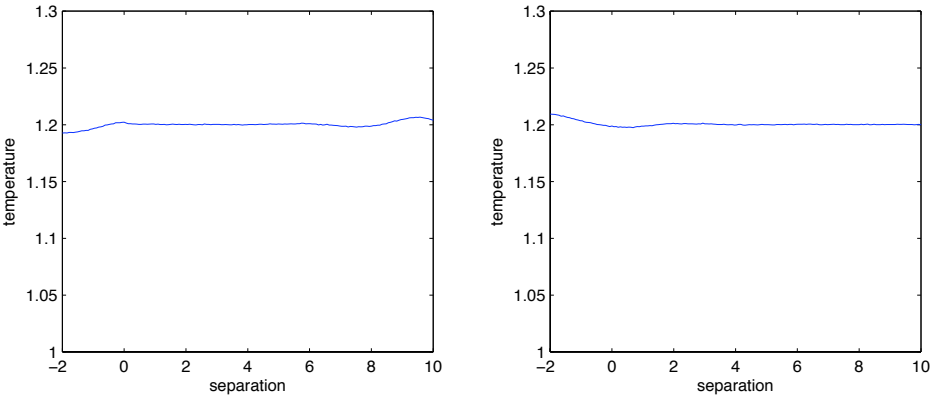

Figure 4.8 The system temperature as a function of separation for a colloid particle moving toward and away from an atomic wall with a velocity U=0.068. (left) colloid particle approached the wall. (right) colloid particle left the wall.

Figure 4.9, **Figure 4.10** show the static and dynamic components of the drag force for the colloid of a core radius 2 and compared with Brenner's solution. **Figure 4.11** and **Figure 4.12** show the system pressure and temperature. These results agree with those of the r=4 and r=2 simulations, and the only differences are that since the colloid radius is smaller, there are more fluid particles in the system, thus the system pressure and temperature are higher than in r=4 and r=2 systems.

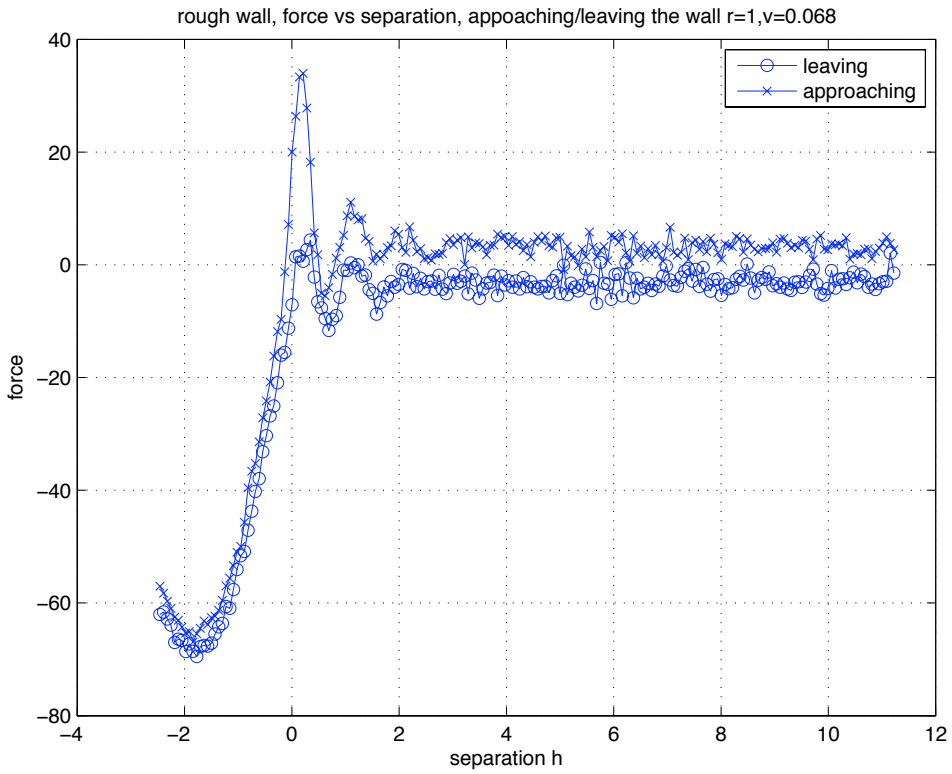

Figure 4.9 The drag force as a function of separation for a colloid of radius 2, moving toward (and away) from the atomic wall at a velocity U=0.068. The solid curve with crosses denotes the force while the colloid approaching the wall; the curve with circles denotes the force while moving away from the wall.

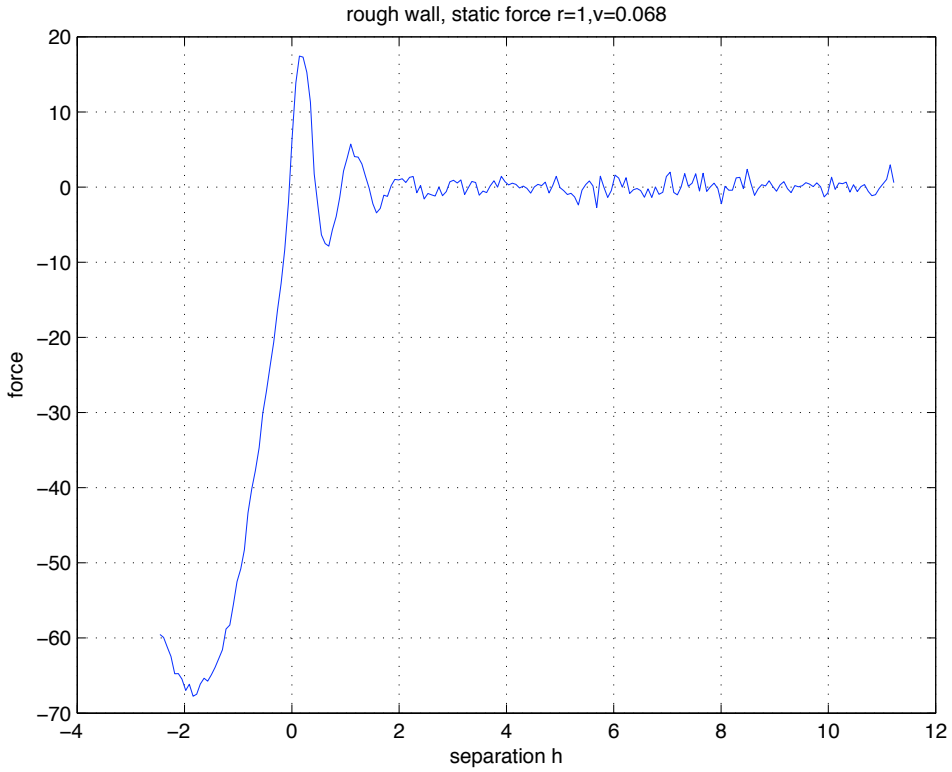
rough wall, static force r=1,v=0.068
force
separation h
20
10
0
−10
−20
−30
−40
−50
−60
−70
−4
−2
0
2
4
6
8
10
12

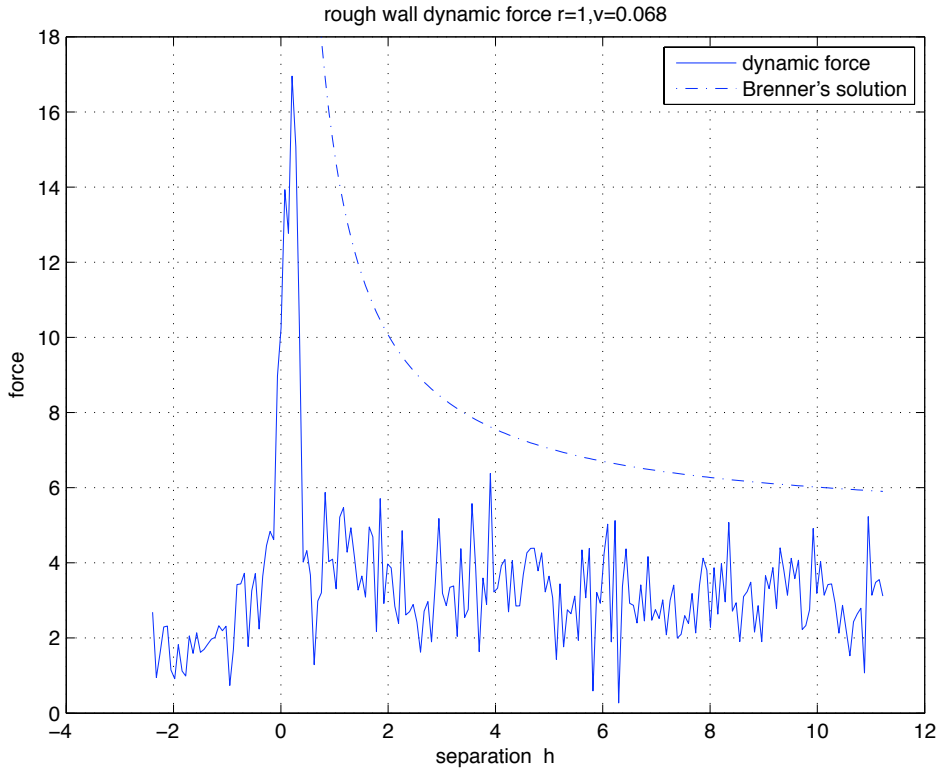

Figure 4.10 The static and dynamic component of the drag force as a function of separation for a colloid particle moving toward an atomic wall with a velocity U=0.068. The broken curve is Brenner's solution.

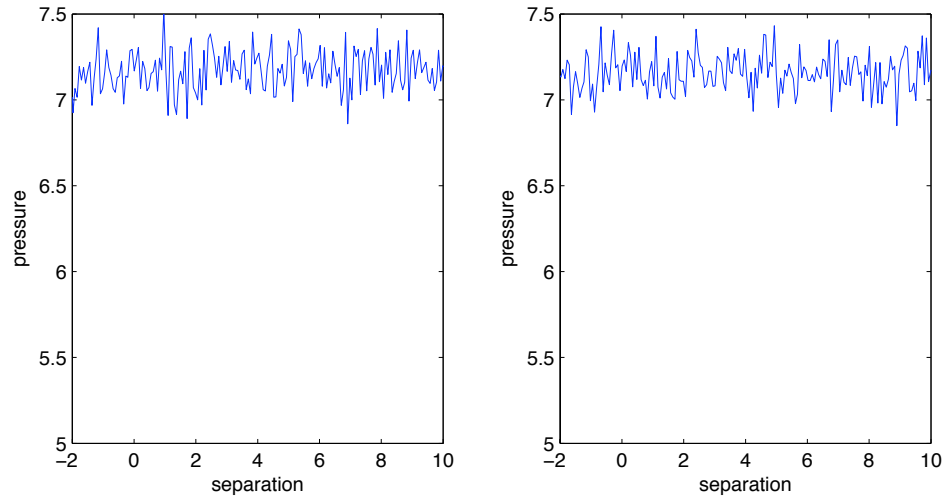

Figure 4.11 The system pressure as a function of separation for a colloid particle moving toward and away from an atomic wall with a velocity U=0.068. (left) colloid particle approached the wall. (right) colloid particle left the wall.

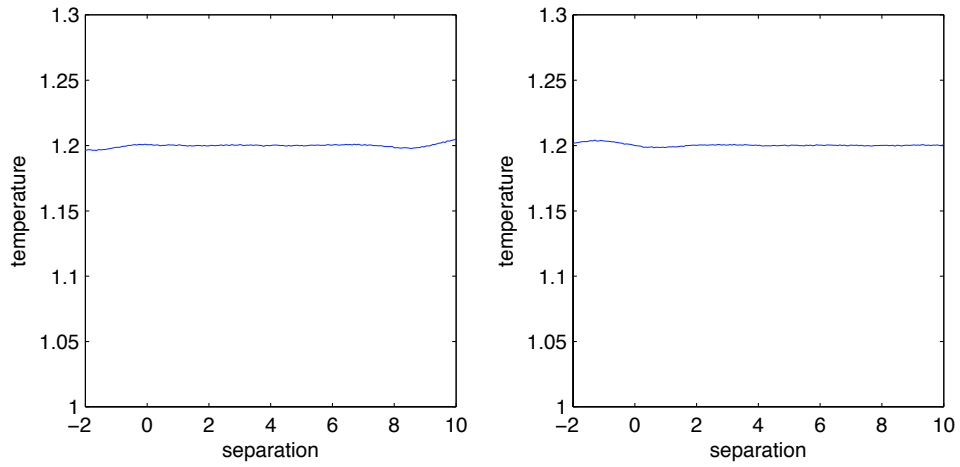

Figure 4.12 The system temperature as a function of separation for a colloid particle moving toward and away from an atomic wall with a velocity U=0.068. (left) colloid particle approached the wall. (right) colloid particle left the wall.

We also tried the same simulations with a higher velocity U=0.1, with the same systems.

Figure 4.13 shows the drag forces when the colloidal particle moves towards and away from the atomic wall. When the colloidal particle is approaching the wall, the maximum value of the force is similar to the case of smaller velocity but when leaving, the curve is more flat, thus the peak value of the dynamic force is larger due to a higher velocity (**Figure 4.14**). The system pressure is about the same, but the temperature changes more dramatically due to a higher velocity (**Figure 4.16**).

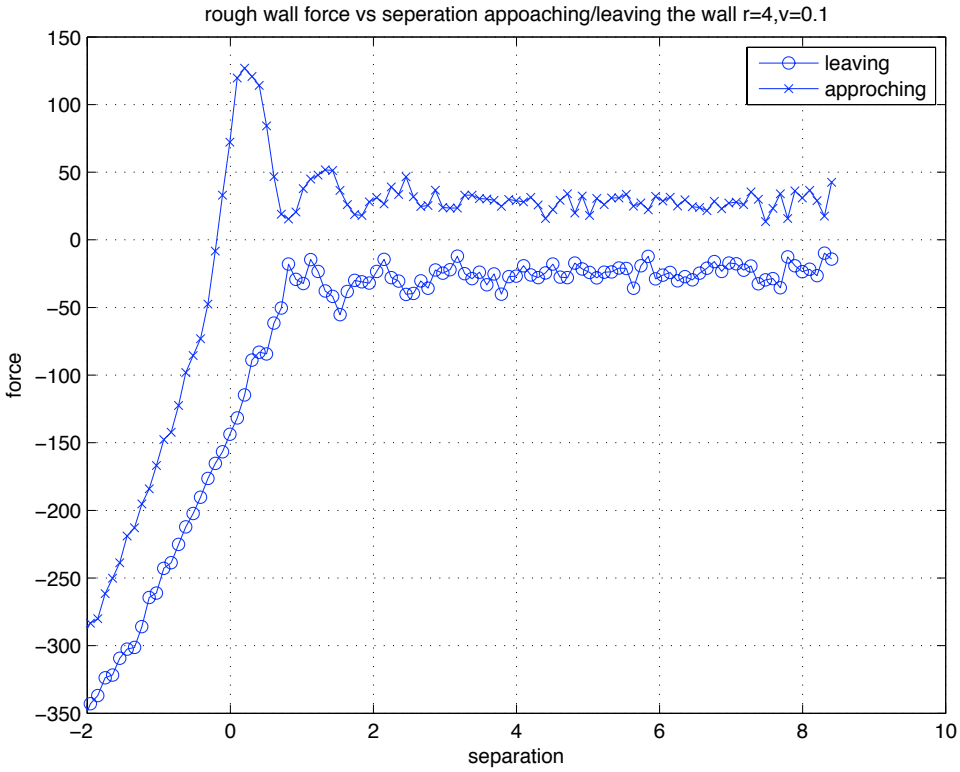

Figure 4.13 The drag force as a function of separation for a colloid of radius 4, moving toward (and away) from the atomic wall at a velocity U=0.1. The solid curve with crosses denotes the force while the colloid approaching the wall; the curve with circles denotes the force while moving away from the wall.

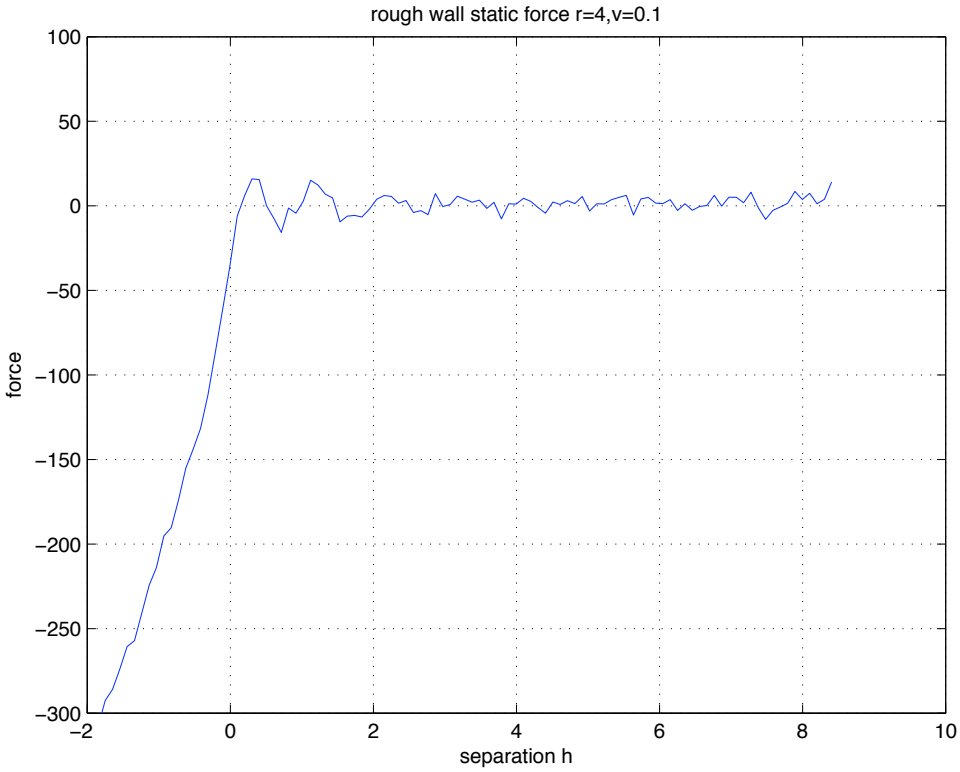
rough wall static force r=4,v=0.1
100
50
0
−50
−100
−150
−200
−250
−300
force
−2
0
2
4
6
8
10
separation h

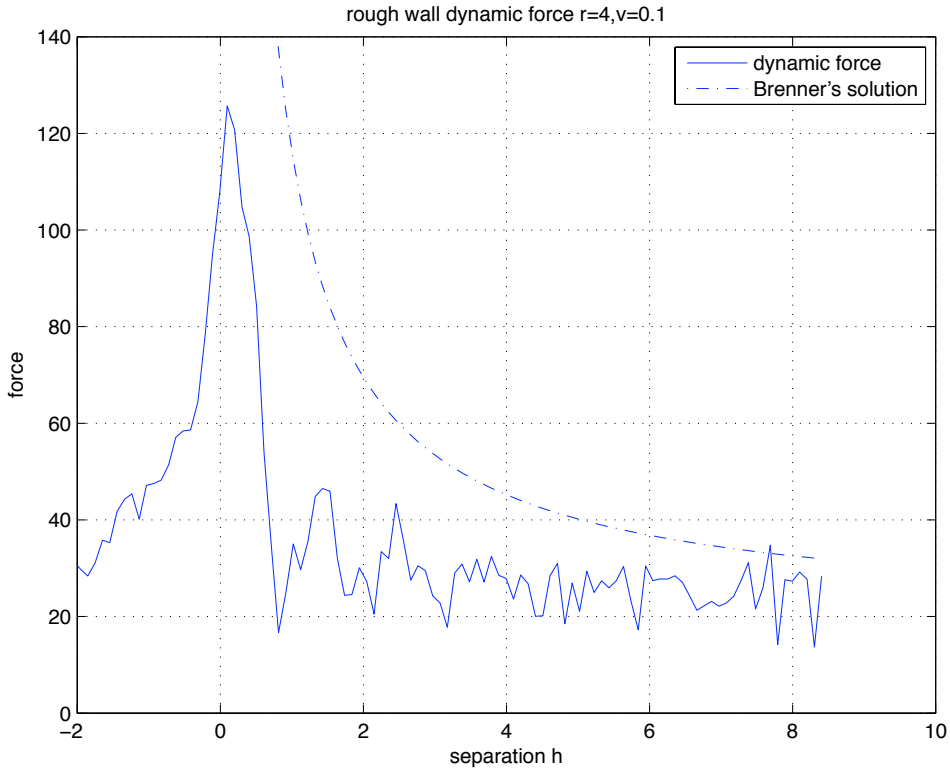

Figure 4.14 The static and dynamic component of the drag force as a function of separation for a colloid particle moving toward an atomic wall with a velocity U=0.1. The broken curve is Brenner's solution.

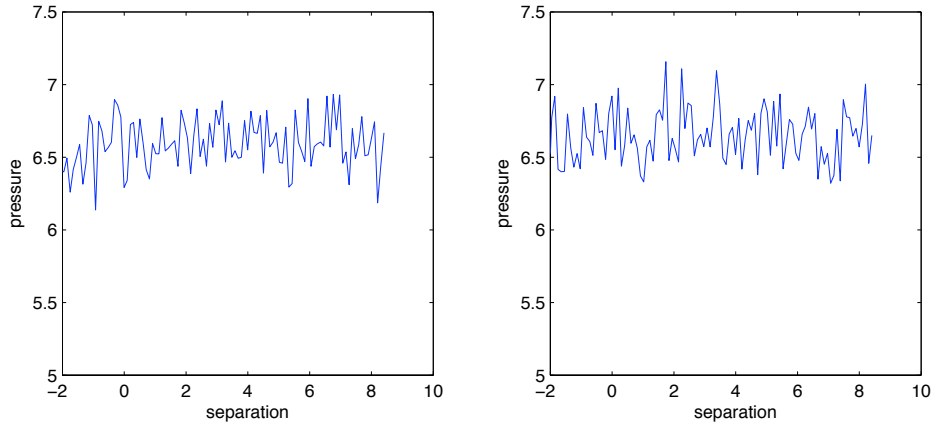

Figure 4.15 The system pressure as a function of separation for a colloid particle moving toward and away from an atomic wall with a velocity U=0.1. (left) colloid particle approached the wall. (right) colloid particle left the wall.

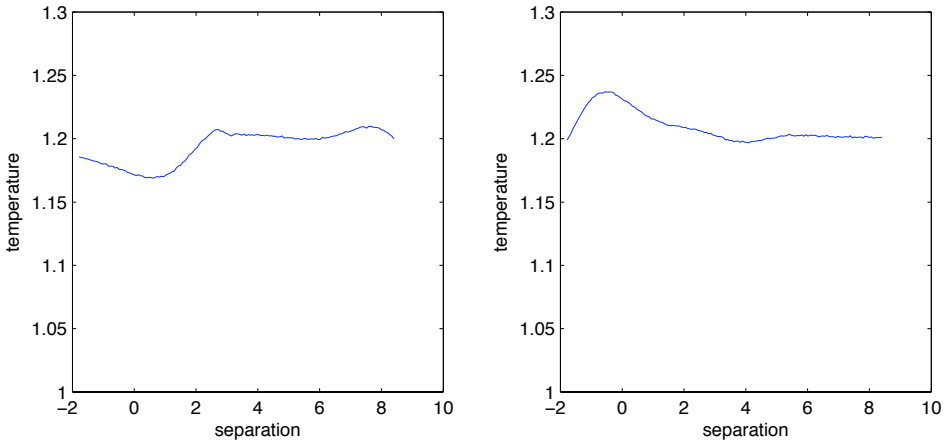

Figure 4.16 The system temperature as a function of separation for a colloid particle moving toward and away from an atomic wall with a velocity U=0.1. (left) colloid particle approached the wall. (right) colloid particle left the wall.

The following figures show the similar simulations with r=2 and r=1. They all support the results from r=4 simulations.

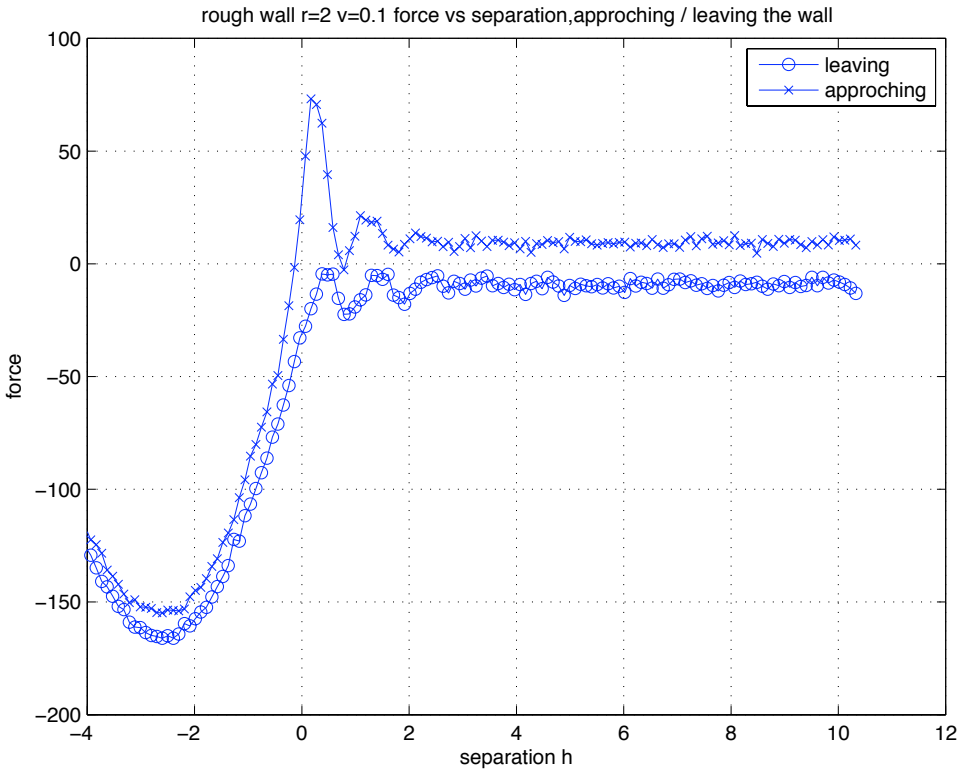

Figure 4.17 The drag force as a function of separation for a colloid of radius 2, moving toward (and away) from the atomic wall at a velocity U=0.1. The solid curve with crosses denotes the force while the colloid approaching the wall; the curve with circles denotes the force while moving away from the wall.

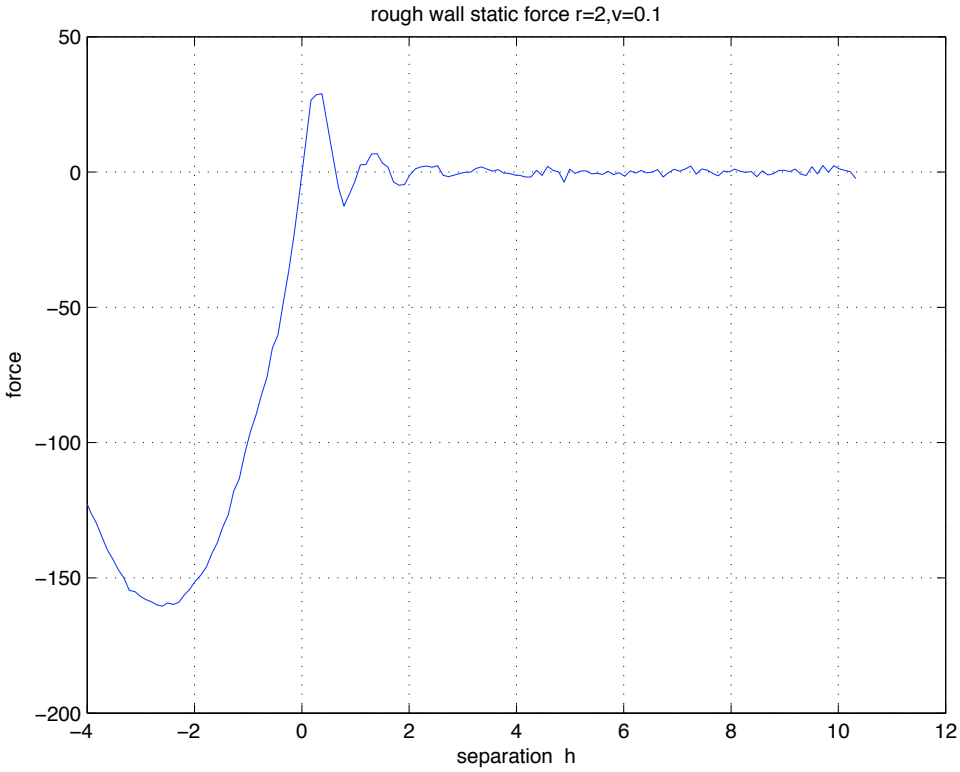
rough wall static force r=2,v=0.1
50
0
−50
−100
−150
−200
force
−4
−2
0
2
4
6
8
10
12
separation h

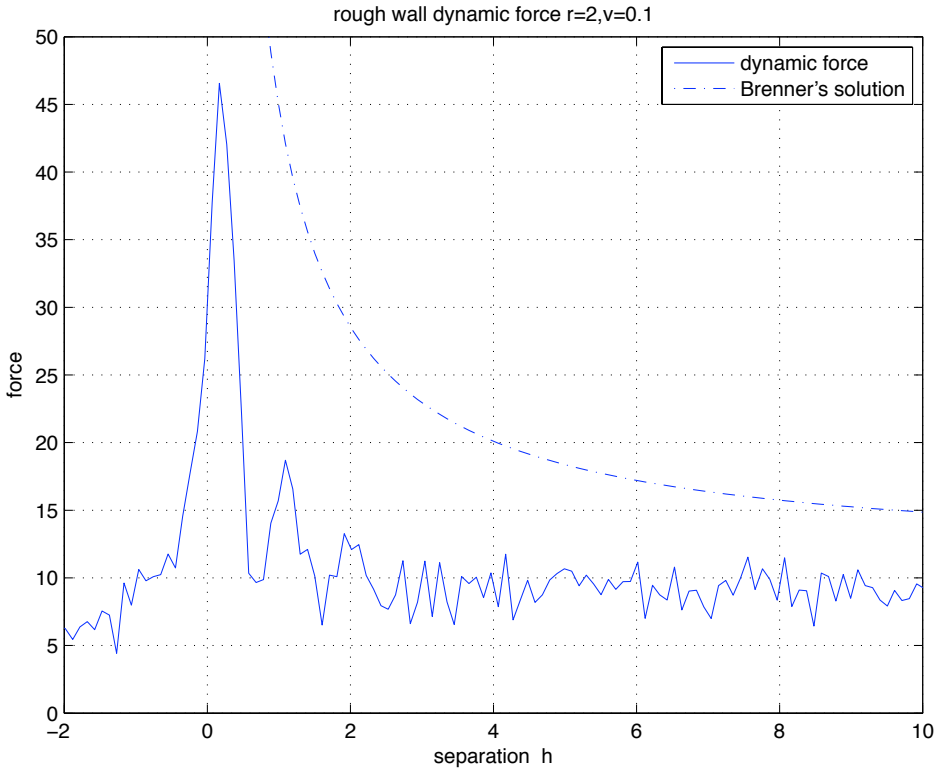

Figure 4.18 The static and dynamic component of the drag force as a function of separation for a colloid particle moving toward an atomic wall with a velocity U=0.1. The broken curve is Brenner's solution.

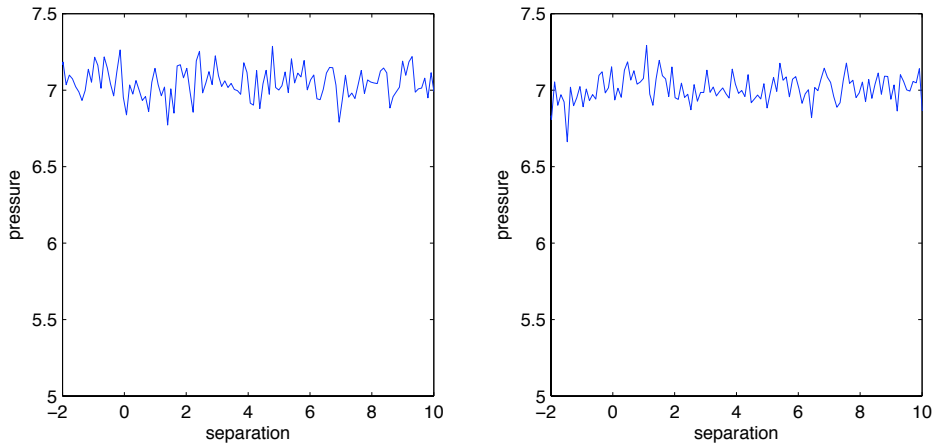

Figure 4.19 The system pressure as a function of separation for a colloid particle moving toward and away from an atomic wall with a velocity U=0.1. (left) colloid particle approached the wall. (right) colloid particle left the wall.

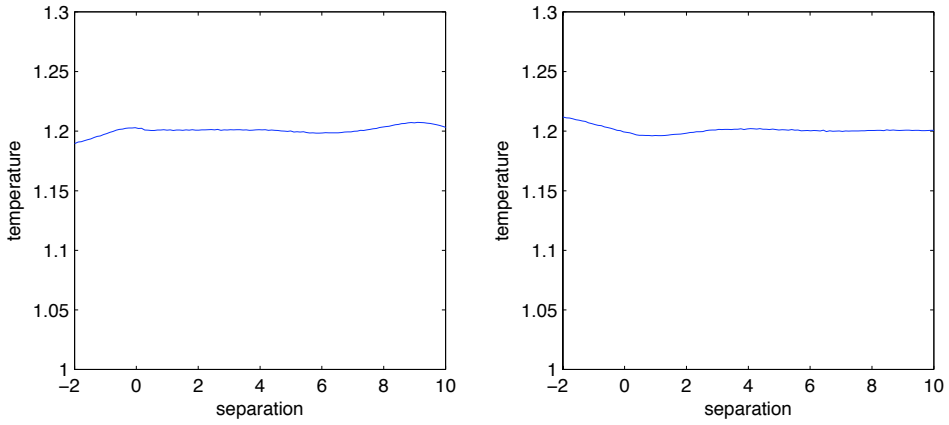

Figure 4.20 The system temperature as a function of separation for a colloid particle moving toward and away from an atomic wall with a velocity U=0.1. (left) colloid particle approached the wall. (right) colloid particle left the wall.

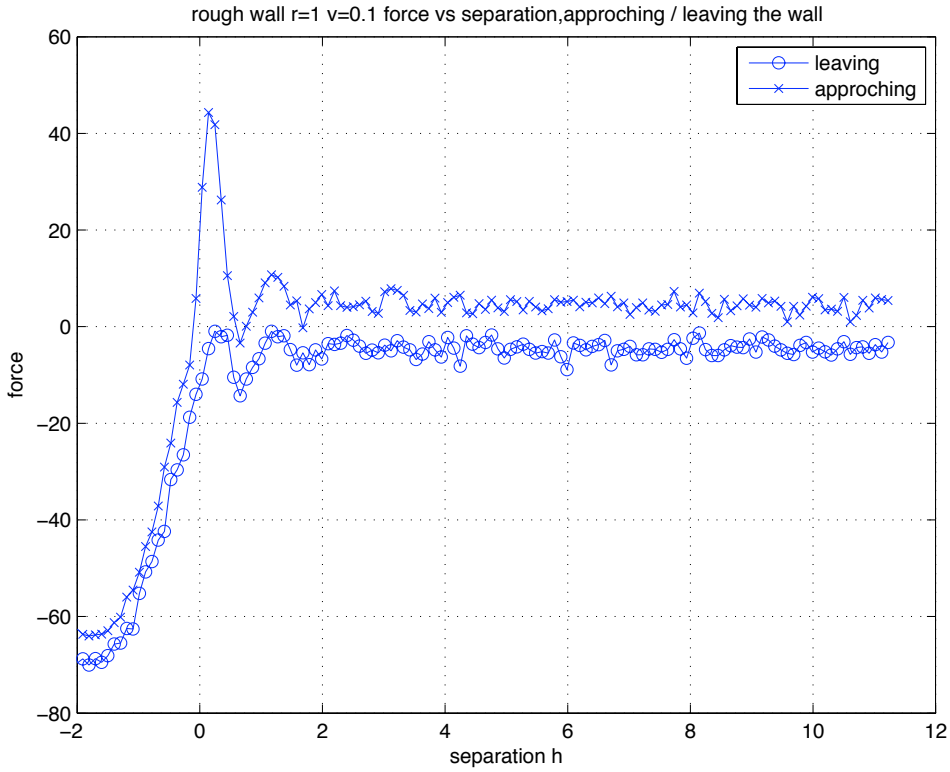

Figure 4.21 The drag force as a function of separation for a colloid of radius 1, moving toward (and away) from the atomic wall at a velocity U=0.1. The solid curve with crosses denotes the force while the colloid approaching the wall; the curve with circles denotes the force while moving away from the wall.

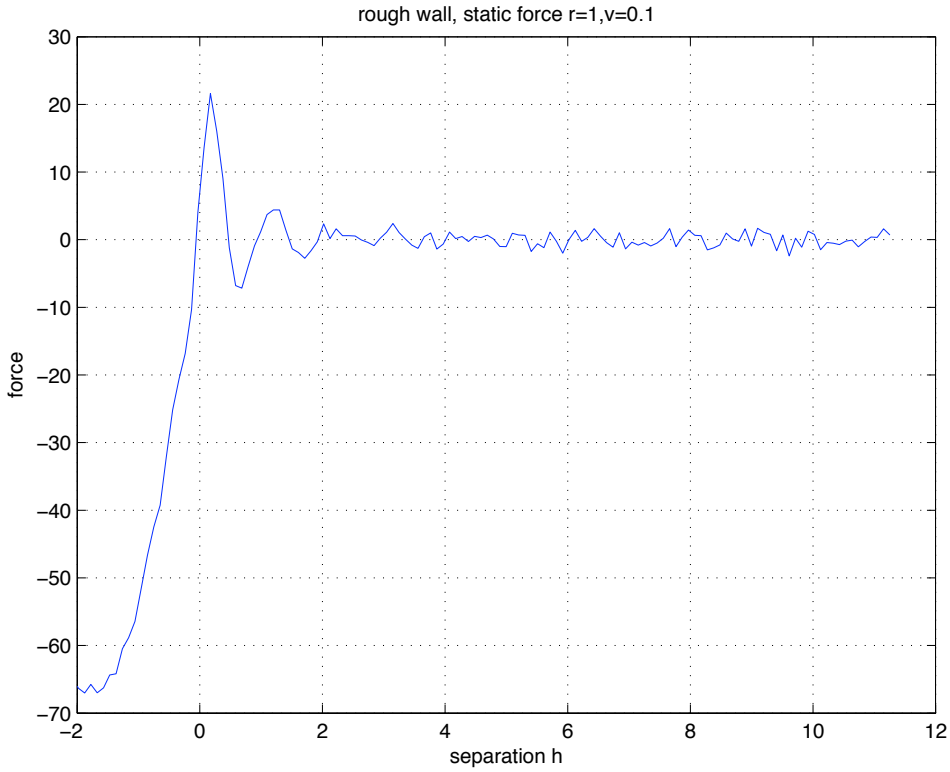
rough wall, static force r=1,v=0.1
force
separation h
30
20
10
0
−10
−20
−30
−40
−50
−60
−70
−2
0
2
4
6
8
10
12

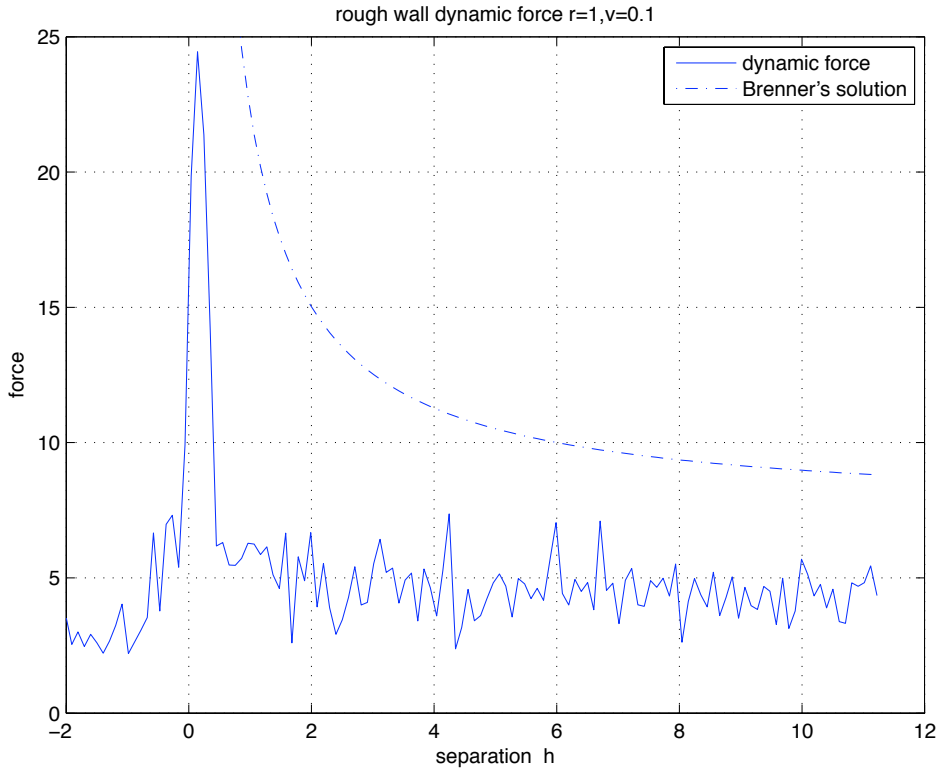

Figure 4.22 The static and dynamic component of the drag force as a function of separation for a colloid particle moving toward an atomic wall with a velocity U=0.1. The broken curve is Brenner's solution.

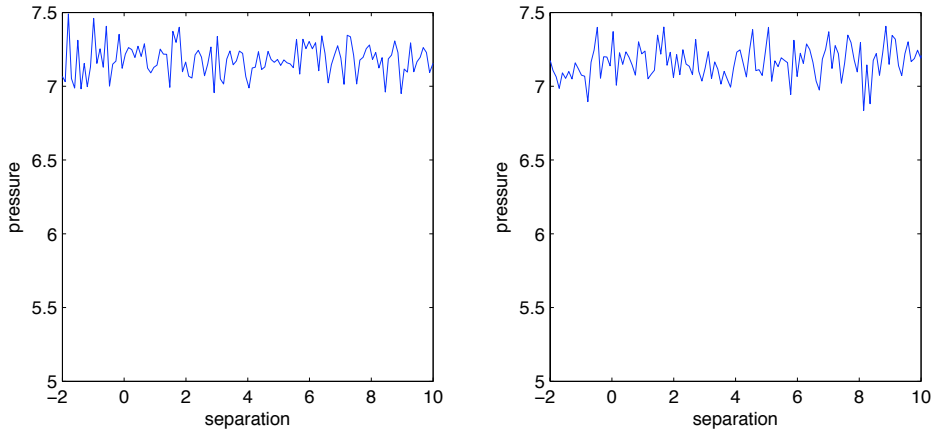

Figure 4.23 The system pressure as a function of separation for a colloid particle moving toward and away from an atomic wall with a velocity U=0.1. (left) colloid particle approached the wall. (right) colloid particle left the wall.

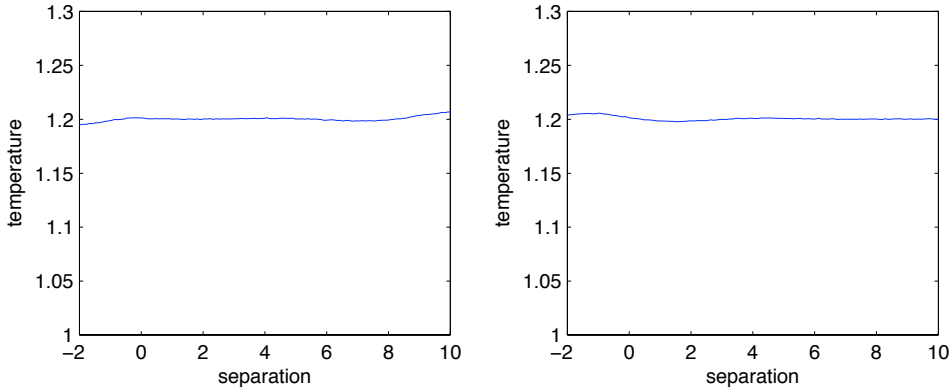

Figure 4.24 The system temperature as a function of separation for a colloid particle moving toward and away from an atomic wall with a velocity U=0.1. (left) colloid particle approached the wall. (right) colloid particle left the wall.

4.3.2 Smooth Wall Results

With the same system, we tried a smooth LJ-93 wall instead of the atom wall to repeat the simulations again. The following figures are the results of r=4,2,1 with U=0.068, 0.1.

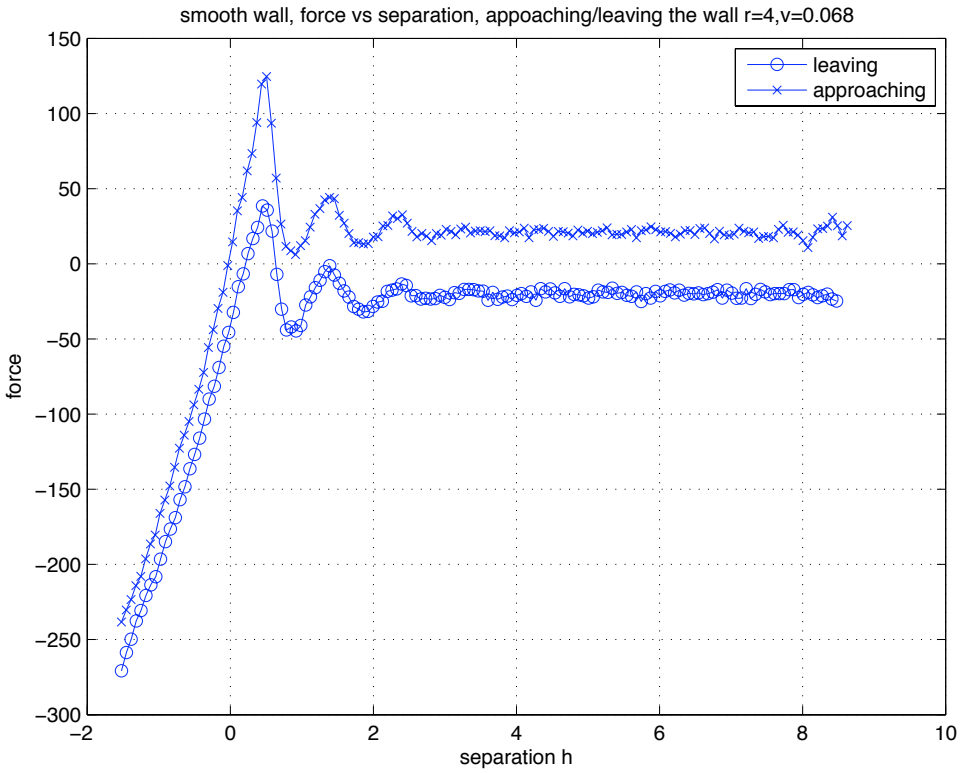

Figure 4.25 The drag force as a function of separation for a colloid of radius 4, moving toward (and away) from the smooth wall at a velocity U=0.068. The solid curve with crosses denotes the force while the colloid approaching the wall; the curve with circles denotes the force while moving away from the wall.

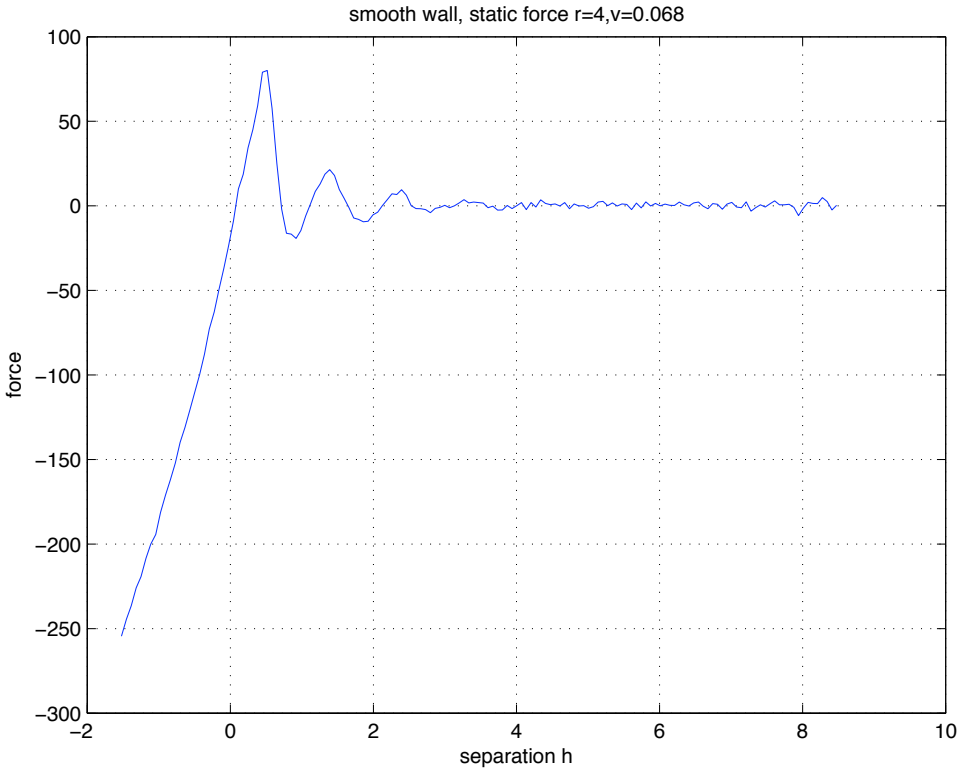
smooth wall, static force r=4,v=0.068
100
50
0
−50
−100
−150
−200
−250
−300
force
−2
0
2
4
6
8
10
separation h

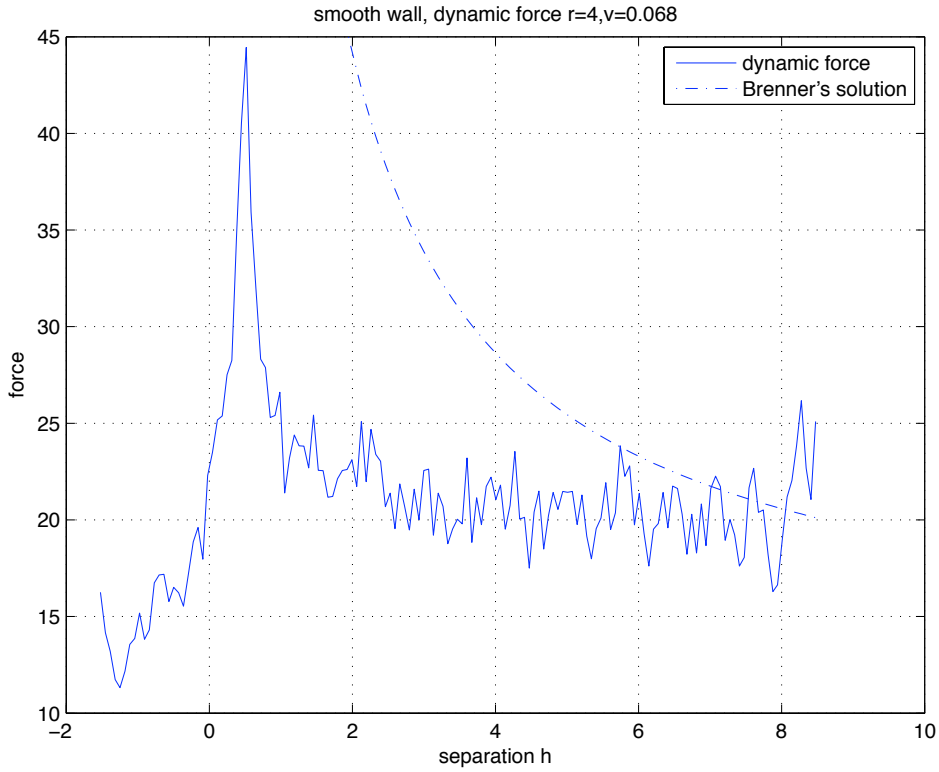

Figure 4.26 The static and dynamic component of the drag force as a function of separation for a colloid particle moving toward an smooth wall with a velocity U=0.068. The broken curve is Brenner's solution.

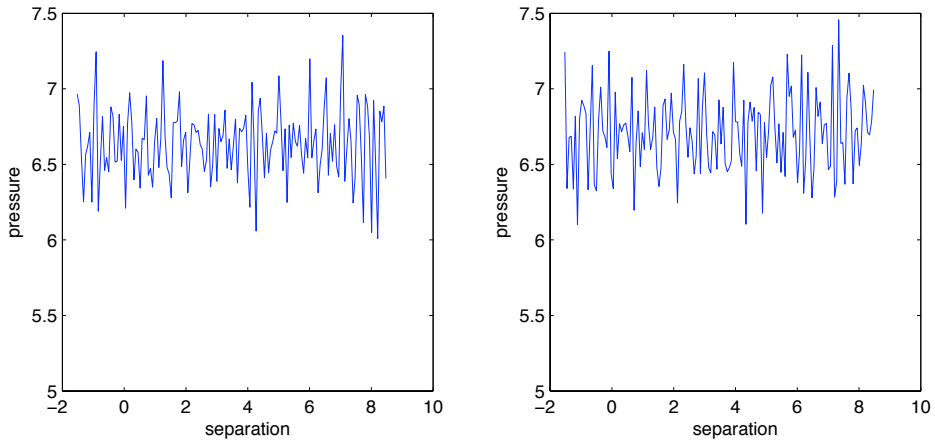

Figure 4.27 The system pressure as a function of separation for a colloid particle moving toward and away from an smooth wall with a velocity U=0.068. (left) colloid particle approached the wall. (right) colloid particle left the wall.

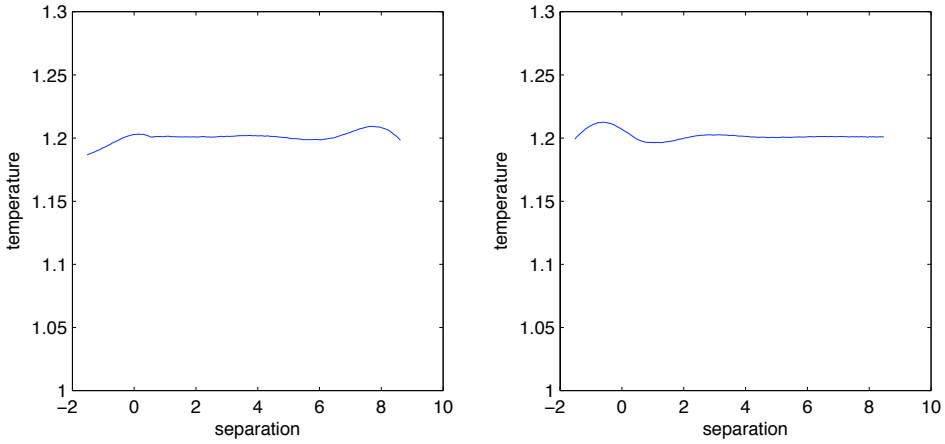

Figure 4.28 The system temperature as a function of separation for a colloid particle moving toward and away from an smooth wall with a velocity U=0.068. (left) colloid particle approached the wall. (right) colloid particle left the wall.

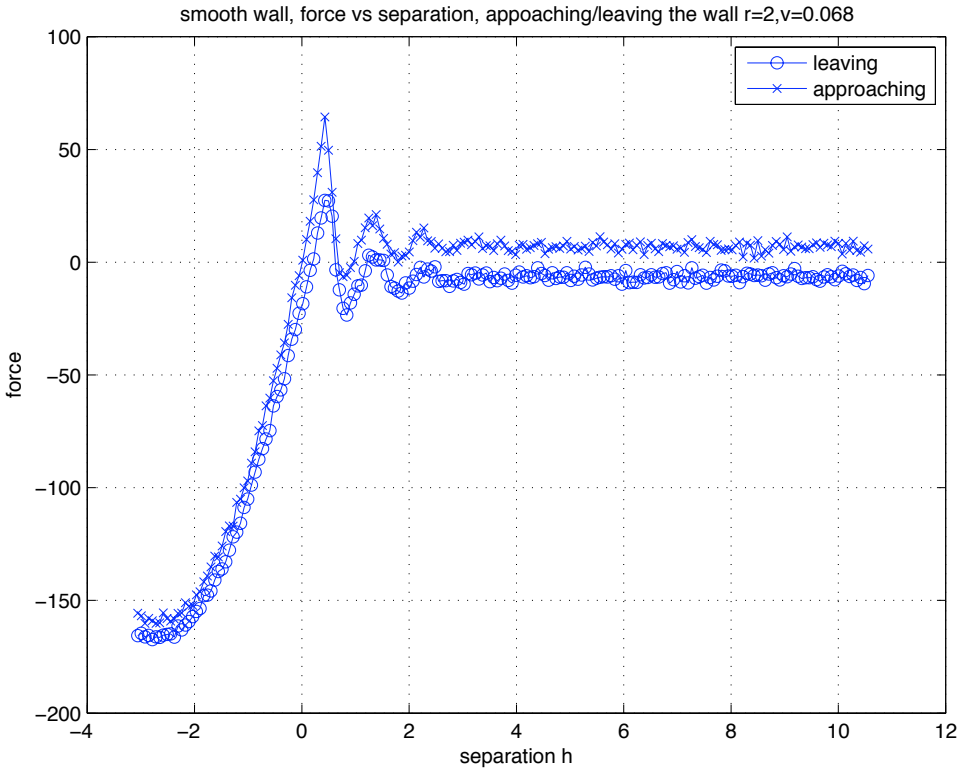

Figure 4.29 The drag force as a function of separation for a colloid of radius 2, moving toward (and away) from the smooth wall at a velocity U=0.068. The solid curve with crosses denotes the force while the colloid approaching the wall; the curve with circles denotes the force while moving away from the wall.

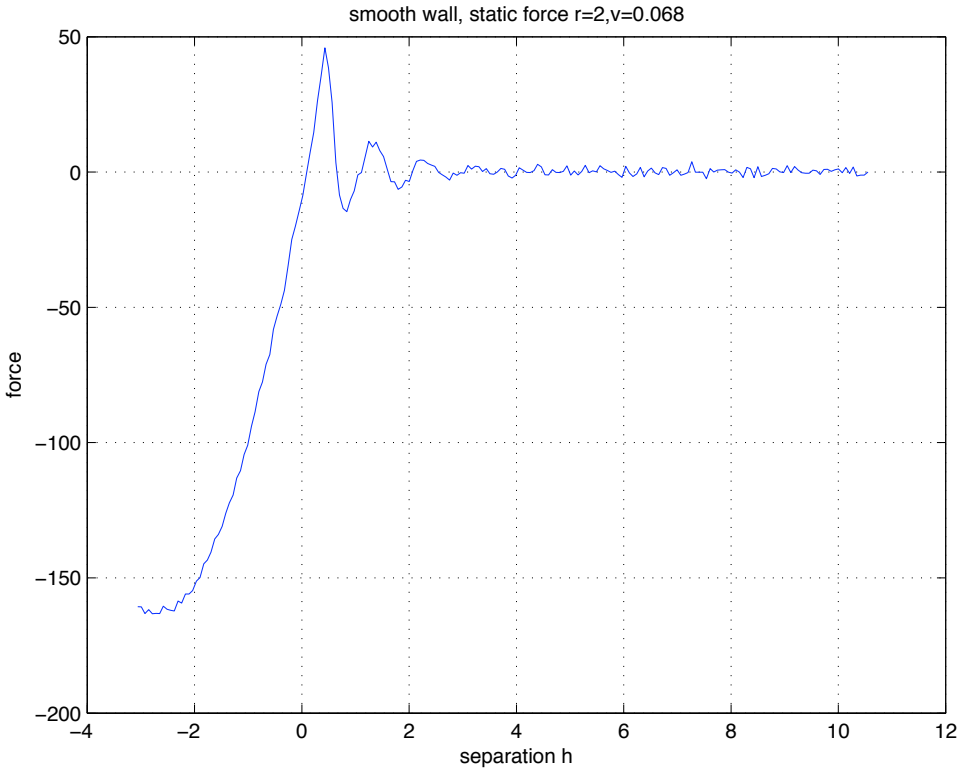
smooth wall, static force r=2,v=0.068
50
0
−50
−100
−150
−200
force
−4
−2
0
2
4
6
8
10
12
separation h

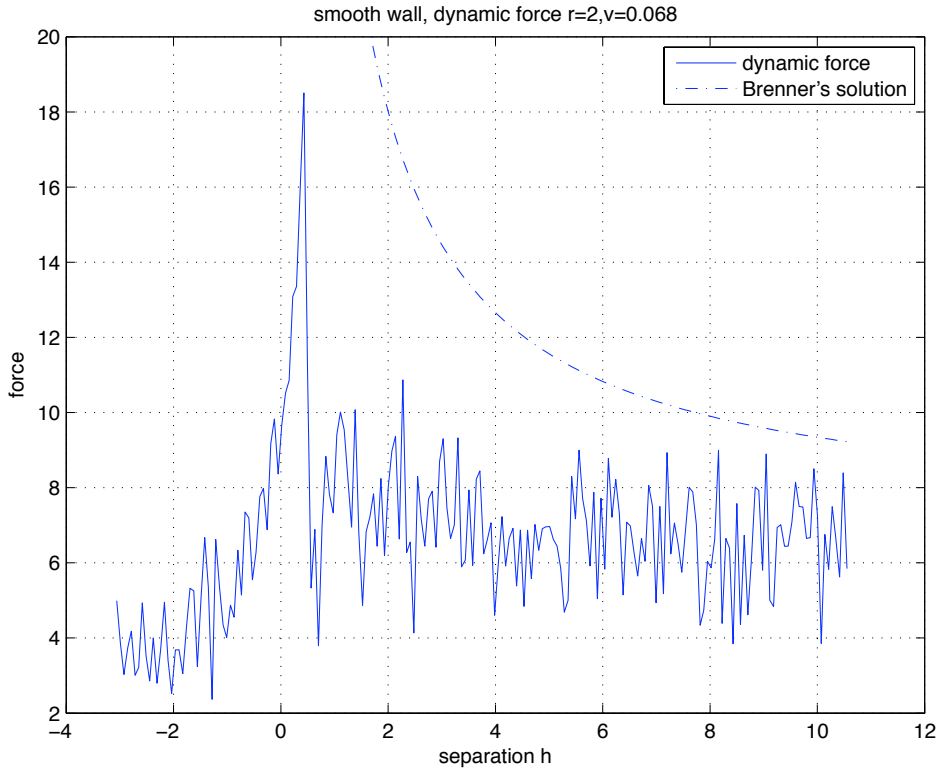

Figure 4.30 The static and dynamic component of the drag force as a function of separation for a colloid particle moving toward an smooth wall with a velocity U=0.068. The broken curve is Brenner's solution.

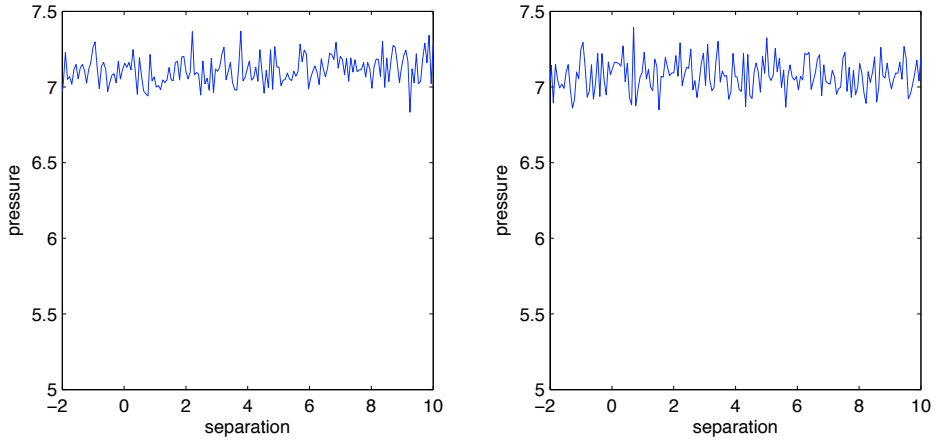

Figure 4.31 The system pressure as a function of separation for a colloid particle moving toward and away from an smooth wall with a velocity U=0.068. (left) colloid particle approached the wall. (right) colloid particle left the wall.

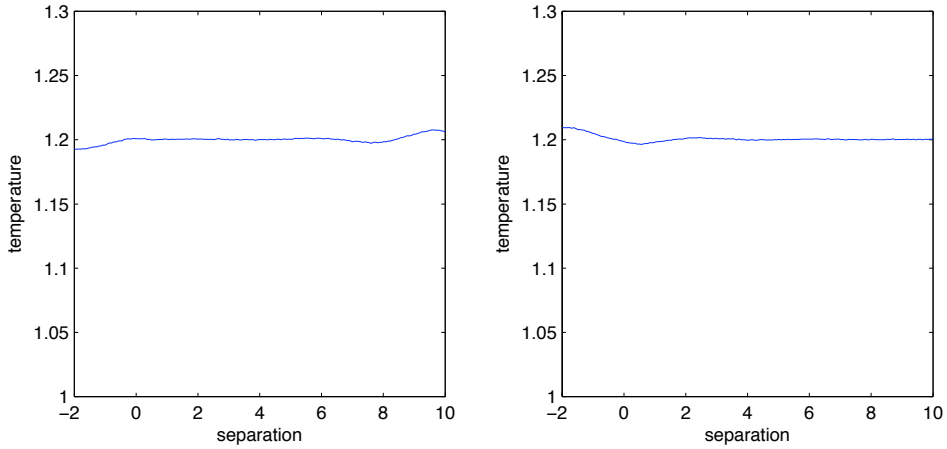

Figure 4.32 The system temperature as a function of separation for a colloid particle moving toward and away from an smooth wall with a velocity U=0.068. (left) colloid particle approached the wall. (right) colloid particle left the wall.

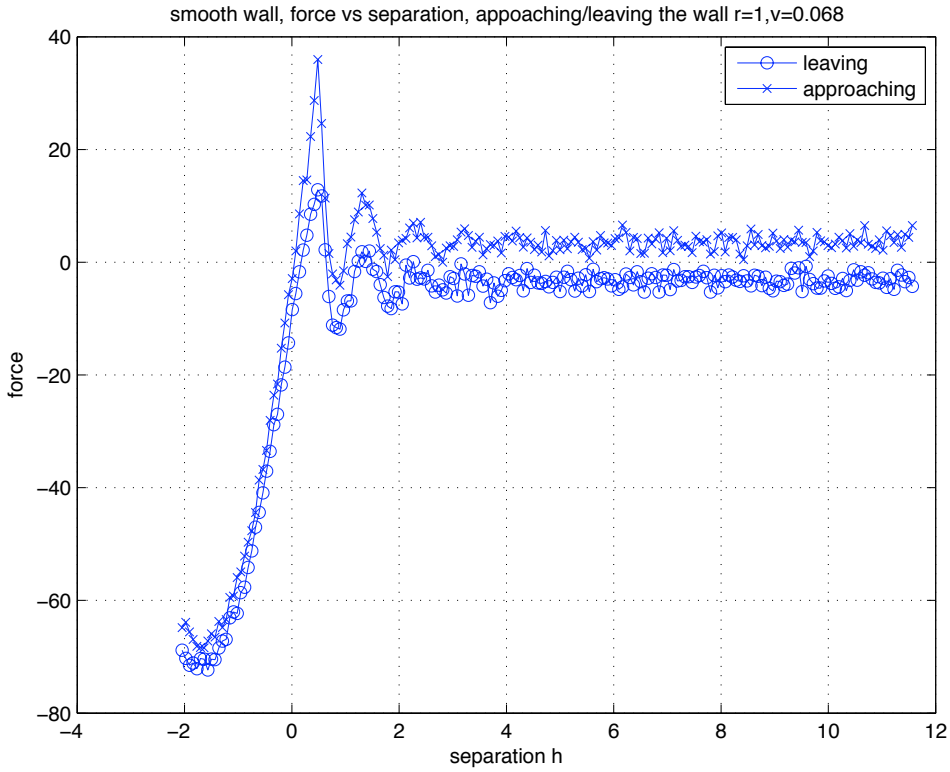

Figure 4.33 The drag force as a function of separation for a colloid of radius 1, moving toward (and away) from the smooth wall at a velocity U=0.068. The solid curve with crosses denotes the force while the colloid approaching the wall; the curve with circles denotes the force while moving away from the wall.

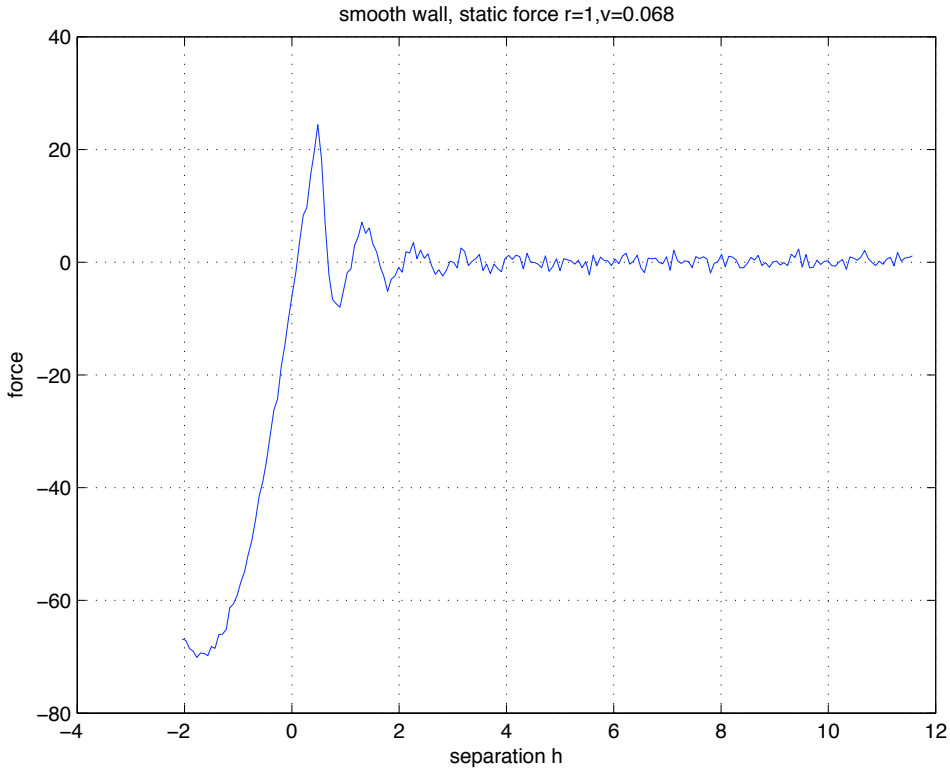
smooth wall, static force r=1,v=0.068
40
20
0
−20
−40
−60
−80
force
−4
−2
0
2
4
6
8
10
12
separation h

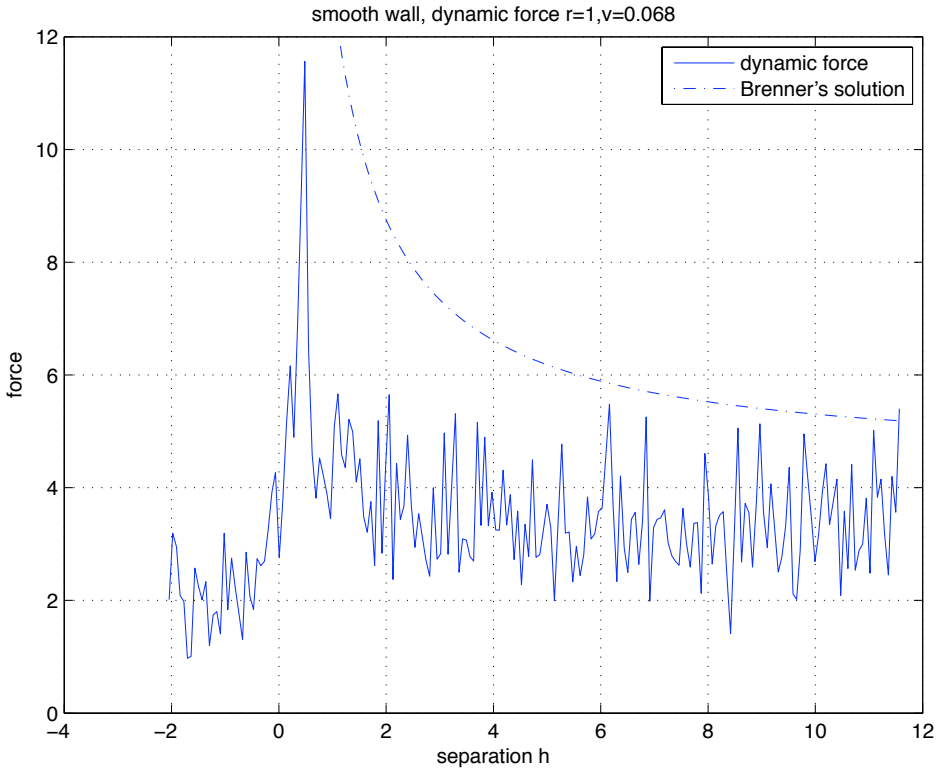

Figure 4.34 The static and dynamic component of the drag force as a function of separation for a colloid particle moving toward an smooth wall with a velocity U=0.068. The broken curve is Brenner's solution.

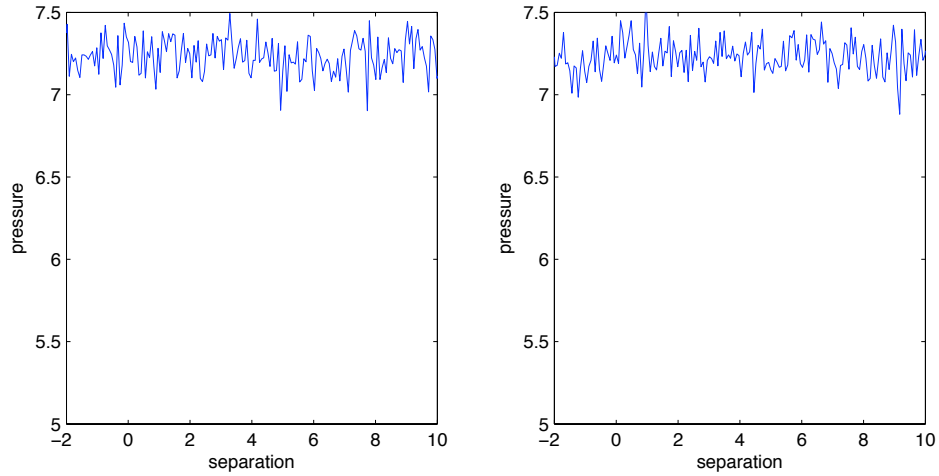

Figure 4.35 The system pressure as a function of separation for a colloid particle moving toward and away from an smooth wall with a velocity U=0.068. (left) colloid particle approached the wall. (right) colloid particle left the wall.

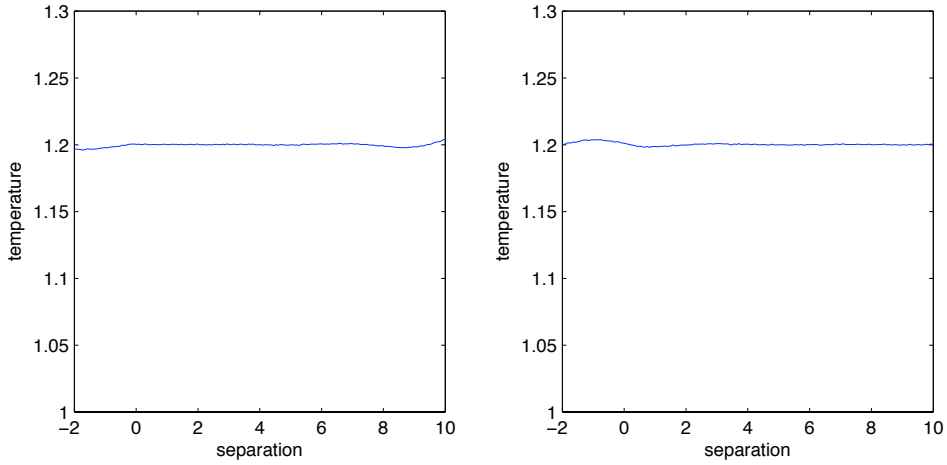

Figure 4.36 The system temperature as a function of separation for a colloid particle moving toward and away from an smooth wall with a velocity U=0.068. (left) colloid particle approached the wall. (right) colloid particle left the wall.

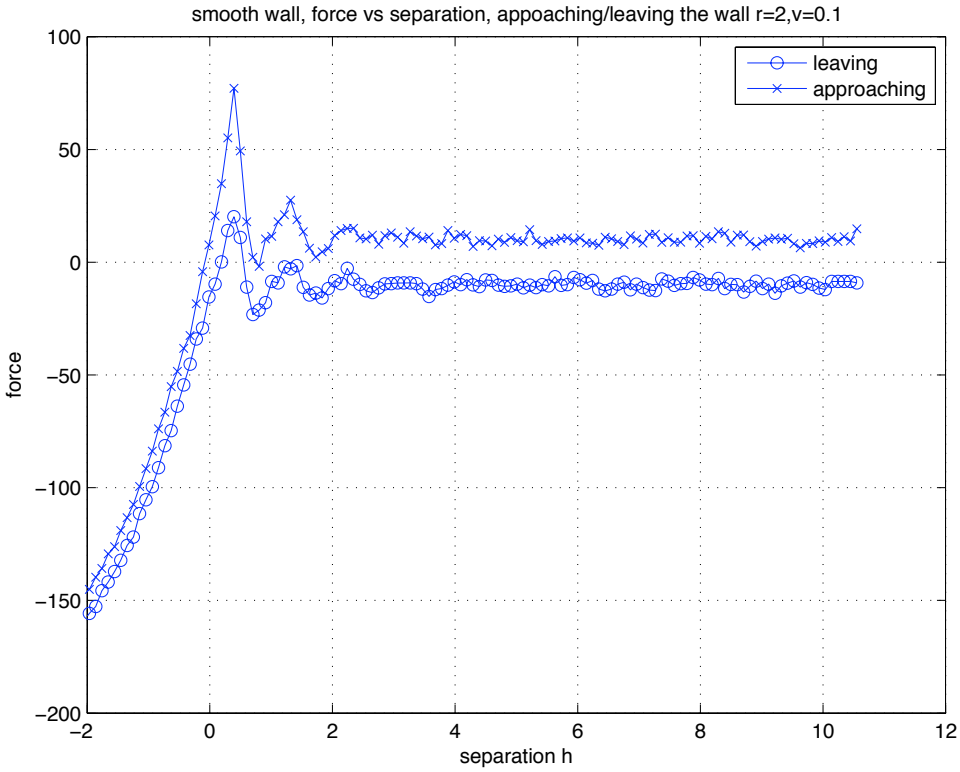

Figure 4.37 The drag force as a function of separation for a colloid of radius 2, moving toward (and away) from the smooth wall at a velocity U=0.1. The solid curve with crosses denotes the force while the colloid approaching the wall; the curve with circles denotes the force while moving away from the wall.

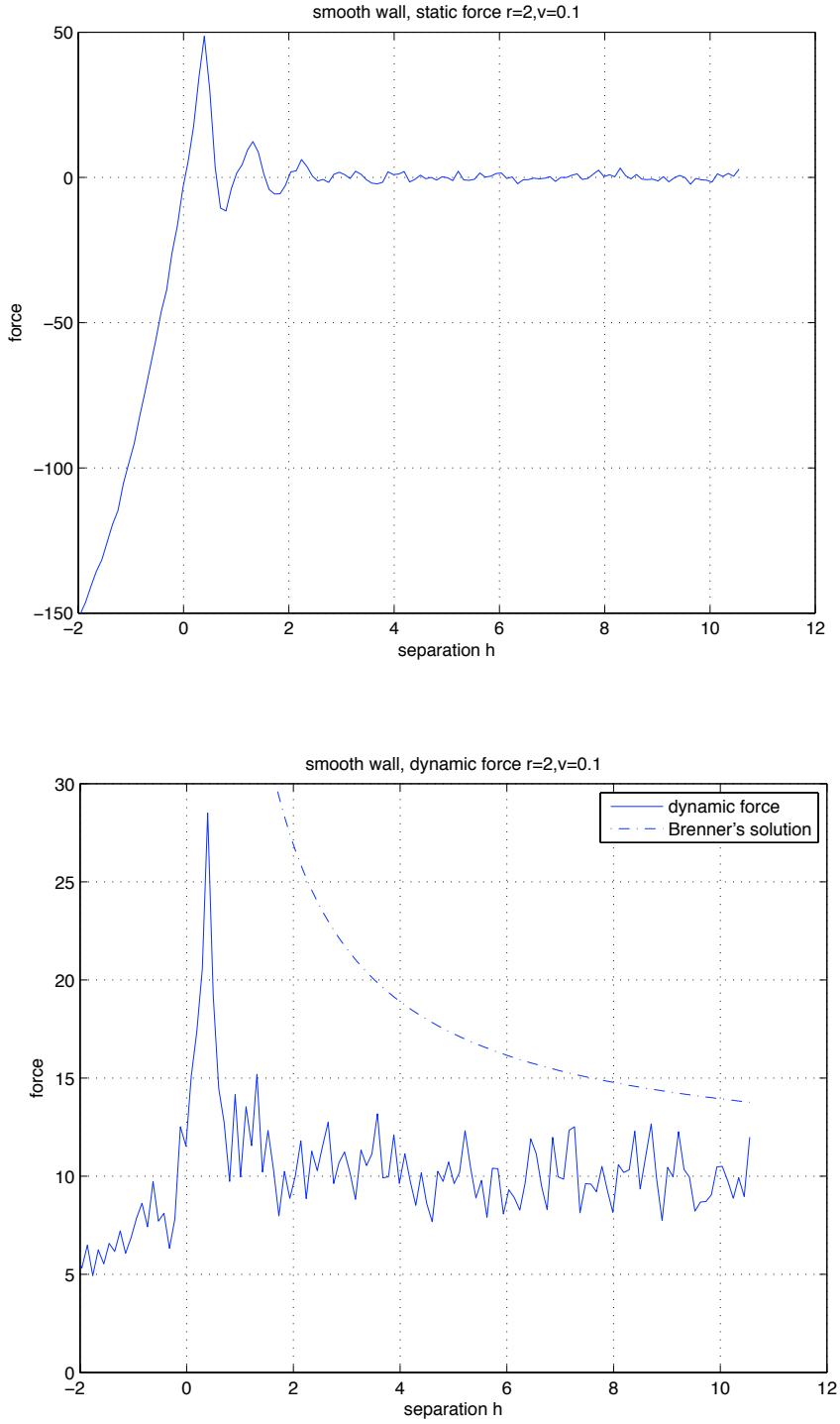

Figure 4.38 The static and dynamic component of the drag force as a function of separation for a colloid particle moving toward an smooth wall with a velocity U=0.1. The broken curve is Brenner's solution.

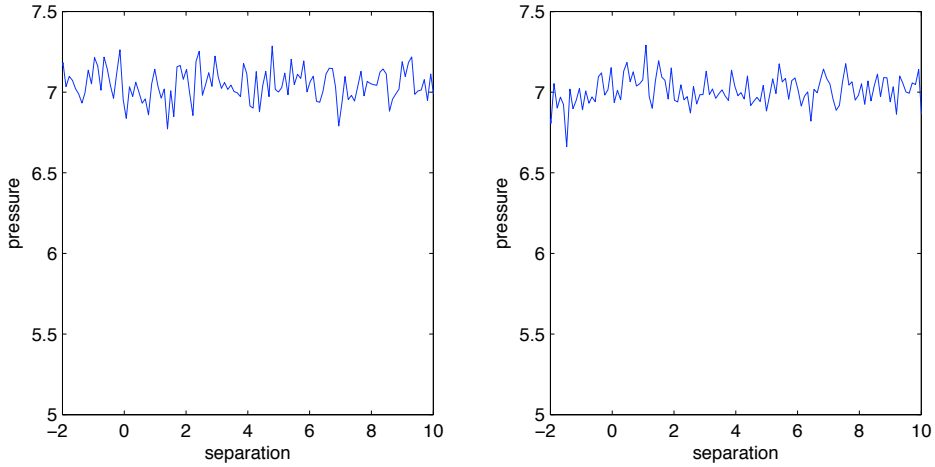

Figure 4.39 The system pressure as a function of separation for a colloid particle moving toward and away from an smooth wall with a velocity U=0.1. (left) colloid particle approached the wall. (right) colloid particle left the wall.

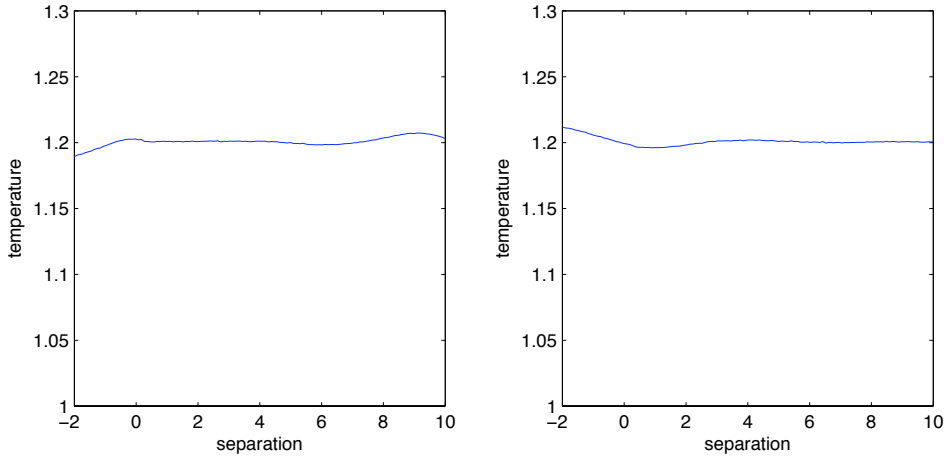

Figure 4.40 The system temperature as a function of separation for a colloid particle moving toward and away from an smooth wall with a velocity U=0.1. (left) colloid particle approached the wall. (right) colloid particle left the wall.

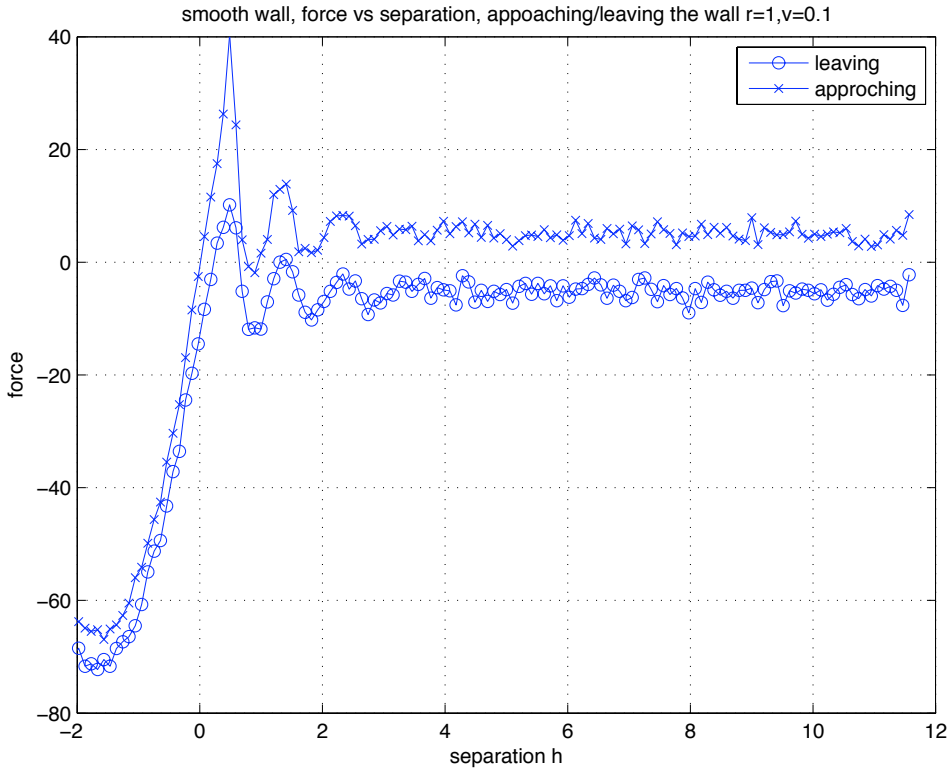

Figure 4.41 The drag force as a function of separation for a colloid of radius 1, moving toward (and away) from the smooth wall at a velocity U=0.1. The solid curve with crosses denotes the force while the colloid approaching the wall; the curve with circles denotes the force while moving away from the wall.

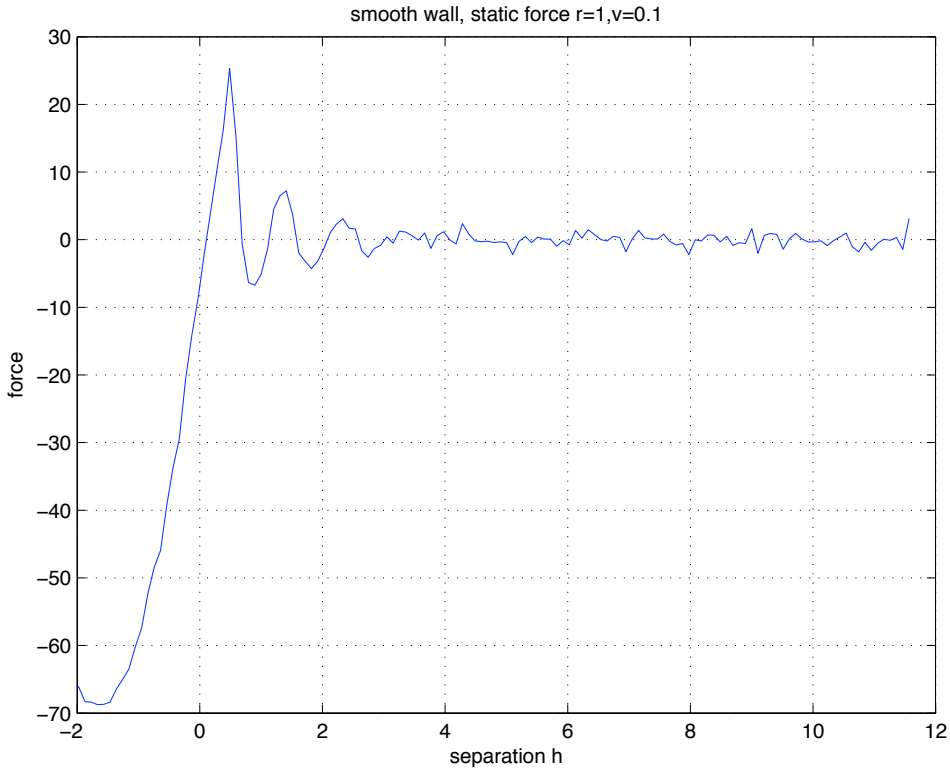
smooth wall, static force r=1,v=0.1
force
separation h
30
20
10
0
−10
−20
−30
−40
−50
−60
−70
−2
0
2
4
6
8
10
12

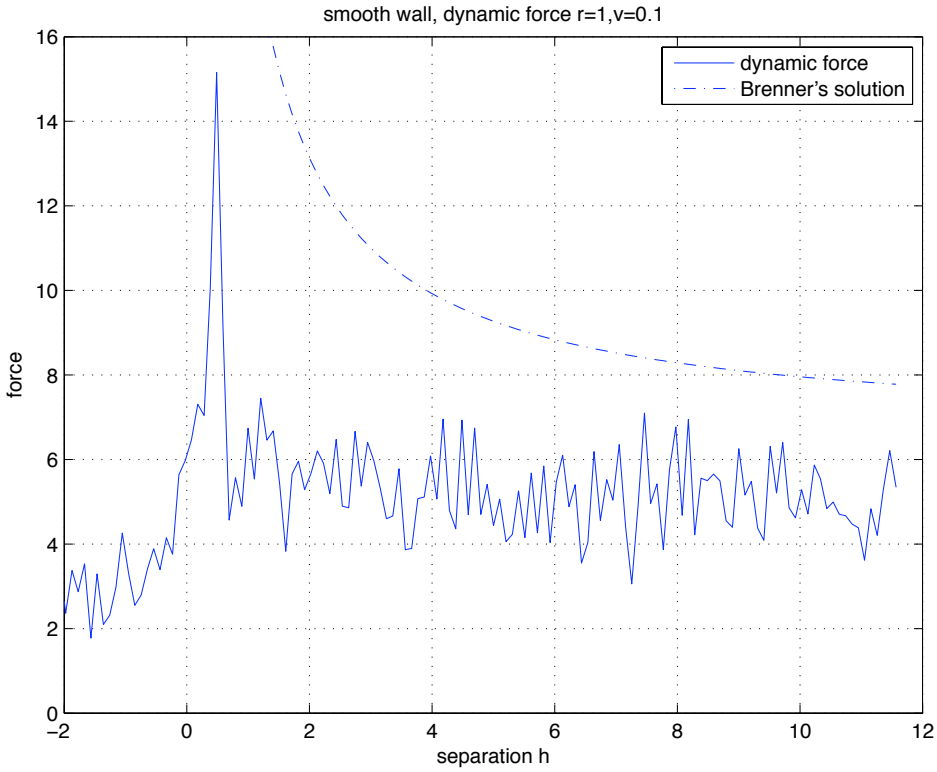

Figure 4.42 The static and dynamic component of the drag force as a function of separation for a colloid particle moving toward an smooth wall with a velocity U=0.1. The broken curve is Brenner's solution.

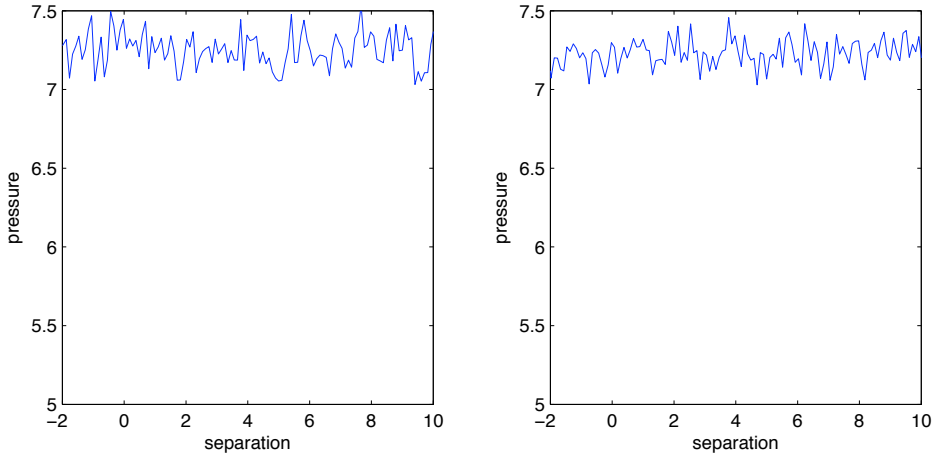

Figure 4.43 The system pressure as a function of separation for a colloid particle moving toward and away from an smooth wall with a velocity U=0.1. (left) colloid particle approached the wall. (right) colloid particle left the wall.

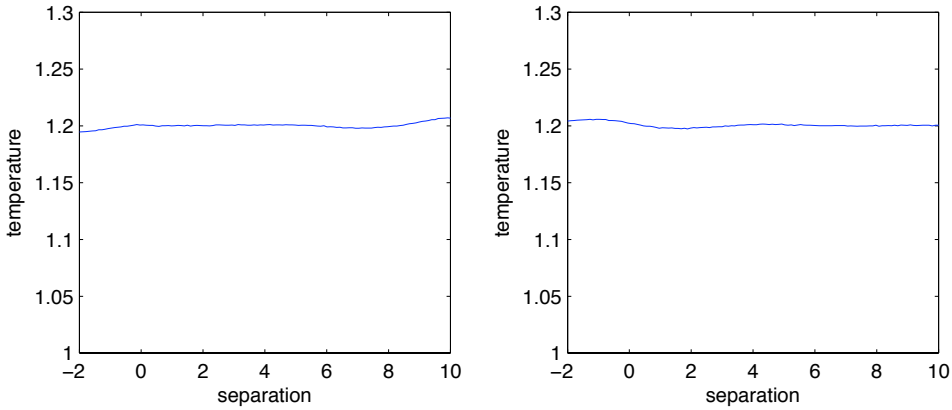

Figure 4.44 The system temperature as a function of separation for a colloid particle moving toward and away from an smooth wall with a velocity U=0.1. (left) colloid particle approached the wall. (right) colloid particle left the wall.

From the results of the dynamic forces, our results indicate that the Brenner term does not exist, since we only observe a spike when the colloidal particle is about to penetrate the

wall. The spike is narrower with a smooth wall, and the peak value depends on the colloidal moving velocity: the higher the velocity is, the higher the peak value is.

4.4 Boundary Condition

In previous chapter we discussed the boundary condition of the system. Here let us compare the dynamic force with the Brenner's solution and the Stokes' solution with both slip and no-slip boundary conditions.

We use the same data from the simulations we have, and compare the dynamic forces with the Stokes' solution with slip boundary condition ($F=4\pi\mu b$) and no slip boundary condition ($F=6\pi\mu b$).

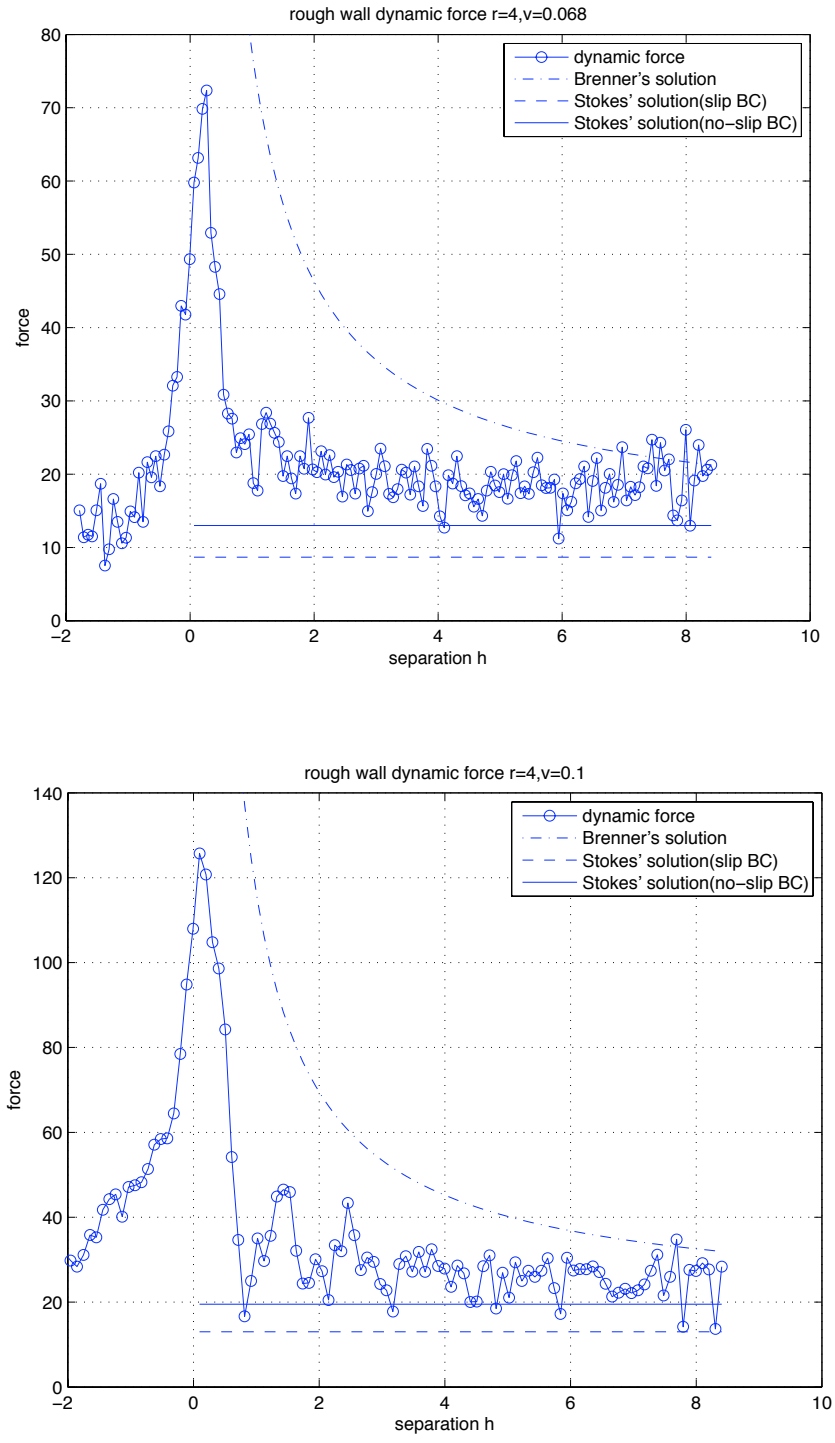

Figure 4.45 Rough wall r=4 simulation with a lower velocity U=0.068 and a higher velocity U=0.1. Dynamic force vs Brenner's solution and Stokes' solution with slip boundary condition and no slip boundary conditions.

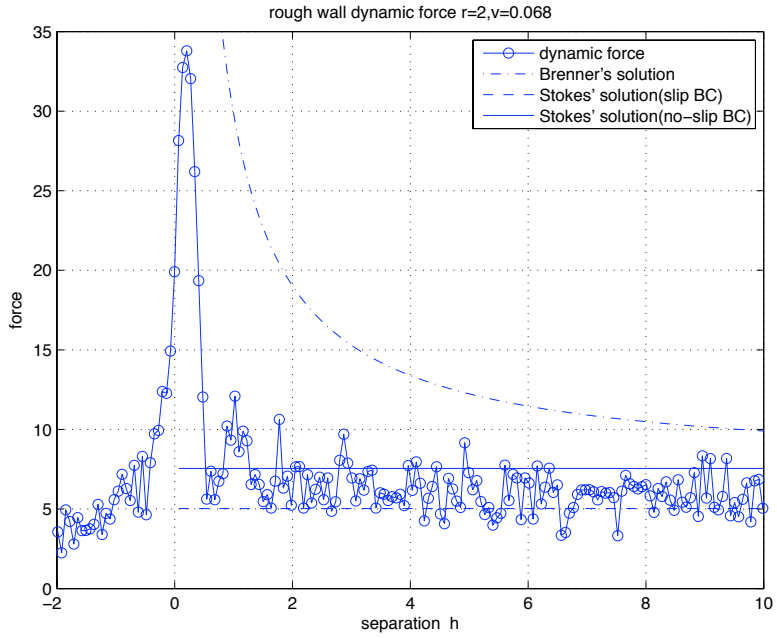

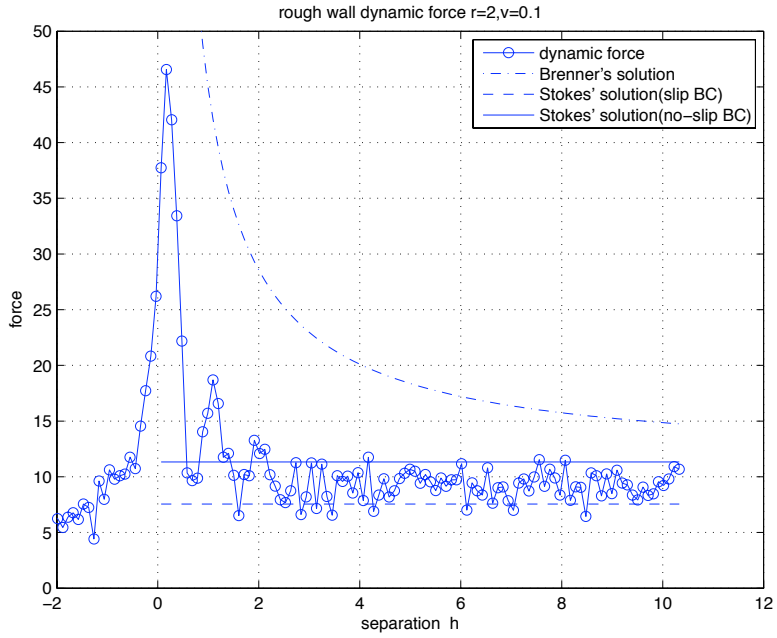

Figure 4.46 Rough wall r=2 simulation with a lower velocity U=0.068 and a higher velocity U=0.1. Dynamic force vs Brenner's solution and Stokes' solution with slip boundary condition and no slip boundary conditions.

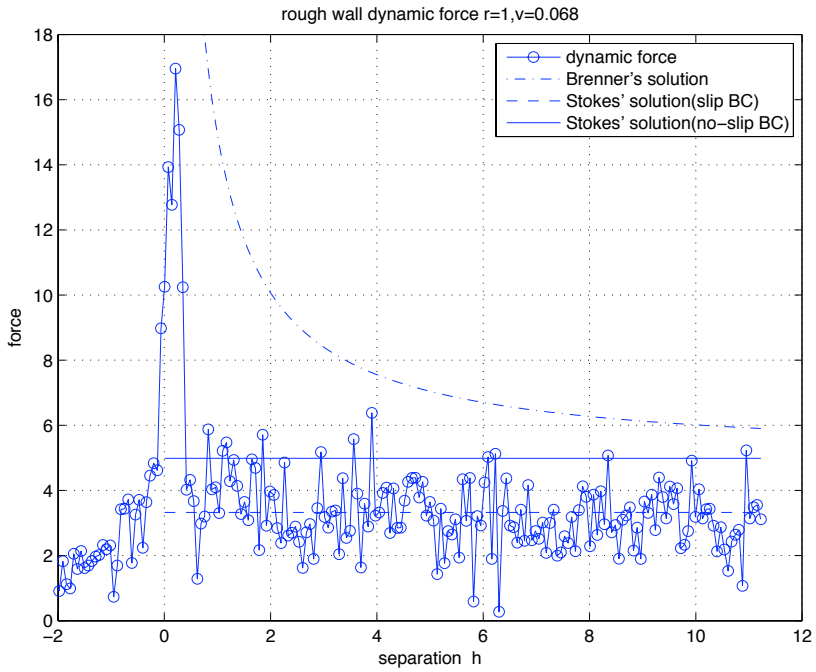

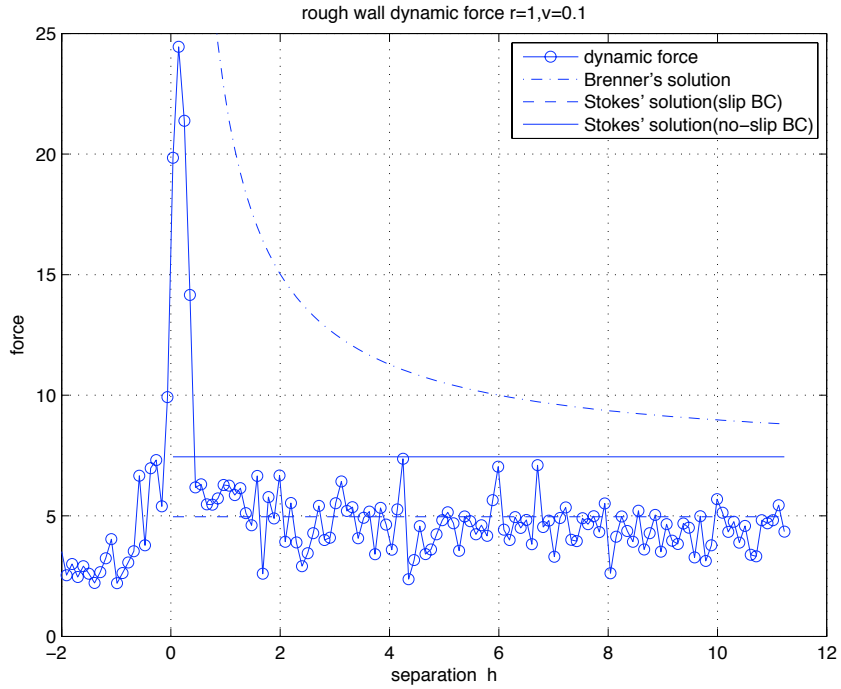

Figure 4.47 Rough wall r=1 simulation with a lower velocity U=0.068 and a higher velocity U=0.1. Dynamic force vs Brenner's solution and Stokes' solution with slip boundary condition and no slip boundary conditions.

From the rough wall simulations, we can tell for r=2 and r=1 cases, the Stokes solutions with slip boundary conditions agree more with the dynamic forces. The r=4 simulations, both the slip and no slip boundary conditions are not behave so well, we think that is caused by the colloidal particle size. For r=4, the colloidal particle is a little bit larger for the simulation box size $Lx/\sigma \times Ly/\sigma \times Lz/\sigma = 13.68 \times 13.68 \times 32.20$.

The smooth wall simulations give the similar results, the following are the corresponding figures. Compare to the rough wall results, the spikes of the smooth wall simulations are narrower and sharper, the peak values are lower than those of the rough wall simulations.

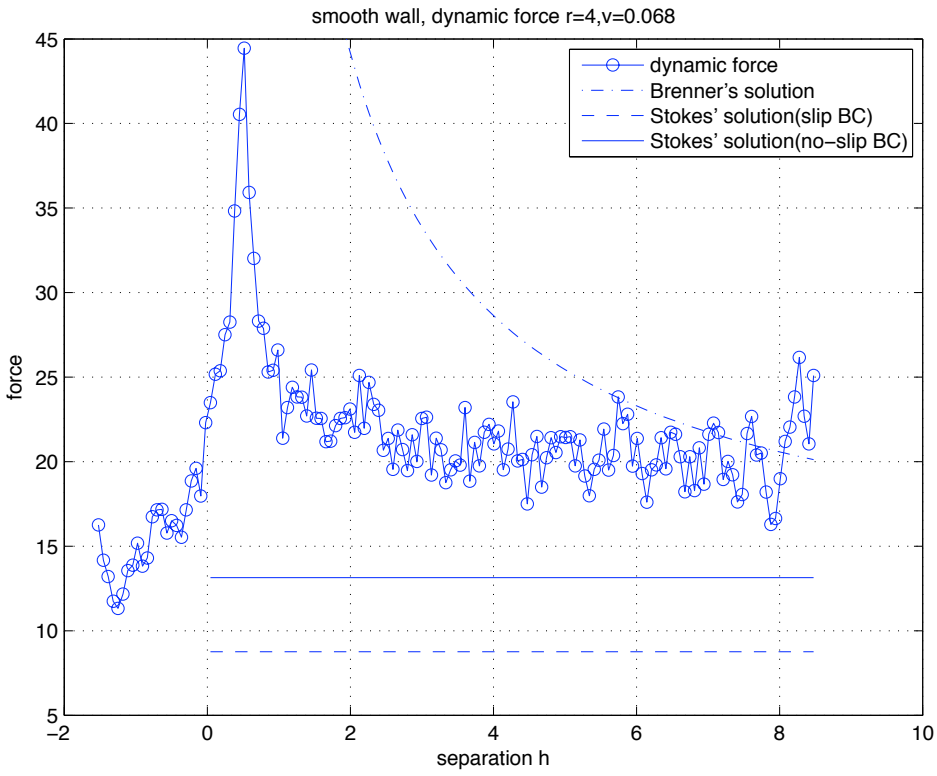

Figure 4.48 Smooth wall r=4 simulation with a lower velocity U=0.068 and a higher velocity U=0.1. Dynamic force vs Brenner's solution and Stokes' solution with slip boundary condition and no slip boundary conditions.

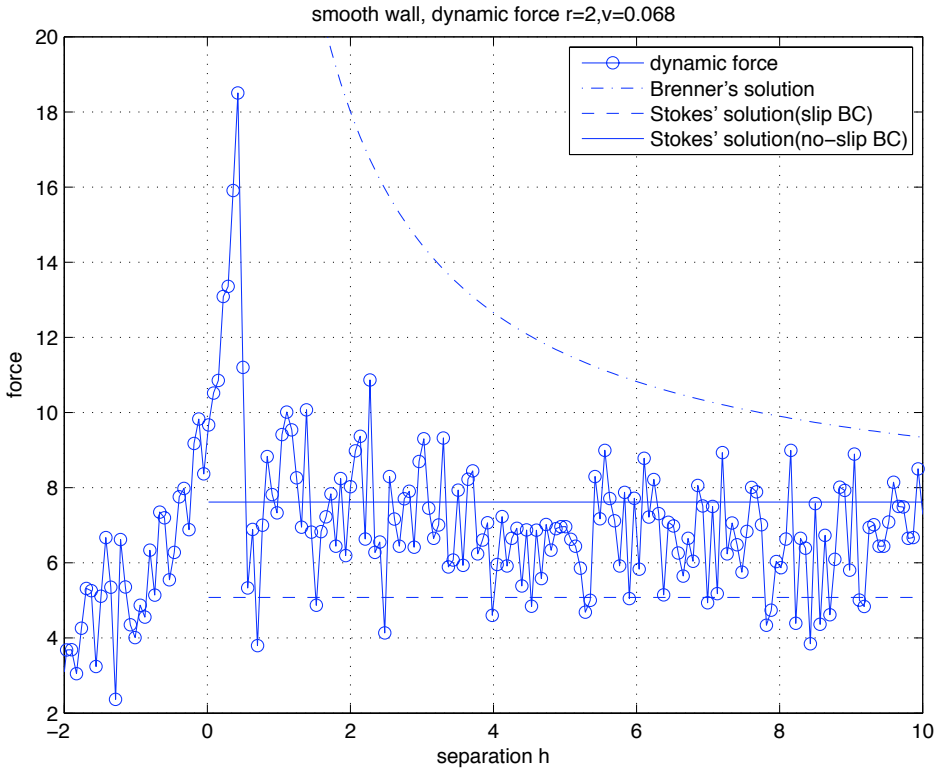
smooth wall, dynamic force r=2,v=0.068
dynamic force
Brenner's solution
Stokes' solution(slip BC)
Stokes' solution(no−slip BC)
force
separation h
20
18
16
14
12
10
8
6
4
2
−2
0
2
4
6
8
10

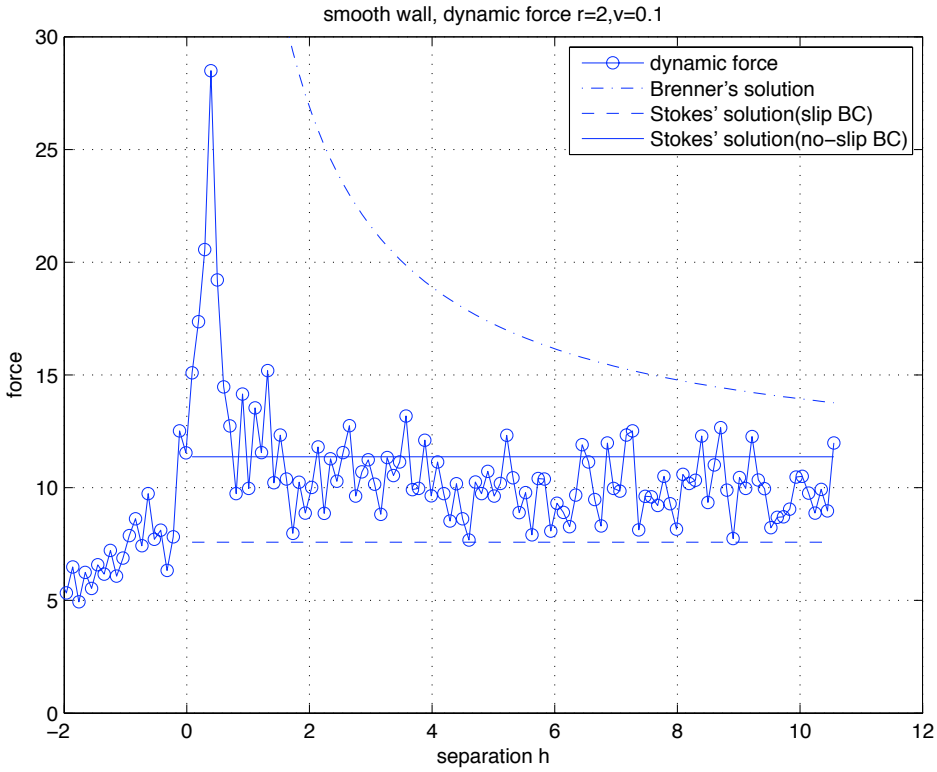

Figure 4.49 Smooth wall r=2 simulation with a lower velocity U=0.068 and a higher velocity U=0.1. Dynamic force vs Brenner's solution and Stokes' solution with slip boundary condition and no slip boundary conditions.

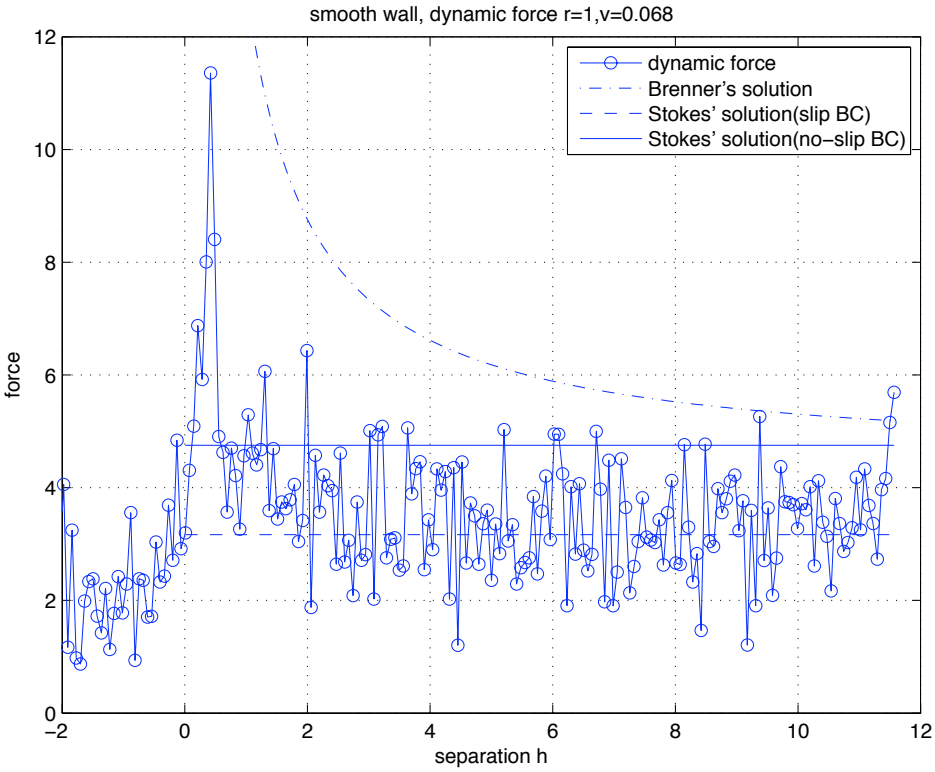
smooth wall, dynamic force r=1,v=0.068
dynamic force
Brenner's solution
Stokes' solution(slip BC)
Stokes' solution(no−slip BC)
force
separation h
0
2
4
6
8
10
12
−2
0
2
4
6
8
10
12

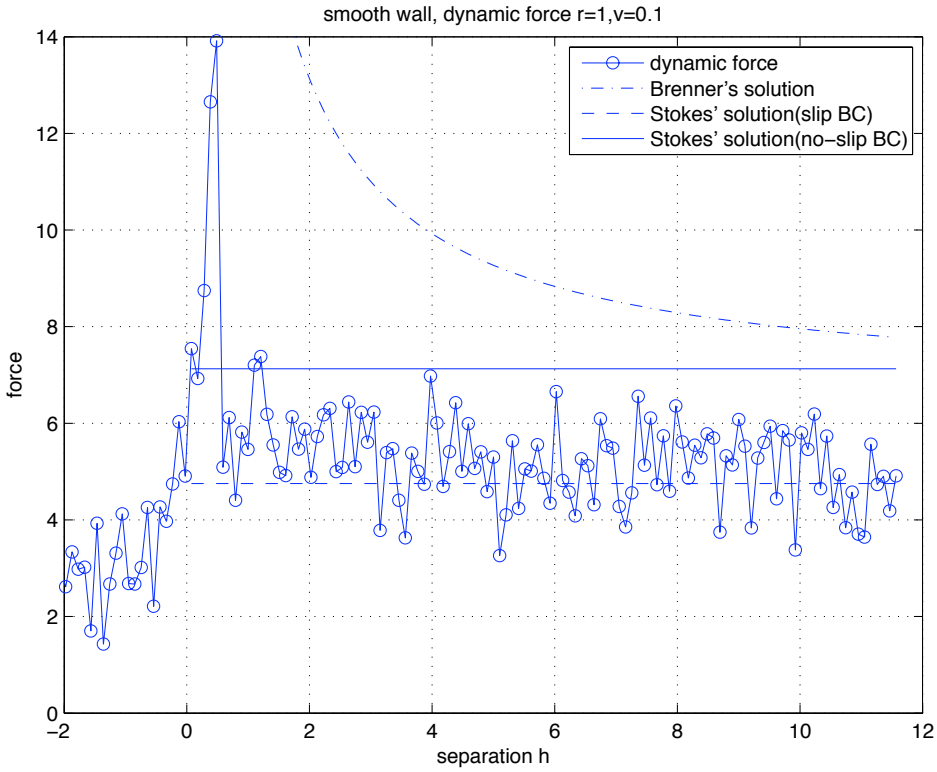

Figure 4.50 Smooth wall r=1 simulation with a lower velocity U=0.068 and a higher velocity U=0.1. Dynamic force vs Brenner's solution and Stokes' solution with slip boundary condition and no slip boundary conditions.

4.5 Discussion

We have step up these simulations to directly test the Brenner model and its assumptions. Compared to previous analyses (Vergeles, van Swol) which used somewhat ad hoc assumptions for the particle diameter and wall position, we will rely on the values established in the previous chapters. It is emphasized that the Brenner model is only appropriate for pure stick conditions. Pozrikidis has recently developed a model to cover

the full-range of slip to stick, incorporating a variable slip-length parameter. According to their research, the drag force exerted on the sphere in free solution is

$F = -8\pi\mu ag = -6\pi a \frac{\beta_p + 2}{\beta_p + 3}(V - U)$, where βp is Basset parameter which depends on the inverse of the slip-length. As βp → 0, which corresponds to an increasing value of slip-length from 0 (pure stick conditions) to infinity (pure slip conditions), the Stokes-law coefficient smoothly changes from 6 for pure stick to 4 for pure slip (the Maxwell limit). Pozrikidis had also extended this model to the case of a sphere approaching a wall, but their expression was not reduced to a simple analytic form. An important conclusion of that analysis is that if either the wall or the particle has pure slip, there should be no Brenner term, just constant drag up to wall contact. One might expect that there would still be a Brenner type contribution if either the wall or the sphere were rough, but the Pozrikidis analysis suggests not.

Our results for the smallest particle, r = 1, are in excellent agreement with the pure slip case: there is no increase in the hydrodynamic drag as the particle approaches the wall, and the magnitude of the drag is in very good agreement with c=4. These are independent of whether the wall is smooth or rough. There is a spike in the drag force at close distances to the wall whose width and magnitude do depend on the wall characteristics. This likely arises from second-order terms, such as high gradients in the local solvent velocity, that are not included in the analyses by Brenner or Pozrikidis. But these are highly localized, and there is an obvious lack in the increased resistance predicted by the Brenner model for distances further away from the wall. The position of that spike coincides quite well with how we defined position of the wall and the size of the colloid

particle in earlier chapters. This both validates that work and limits any shifts that might be made to obtain a better fit to the Brenner model. That is, similar spikes at contact were observed in the previous Vergeles and van Swol work, and were interpreted as arising from the Brenner term.

For r = 2, we get fairly good agreement with the pure slip case. The drag term is fairly constant, though now with an apparent c values of ~5. There is perhaps a slight increase in drag at very short distances, but this is still much smaller than the Brenner prediction. The spike at the wall is now significantly greater in magnitude and slightly greater in width, which is consistent with it arising from second-order, velocity gradient terms.

For r = 4, drag term is still fairly constant away from the wall, though its value is now greater than that predicted by the stick / Brenner solution. Treated at face value, its apparent c value would be ~8 which is outside the range that is physically expected. However, there is still no significant increase in drag on approaching the wall compared to what is predicted by the Brenner solution. The spike term at contact with the wall has again increased dramatically in intensity and somewhat in width.

We have used a smooth particle in all cases with a radially symmetric potential. Consequently, there is no mechanism by which these particles themselves can develop a tangential force that would correspond to "stick". Analysis by Bouquet showed that the sticking coefficient (slip length) results from atomistically detailed surfaces; a particle sliding across those surfaces experiences friction by sliding across one atom on the surface, but then bumping into the next atom. Consequently, our smooth particles should

be considered as having a pure slip surface. Therefore, we expect our results to reproduce the c = 4 result, which is what we have observed for r = 1.

The minor deviation for r=2 and large deviation for r=4 in the constant drag term away from the wall likely arises from using too small of a simulation box. That is, the displacement of the solvent around the colloid particle as it moves towards or away from the wall interacts with the periodic images defined by the size of our simulation box. If the box is too small, that flow around the colloid becomes restricted and this would add an additional drag term. This would not depend on the distance from the wall, but arises because the wall is present forcing that flow to occur. The lack of a significant increase with distance from the wall supports this explanation for that increased resistance, rather than it arising from the Brenner term. These results are then consistent with the c=4 conclusion reached for the r=1 simulations. This conclusion could be verified by repeating these simulations with a larger box.

The appearance of a spike in the drag force as the particle contacts the wall deserves some discussion. This increases with both the size of the particle and its velocity, and that dependence appears to be quadratic. This supports the argument that these arise from second order effects, such as the gradient in the velocity of the solvent around the colloid particle. They also differ significantly between the smooth wall and rough wall, indicating that surface roughness plays a role here while it does not effect the drag in approaching the wall. This suggests that perhaps one could add some second order corrections to the Pozrikidis model to account for them. What is particularly interesting is that the widths of these spikes are smaller than the size of the solvent atoms.

Consequently, we again reach the conclusion that the continuum fluid flow laws can be applied down at the atomic level.

Overall, these results are in excellent agreement with the Pozrikidis model that allows for slip, and disproves the application of the Brenner no-slip model for this situation. The agreement with the Pozrikidis model is especially noteworthy for the lack of a drag term for the mixed case of smooth particle and rough wall. Both Brenner and Vinogradova have formulated more complex models for the drag terms that allowed for slip. However, both of their formulations differ from the Pozrikidis model in that they did not limit to the pure slip drag (c=4) in the bulk solution. Our results are clearly consistent with the Pozrikidis model in that regard.

References

[Batchelor00] G. K. Batchelor, “An Introduction to Fluid Dynamics”, Cambridge University Press (New York, 2000).

[Bocquet2007] L. Bocquet and Jean-Louis Barrat, “ Flow Boundary Conditions from Nano- to Micro-Scales,” *Soft Matter* **3**, 685-693 (2007)

[Brenner61] H. Brenner, “The slow motion of a sphere through a viscous fluid toward a plane surface,” *Chem. Eng. Sci.* **16**, 242-251 (1961).

[Challa06] S. Challa and F. van Swol, “Molecular simulations of lubrication and solvation forces,” *Phys. Rev. E* **73**, 016306-1-8 (2006).

[Gaskell86] T. Gaskell, U.Balucani, M. Gori and R. Vallauri, “Wavevector-Dependent Shear Viscosity in Lennard-Jones Liquids”, *Physica Scripta.* Vol.35,37-39, (1987).

[Hasen07] J. S. Hasen, Peter J. Daivis, Karl P. Travis and B. D. Todd, “Parameterization of the nonlocal viscosity kernel for an atomic fluid”, *Phys. Rev*. E 76.041121 (2007).

[Hernandez2005] J. P. Hernandez-Ortuz, C. G. Stoltz, and M. D. Graham, “Transport and Collective Dynamics in Suspensions of Confined Swimming Particles”, *Phys. Rev. Lett.* **95**, 204501 (2005).

[Heyes96] D. M. Heyes, M. J. Nuevo and J. J. Morales "Self-Diffusion of Large Solid Clusters in a Liquid by Molecular Dynamics Simulation" *Mol. Phys.* **88**, 1503-1516 (1996).

[Holian] B. L. Holian, A. F. Voter, N.J. Wagner, R. J. Ravelo, and S. P. Chen, "Effectis of Pairwise Versus Many-body Forces on High-Stress Plastic Deformation" Physical Review A, Vol. 43, Number 6, (1991).

[Kohale2008] S. C. Kohale and R. Khare, "Molecular Simulation of Cooperative Hydrodynamic Effects in Motion of A Periodic Array of Spheres Between Parallel Walls," *J. Chem. Phys.***129** 164706 (2008).

[Kohale10] S. C. Kohale and R. Khare " Molecular Dynamics Simulation Study of Friction Force and Torque on a Rough Spherical Particle" *J. Chem. Phys.* **132**, 234706 (2010).

[Koplik89] J. Koplik, J. R. Banavar and J. F. Willemsen "Molecular Dynamics of Fluid Flow at Solid Surfaces" *Phys. Flui A* 1, 781-794 (1989).

[LAMMPS] A classical molecular dynamics code, and an acronym for Large-scale Atomic/Molecular Massively Parallel Simulator. LAMMPS is distributed by Sandia National Laboratories, a US Department of Energy laboratory.

[Luo07] H. Luo, C. Pozrikidis "Effect of surface slip on Stokes flow past a spherical particle in infinite fluid and near a plane wall", *Journal of Engineering Math* (2008) 62:1-21.

[Muller99] Florian Müller-Plathe, "Reversing the perturbation in nonequilibrium molecular dynamics: An easy way to calculate the shear viscosity of fluids", *Phys. Rev*. E 59, 4894 (1999).

[Nuevo97] M. J. Nuevo, J. J. Morales and D. M. Heyes "Hydrodynamic Behavior of a Solute Particle by Molecular Dynamics", *Mol. Phys.* **91**, 769-774 (1996).

[Riedel2005] I. Riedel, K. Kruse, and J. Howard, "A Self-organized Vortex Array of Hydrodynamically Entrained Sperm Cells", *Science* **309, 300** (2005).

[Todd08] B. D. Todd, J. S. Hansen and Peter J. Daivis, "Nonlocal Shear Stress for Homogeneous Fluids", *Phys. Rev. Lett.* PRL 100, 195901 (2008).

[Todd08] B. D. Todd and J. S. Hansen, " Nonlocal Viscous Transport and the Effect on Fluid Stress", *Phys. Rev*. E 78, 051202 (2008).

[Vinogradova2010] O. I. Vinogradova and A. V. Belyaev, "Wetting, Roughness and Flow Boundary Conditions," *J. Phys.: Condens. Matter* **23** 184104 (2011).

[Vinogradova2011] E. S. Asmolov, A. V. Belyaev, and O. I. Vinogradova, "Drag Froce on A Sphere Moving Toward An Anisotropic Superhydrophobic Plane," *Phys. Rev.E* **84** 026330 (2011).

[Vergeles96] M. Vergeles, P. Keblinski, J. Koplik and J. R. Banavar, "Stokes drag and lubrication flows: a molecular dynamics study," *Phys. Rev. E* **53**, 4852-4864 (1996).

[Vergeles97] M. Vergeles, P. Keblinski, J. Koplik and J. R. Banavar, "Stokes drag at the molecular level," *Phys. Rev. Lett.* **75**, 232-235 (1995).

[Voth2002] G. A. Vothm, B. Bigger, M. R. Buckley, W. Losert, M. P. Brenner, H. A. Stone, and J. P. Gollub, "Ordered clusters and dynamical states of particles in a vibrated fluid", *Phys. Rev. Lett*. **88**, 234301 (2002).

[Zhu2006] L. Zhu, P. Attard and C. Neto, " Reliable Measurements of Interfacial Slip by Colloid Probe Atomic Force Microscopy. I . Mathematical Modeling," *Langmuir* **27**, 6701-6711 (2011).